REACTOR MATERIALS

A Quarterly Technical Progress Review

Prepared for DIVISION OF TECHNICAL INFORMATION, U. S. ATOMIC ENERGY COMMISSION,
by BATTELLE MEMORIAL INSTITUTE, COLUMBUS LABORATORIES

Winter 1969-1970

● VOLUME 12

● NUMBER 4

Index Issue

TECHNICAL PROGRESS REVIEWS

The United States Atomic Energy Commission publishes the Technical Progress Reviews to meet the needs of industry and government for concise summaries of current nuclear developments. Each journal digests and evaluates the latest findings in a specific area of nuclear technology and science. *Nuclear Safety* is a bimonthly journal; the other three are quarterly journals.

Isotopes and Radiation Technology
P. S. Baker, A. F. Rupp, and associates
Isotopes Information Center, Oak Ridge National Laboratory

Nuclear Safety
Wm. B. Cottrell, W. H. Jordan, J. P. Blakely, and associates
Nuclear Safety Information Center, Oak Ridge National Laboratory

Reactor Technology

Reactor Materials
E. M. Simons and associates
Battelle Memorial Institute, Columbus Laboratories

All are available from the U. S. Government Printing Office. See the back cover for ordering instructions.

The views expressed in this publication do not necessarily represent those of the United States Atomic Energy Commission, its divisions or offices, or of any Commission advisory committee or contractor.

Availability of Reports Cited in This Review

United States Atomic Energy Commission (USAEC) reports are available at USAEC depository libraries and are sold by the Clearinghouse for Federal Scientific and Technical Information (CFSTI), National Bureau of Standards, U. S. Department of Commerce, Springfield, Va. 22151. All reports sold by CFSTI are $3.00 for printed copy and $0.65 for microfiche. Each separately bound part of a report is priced as a separate report. Some reports may not be available because of their preliminary nature; however, the information contained in them will generally be found in later progress or topical reports on the subject.

Other U. S. Government agency reports identified in this journal generally are available from CFSTI.

Private-organization reports should be requested from the originator.

United Kingdom Atomic Energy Authority (UKAEA) and Atomic Energy of Canada Limited (AECL) reports are available at USAEC depository libraries. UKAEA reports are sold by Her Majesty's Stationery Office, London; AECL reports are sold by the Scientific Document Distribution Office, Atomic Energy of Canada Limited, Chalk River, Ontario, Canada. UKAEA and AECL reports issued after March 1, 1967, are sold by CFSTI to purchasers in the United States and its territories.

REACTOR MATERIALS

Vol. 12, No. 4 Winter 1969–1970

Contents

Fuel and Fertile Materials (Section I)

Basic Studies of Radiation Effects in Fuel Materials . . . 221
Fuel Reactions Following Loss-of-Coolant Accidents . . . 223
Plutonium Compounds . . . 223
Uranium and Thorium Oxides . . . 225
Uranium Carbides and Nitrides . . . 226
Metal–Ceramic Fuels . . . 228
Plutonium Metal and Alloys . . . 228
Thorium Metal and Alloys . . . 231
Uranium and Uranium Alloys . . . 231
References . . . 233

Moderator and Control Materials (Section II)

Graphite . . . 236
Beryllium Metal and Alloys . . . 237
Solid Hydrides . . . 242
Metallic Poison Materials . . . 245
Dispersions and Nonmetallic Poisons . . . 245
References . . . 247

Special Fabrication Techniques (Section III)

Powder-Metallurgy Materials . . . 248
Melting, Casting, and Fabrication of Cast Structures . . . 248
Chemical Plating . . . 250
Explosive Metalworking . . . 251
Welding and Brazing . . . 251
Nondestructive Testing . . . 254
References . . . 255

Index

Volume 12 . . . 257

Superintendent of Documents, U. S. Government Printing Office, Washington, D. C. 20402, $2.50 per year

Reactor Materials

is one of a series of nuclear science and technology progress reviews being published under the auspices of the USAEC Division of Technical Information. About 35 specialists from the staff of the Columbus Laboratories of Battelle Memorial Institute prepare topical reviews periodically from worldwide literature. *Reactor Materials* covers properties, behavior, and fabrication processes of materials applicable to nuclear reactor components and associated equipment.

The authors and editors attempt to combine the highlights of significant new developments into a concise summary for both management and the technical specialist. Generally, enough of the results are presented to define the research and summarize the findings. For readers desiring more detailed information on any particular topic, the coverage is documented by references at the end of each section.

This issue marks the completion of our 12th year of publication. Unfortunately, we are at the same time faced with a significantly reduced budget. To maintain continuity, we will continue to publish *Reactor Materials* quarterly, but the specific subjects covered will vary from issue to issue. This issue treats fuel and fertile materials, moderator and control materials, and special fabrication techniques. The next issue will concentrate on properties, corrosion, and radiation effects in cladding and structural materials.

E. M. Simons
D. L. Keller

BATTELLE MEMORIAL INSTITUTE
COLUMBUS LABORATORIES

Issued quarterly by the U. S. Atomic Energy Commission. Use of funds for printing this publication approved by the Director of the Bureau of the Budget on May 12, 1969.

Section

I

Reactor Materials

Fuel and Fertile Materials

Basic Studies of Radiation Effects in Fuel Materials

Metals

A discussion, based on capillarity principles, of the stability of gas bubbles in solids has been given by Tiwari,[1] who concludes that one should expect a solid containing trapped gases to swell spontaneously. Moreover, the kinetics of the process should be governed by the diffusion of atoms through their own lattice.

A fuel-swelling model, which takes into account the distribution in size space of bubble radii, has been developed by August.[2] A nonlinear integrodifferential equation was derived for the bubble-distribution function and was transformed into an ordinary infinite system of differential equations. Numerical integration of this system of equations yielded the amount of swelling. Analogous discussions of this subject have previously been given by Baroody,[3] Gruber,[4] and Agranovich et al.[5]

A discussion of the possible nature of the change in volume of fuel compositions in solid swelling has been given by Guseva et al.[6] They concluded that a linear dependence of solid swelling on burnup is inherent in many fuel compositions within the range of temperatures and compositions where gas swelling and phase transformations are absent.

The mechanism of the radiation growth of uranium at small irradiation doses has been discussed by Konobeevskii et al.[7] Among the several conclusions drawn was the following: The growth of alpha uranium under irradiation is a two-stage process, starting with the accumulation of single-vacancy defects and intermediate atoms within the crystalline lattice. The formation of such defects occurs in the whole volume of the metal and is of a rather homogeneous character.

The radiation resistance of fuel elements in the "Arbus" reactor was evaluated by Chushkin et al.[8] The fuel material was a U–Al alloy containing 35 wt.% uranium. The maximum heat flux from the surfaces of the elements was 8×10^4 kcal/(m^2)(hr), and the maximum can temperature was 350°C. In use, the elements reach a burnup of 3.7%, and it was concluded, on the basis of the analysis, that this figure represents only a small fraction of the permissible burnup limit.

The effect of externally applied hydrostatic pressure from 0 to 1000 bars at 900°C on the fission-gas-induced swelling in uranium has been studied by Kulcinski et al.[9] The swelling was a sensitive function of pressure below 110 bars and relatively insensitive to pressure above 110 bars. Metallography of the samples showed that the average diameter of the bubbles was reduced from 3300 to 1800 A and the total number increased from 0.9 to $4.2 \times 10^{12}/cm^3$ as the annealing pressure was increased from 0 to 110 bars, respectively. Further increases in pressure from 110 to 1000 bars had little effect on average bubble size and density. The mechanism of pressure-reduced swelling was related to the equilibrium number of vacancies that can be associated with fission-gas atoms under stress. It was also shown, both experimentally and theoretically, that a loss of surface area occurs when bubbles coalesce under pressure.

X-ray diffraction analysis has been used by Bethune[10] to examine the phase change introduced in U_3Si thermally, by irradiation at 60°C, and by plastic deformation. Short irradiation exposures (burnup $\leq 0.12 \times 10^{-3}$% of all atoms) and plastic deformation modified the room-temperature structure of U_3Si, bct, to a disordered fcc structure, whereas heating above 756 ± 5°C caused an allotropic transformation to an ordered fcc structure of the Cu_3Au type. Lattice-parameter determinations indicated that the radiation-induced phase transformation was accompanied by a volume increase of 0.6%. Further irradiation resulted in nearly complete destruction of the diffraction pattern as the U_3Si became amorphous. The damage introduced by irradiation or by plastic deformation annealed in the range 250 to 500°C with a complete recovery to the bct structure.

Ceramics

A simulation experiment on columnar-grain formation in UO_2 was performed by Taketani and Ichikawa[12] using NaCl single crystals to examine the progress of void formation and migration. When two single crystals of NaCl were held together under a temperature gradient, platelike or lenticular voids were observed to generate and migrate toward the hot side, forming columnar grains in the NaCl crystal. The crystallographic orientation of the colder crystal was found to affect the void shapes observed in the hotter crystal. This void behavior was explained by calculations concerning the evaporation and condensation of the NaCl molecule.

The temperature-gradient-induced migration of helium-filled pores in KCl has been investigated by Carter et al.[13a] in order to test the theories of temperature-induced bubble migration in solids. The rate of migration was found to be in remarkably good agreement with that which would be expected if the transport of material occurred by an evaporation–condensation mechanism, with matter transport being controlled by diffusion of the vapor through the gas phase.

The fission-product-gas pressure in macroscopic voids was calculated at NASA–Lewis[14] over the temperature range 1000 to 2500°K for clad UO_2 fuel elements operating in a fast-neutron spectrum. The contributions of the partial pressures of cesium, rubidium, and other fission products which have generally been neglected in other investigations were included in the pressure calculations. At low temperatures, xenon and krypton are the major contributors to the total pressure. However, it was shown that the partial pressures of cesium and rubidium at high temperatures can be as much as 70% of the partial pressures of xenon and krypton.

Homogeneous nucleation theory was applied by Harrison[15] to uranium carbide to describe bubble formation and swelling. It was concluded that, at temperatures $\leqslant$700°C and for burnups less than 5×10^{20} fissions/cm^3, bubble formation is unlikely. A bubble nucleation time was predicted and its temperature dependence discussed. Comparisons were illustrated between calculated and observed swelling of unrestrained uranium carbide, and, finally, results of calculations of carbide swelling under various idealized conditions were presented.

The dynamic re-solution of small gas bubbles in UO_2 has been discussed by Nelson,[16] for conditions when the dissolved gas both can and cannot diffuse back into the bubbles. In accord with experimental observations, the model predicts that the bubble nucleation density is virtually independent of both the irradiation temperature and the fission rate. Further, the model enables the fraction of gas in "dynamic solution" and the fraction of gas contained within bubbles to be calculated for different values of gas-atom diffusion coefficient.

An extrapolation was made by Harrison[17] of the existing argon equation of state to higher pressures and temperatures. Because there is good experimental evidence that the theorem of corresponding states is obeyed for argon and xenon over the range of existing experimental measurements, the extrapolated argon equation may be used for xenon with suitable scaling. Examples were given of the use of the new xenon equation of state in the calculation of gas contents of bubbles and in the prediction of uranium carbide swelling. These were compared with similar calculations using the modified van der Waals law, showing how the latter underestimates the gas content of bubbles and overestimates gas swelling.

The role of bubbles in fission-gas release from UO_2 has been evaluated by Cornell et al.[13b] Experimental evidence for the mechanisms of bubble mobility in irradiated UO_2 was reviewed, and a description was given of the theory of gas transport to grain boundaries involving radiation-induced re-solution of intra- and intergranular bubbles.

Studies of the postirradiation release of fission gas from lightly irradiated UC have been conducted at Battelle–Columbus[18] over the temperature range 1300 to 2000°C. The diffusion coefficient of xenon in UC was measured and found to be given by an expression of the type

$$D = D_0 \exp\left(\frac{-Q}{RT}\right)$$

where $D_0 = 4.8 \times 10^{-2}$ cm^2/sec and $Q = 70$ kcal/mole. This diffusivity exhibits a temperature dependence similar to that for uranium self-diffusion in UC, and at any given temperature it is roughly an order of magnitude higher. The former observation suggests that xenon may diffuse via a uranium vacancy mechanism in UC, and the latter observation is consistent with the general finding that diffusion in a chemical concentration gradient is more rapid than self-diffusion.

The effect of stored energy in UO_2 and UN on in-reactor measurements of thermal diffusivity is being evaluated at Oak Ridge.[19a] Experimental methods are being used to study effects of energy release (or storage) during temperature transients. The presence of

an energy release during the time that the rate at which point defects are annealed exceeds the rate at which they are produced (an increase of specimen temperature) or the presence of an energy absorption when the annealing rate is less than the production rate (specimen cooling) will affect the measurement of thermal diffusivity during irradiation when a temperature-transient method is used.

The proceedings of the American Nuclear Society Topical Meeting (held at the General Electric Research and Development Center, Schenectady, New York, August 22–23, 1968) on Fundamental Properties of Materials in Nuclear Fuel Assemblies have been published in the *Journal of Nuclear Materials*.[13] The topics discussed include ionic motion in UO_2, rare-gas behavior in solids, and cladding materials.

(A. J. Markworth)

Fuel Reactions Following Loss-of-Coolant Accidents

Workers at Argonne[20] are continuing their study of the effect of violent meltdown on stainless-steel-clad UO_2 fuel rods in a sodium-cooled reactor. Five fuel rods were placed in a sodium-filled autoclave and subjected to two transients in the TREAT reactor of 236 and 460 cal/g of UO_2 during which the sodium reached a peak temperature of 1100°C. All five fuel rods were completely destroyed; only small cylindrical sections of UO_2 about ½ in. long remained. These sections were hollow and had an outside diameter greater than that of the original fuel pellet. The researchers postulated that the UO_2 pellets expanded by virtue of partial melting and thus contacted the cladding, whereupon the cladding melted, and perhaps vaporized, and the outer portion of the UO_2 solidified. The hollow core was the result of molten oxide flowing from the solid oxide annulus. (H. S. Rosenberg)

Plutonium Compounds

Oxides

Savannah River[21] has developed a process for preparing $^{238}PuO_2$ depleted in ^{17}O and ^{18}O to lower the neutron emission. The process involves oxygen-isotope exchange between $^{16}H_2O$ vapor and $^{238}PuO_2$ containing natural oxygen. The $^{238}PuO_2$ depleted to about 8% of the natural abundance of ^{18}O emitted only 5.5 neutrons/(sec)(mg of ^{238}Pu). Mound reported[22] on the behavior of $^{238}PuO_2$ microspheres contained in stainless steel and impacted into concrete, granite, and sand targets at velocities of 102 to 456 ft/sec. The percentage of fines (particles $<44\ \mu$ in diameter) increased with increasing velocity to a maximum of 50 to 55% above 375 ft/sec. Mound workers also compiled[23] the available information on the phase diagrams and compatibility of PuO_2 with various materials. A partial list of those systems involving PuO_2 includes the metals Al, Cr, Fe, Mg, Mo, Nb, Ni, Pu, Si, Ta, Th, Ti, U, V, W, and Zr; the alloys Inconel, stainless steel, W–26 Re, and Zircaloy-2; and the oxides of Al, Be, Ce, Cr, Fe, Li, Mg, Na, Si, Ta, Th, U, V, and Zr.

Thermal-reactor fuel studies in Belgium[24] have utilized both vibratory-compacted and swaged fuel elements of UO_2–0.96 mole % PuO_2 in 304L stainless-steel cladding. The effects of irradiation of the fuel in the BR-3 pressurized-water reactor to an average burnup to 3400 Mwd/metric ton with a linear power rating of 110 watts/cm are reported. Workers at Nuclear Materials and Equipment[25] showed the fuel microstructures developed in UO_2–20 PuO_2 after burnups to 60,000 Mwd/metric ton. Both hypostoichiometric coprecipitated and stoichiometric mechanically blended materials were irradiated and examined.

Battelle–Northwest[26] has irradiated hypostoichiometric UO_2–25 PuO_2 fuel pellets (O/M = 1.96) to burnups of approximately 70,000 Mwd/metric ton. A reaction was noted between the fuel and the 304 stainless-steel cladding. The reaction in localized areas extended as much as one-third of the way through the 16-mil cladding. It was indicated that 80% of the fission gas was released from the fuel. Oak Ridge[19b] has also studied the fission-gas release from UO_2–25 PuO_2 pellets at temperatures from 350 to 1130°C. The gas release appeared to depend on temperature throughout the range studied. Sudden cooling from 980 to 200°C produced a burst of gas release. A large amount of the iodine content was released during this burst.

The densities of sol-gel prepared UO_2–20 PuO_2 pellets after sintering for 5 hr in argon or in Ar–4 vol.% H_2 ranged from 81 to 87% of theoretical.[19c] Rocky Flats[27] has reviewed most UO_2–PuO_2 fabrication studies and reports on its own fabrication of UO_2–15 PuO_2 and UO_2–30 PuO_2 pellets from mechanically blended powder.

General Electric[28] has evaluated the compatibility of UO_2–20 PuO_2 fuel with austenitic-stainless-steel cladding, both out-of-pile and in-pile. Stoichiometric and slightly hypostoichiometric fuels were fully compatible with 304, 316, 321, and 347 stainless steels and Incoloy 800 for at least 1000 hr at 1400°F (760°C) out-of-pile. All alloys exhibited slight incompatibility with hyperstoichiometric fuel under similar conditions. In-pile results after fuel burnups of 52,000 to 100,000 Mwd/metric ton showed a heavy grain-boundary precipitate up to a depth of 0.004 in. in 316 and 347 stainless steels. Severely attacked cladding was observed in instances of excessively high operating temperatures (~800°C).

The liquidus–solidus curves for UO_2PuO_2, as determined by General Electric,[29] are shown in Fig. I-1. For high-plutonium compositions the maximum melting temperature occurs at an O/Pu ratio around 1.75.

O'Boyle, Brown, and Sanecki[30] examined the distribution of solid fission products in UO_2–20 PuO_2 fuel irradiated to a burnup of 2.7 at.% in a fast flux. White metallic inclusions located in both the equiaxed and columnar-grain regions contained Mo, Tc, Ru, Rh, and Pd, but no U or Pu. The observed partition of solid fission products between the oxide matrix and the inclusions was in agreement with predictions based on the free energy of formation of the fission-product oxides and the balance between oxygen liberated by the fission process and oxygen required to form stable fission-product oxides. Uranium and plutonium radial distribution measurements indicated a migration of plutonium up the temperature gradient. The plutonium concentration increased from 17.7 wt.% at the center of the columnar grains to 24.0 wt.% near the central void.

Batey et al.[31] have investigated the compatibility of tantalum with UO_2–PuO_2 compositions in the temperature range 1400 to 2100°C. The minimum temperature for a UO_2–PuO_2/Ta reaction for mixed oxides in the range from 40 to 100 wt.% PuO_2 was 1440°C. The tantalum content of the interface-equiaxed-grain zone increased from 2 wt.% for UO_2 to 18 wt.% for PuO_2.

Harwell[32] has conducted phase studies in the PuO_2–ZrO_2 system. The stabilization by PuO_2 of cubic ZrO_2 to room temperature as reported by previous investigators was found to be related to reduced oxides on the $PuO_{1.61}$–ZrO_{2-x} tie. In the fully oxidized state, tetragonal ZrO_2 was stabilized over a wide range of PuO_2 contents at high temperature. At lower temperatures the solubility of PuO_2 in the tetragonal phase appears to pass through a maximum at about 1000°C and then decrease rapidly, resulting in a wide two-phase region.

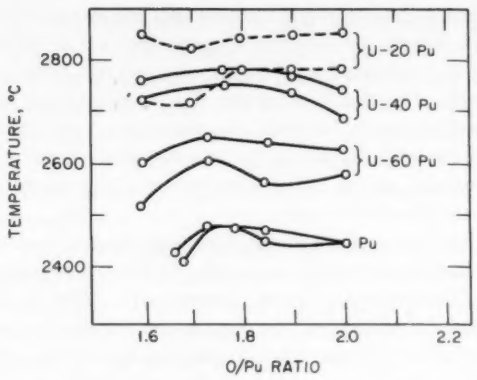

Fig. I-1 Liquidus–solidus curves for U–Pu oxides as a function of stoichiometry.[29]

Carbides

Los Alamos[33] has reported the thermal conductivity of UC–20 PuC to be 0.028 cal/(sec)(cm)(°C) at 118°C and 0.043 cal/(sec)(cm)(°C) at 1001°C. From mass-spectrometric studies the pressures of plutonium vapor above PuC–Pu_2C_3 and above Pu_2C_3–C were ascertained. Upon combining these data with the thermodynamic functions published for PuC and estimated for Pu_2C_3, values for the enthalpy of formation at 298°K of $PuC_{0.87}$(s) and $PuC_{1.50}$(s) were calculated to be −10.2 and −12.2 kcal/mole, respectively. Corresponding values for the entropy of formation were given as +3.0 and +5.3 eu, respectively.

From a mass-spectrometric study in the Pu–C system by Argonne,[34] Pu(g) was found to be the predominant vapor species in the condensed systems Pu_2C_3 + C, Pu_2C_3 + PuC_2, and PuC_2 + C in the temperature ranges 1365 to 1659°C, 1659 to 2026°C, and 1659 to 2075°C, respectively. The eutectoid temperature for which Pu_2C_3(s), PuC_2(s), and C(s) are in equilibrium was determined to be 1659°C.

Harwell, in a study of the UC_2–PuC_2 system,[35] found the U_2C_3 + C → UC_2 formation temperature to be 1590°C and the Pu_2C_3 + C → PuC reaction temperature to be 1650°C. A narrow field of two immiscible fcc phases exists in the UC_2–PuC_2 system. The phase diagram is shown in Fig. I-2. Melting-point data for the system were presented for stoichiometric and hyperstoichiometric compositions.

French investigators studied the U–Pu–Ti–C system[36] and reported on the preparation[37] of (U,Pu)CN. In the latter program a single-phase carbonitride was sought. Synthesis techniques included reactions of nitrides with carbon and carbides with nitrogen. A single-phase carbonitride containing 25 to 50 at.% nitrogen and having a density of 87% of theoretical was prepared by adding carbon to (U,Pu)N and heating for a few hours at 1600°C.

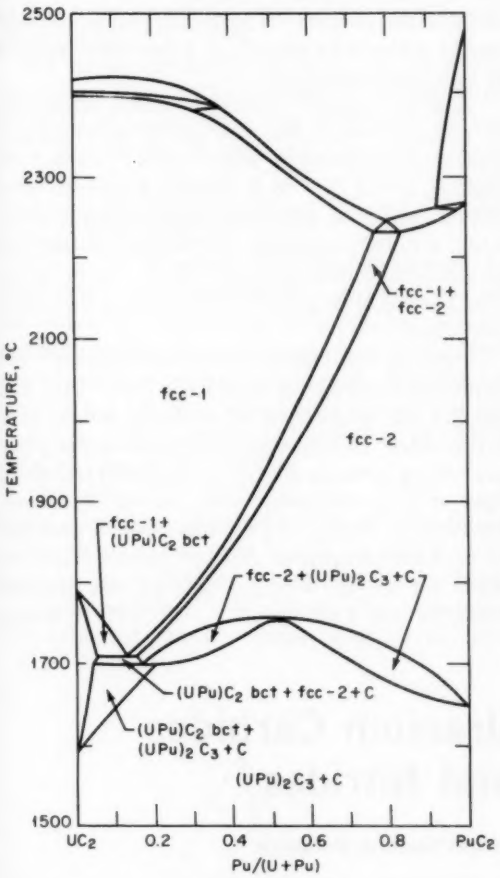

Fig. I-2 Tie between UC_2 and PuC_2 (Ref. 35).

Nitrides

As part of the investigation of mixed nitrides (U,Pu)N as fast-reactor fuels, Battelle–Columbus conducted sintering studies on mixtures[38] of UN and PuN. Volumetric expansion during the process of solid-solution formation was noted—as high as 14.7% when the mixture was held at 1900°C for 3½ hr. The volatilization behavior of UN, PuN, and UN–20 PuN was discussed. Vaporization results for the mixed-nitride material are shown in Table I-1. The volatilization behavior of this composition is governed predominantly by the PuN and not by UN. Irradiation results are given for two capsules. One capsule operated at a linear power rating of 13.5 to 19.6 kw/ft, and the fuel had burnups from 65,000 to 100,000 Mwd/ton. Diametral expansions for the fuel from 0.53 to 5.72% were observed. The other capsule operated at a rating of 25.7 to 29.2 kw/ft to burnups from 81,000 to 92,000 Mwd/ton. Linear expansions for the fuel from 1.29 to 3.9% were noted.

Oak Ridge researchers discussed the effects of nuclear burnup of mixed-nitride fuel in respect to chemical interactions with other components.[19d] Their calculations indicate that the activity of nitrogen in (U,Pu)N increases with irradiation burnup.

(M. D. Houston)

Uranium and Thorium Oxides

Properties and Behavior

The Proceedings of the ANS Topical Meeting on Fundamental Properties of Materials in Nuclear Fuel

Table I-1 Vaporization[38] of $(U_{0.8}Pu_{0.2})N$

Temp., °K	Vapor pressure, atm			pM/pN² ratio	Thermodynamic activity	
	Nitrogen	Plutonium	Uranium		Uranium	Plutonium
1400	3×10^{-11}	2×10^{-10}	10^{-14}	5.8	0.03	0.004
1600	2.5×10^{-9}	1.5×10^{-8}	3×10^{-12}	5.8	0.06	0.015
1800	8.8×10^{-8}	5.1×10^{-7}	6.3×10^{-10}	5.8	0.21	0.032
2000	1.1×10^{-6}	6.7×10^{-6}	4.0×10^{-8}	5.8	0.51	0.044
2200	2.0×10^{-5}	5.8×10^{-5}	7.0×10^{-7}	5.8	0.78	0.062
2400	5.4×10^{-5}	3.1×10^{-4}	8.1×10^{-6}	5.8	0.78	0.062

Assemblies[13] contains significant articles on ionic motion in UO_2 and rare-gas behavior in solids. The status of oxygen and uranium diffusion in UO_2 is reviewed by Belle,[13c] and recent data on this subject are reported by Marin and Contamin[13d] and Matzke.[13e] Marin and Contamin found that uranium self-diffusion in UO_{2+x} (with x ranging from 0.03 to 0.20) followed the Arrhenius relation

$$D = 0.13x^2\,(1 + 1000x^3) \times \exp(-85{,}000/RT) \quad \text{cm}^2/\text{sec}$$

over the temperature range 1275 to 1650°C. Oxygen diffusion was found to be represented by the equation

$$D = 0.26 \exp(-59{,}300/RT) \quad \text{cm}^2/\text{sec}$$

in the range 780 to 1250°C. Matzke observed that the coefficients for uranium self-diffusion in UO_2 which had been annealed in hydrogen were very small compared with previously published values. He attributed this difference to possible impurity effects or substoichiometric effects resulting from the hydrogen reduction. For UO_{2+x}, larger uranium diffusion coefficients were observed, more in accord with previous results. At 1500°C the dependence of D on x can be described by

$$\log D = -10.85 + 1.5 \log x$$

The most probable value for the enthalpy of activation for uranium diffusion in UO_2 was determined to be 110 ± 7 kcal/mole.

Russian investigators[39] have studied ^{99}Mo diffusion from irradiated UO_{2+x}, where x varied from 0.682 to 0.724. The UO_{2+x} was irradiated to fluences from 10^{16} to 10^{18} thermal neutrons/cm^2 at less than 100°C and then heated at various temperatures. Between 600 and 1200°C, ^{99}Mo release increased with temperature, and nearly quantitative release was observed after 400 to 500 min at 1200°C. At all temperatures, release followed a square-root-of-time dependency, with a break in the curve after 20 to 30 min. The initial stage of release showed an activation energy of 45 to 55 kcal/mole, whereas the second stage had an activation energy in the range 22 to 26 kcal/mole. The first stage is attributed to decomposition of a U_3O_{8+y} phase during heating, and the second release stage is associated with diffusion of ^{99}Mo in the hexagonal phase formed in the decomposition.

(R. H. Barnes)

Fabrication

Yugoslavian studies[40] have shown that the influence of reducing and oxidizing atmospheres on the sintering of UO_2 powders is dependent on the activity, or specific surface area, of the powder. Excess oxygen in nonstoichiometric UO_2 and high surface area may limit the sintered density and lead to the formation of intergranular porosity. In such cases, higher densities may be achieved by sintering at lower temperatures or by sintering in hydrogen.

A British patent[41] claims that a UO_2 ceramic can be prepared which does not exhibit columnar-grain growth at temperatures above 1600°C through the addition of 0.1 to 4 wt.% iridium. A solution of an iridium compound, ammonium chloro-iridite, is slurry-mixed with UO_2 and dried. The resultant powder may be fabricated into dense pellets by normal processing after a drying cycle at 400°C to decompose the iridium compound.

Planetary ball milling has been investigated[42] as a method of comminuting presintered ThO_2–UO_2 granules for the preparation of sinterable solid-solution feed powders. Experimental results indicate that planetary milling offers significant size-reduction-rate advantages over conventional comminution treatments. Solid-solution ThO_2–UO_2 powders, with a sinterability equivalent to that of powders conventionally wet milled for 44 hr, were produced by wet planetary milling for only 4 hr. (T. R. Wright)

Uranium Carbides and Nitrides

Properties and Behavior

The nature of the UO_2–UN system, mentioned in *Reactor Materials*, **12**(3): 164 (Fall 1969), has been clarified by Benz at Los Alamos.[43] His high-temperature X-ray data show that a complete series of solid solutions exists between UO_2 and bcc U_2N_3–UN_2 at temperatures above 1200°C. This solid solution breaks down on cooling below 1200°C to give a eutectoid mixture of UO_2 and U_2N_3 at room temperature. The X-ray data also show that a three-phase region exists in the phase-diagram triangle bounded by UN, hexagonal U_2N_3, and $UO_{0.4}N_{1.4}$ (solid solution) at temperatures from 1200 to 1400°C. Hexagonal U_2N_3 and bcc U_2N_3 cannot exist in equilibrium at the same composition and temperature. Since bcc U_2N_3 forms solutions with

UO_2 and UN_2 and hexagonal U_2N_3 can coexist with UN at 1200°C, it seems likely that bcc U_2N_3 contains slightly more nitrogen (and/or oxygen) than hexagonal U_2N_3. Some information was also obtained on the solidus surface in the U–N–O system. The UO_2 dissolves appreciable UN at the eutectic temperature (2600°C) in the quasi-binary UO_2–UN system. Nitrogen lowers the monotectic temperature between liquid uranium and UO_2 to 2340°C.

The relative insolubility of UO_2 and UN at low temperatures, as noted by the Japanese and mentioned in *Reactor Materials*, **12**(3): 164 (Fall 1969), has also been observed by Moench and Claussen.[44] X-ray studies of pellets annealed at 1800 to 1900°C indicate complete solid solution between UN and CeN and between UN and NdN.[45]

The U–Zr–C system has been reexamined by Nickel et al.[46] As has been found in previous studies of this system, the composition of (U,Zr)C that will not react with carbon to form UC_2 increases in zirconium content with increasing temperature. However, as shown in Fig. I-3, these investigators indicate that this point moves only from ZrC–39 mole % UC at 1700°C to ZrC–23 mole % UC at 2000°C.

The tetragonal phases U_2OsC_2, U_2PtC_2, and U_2RuC_2 have been identified by Holleck[47] in addition to the phases U_2IrC_2 and U_2RhC_2 reported earlier [*Reactor Materials*, **10**(4): 209 (Winter 1967–1968)].

An investigation[36] of the UC–TiC system has confirmed that this is a simple eutectic-type quasi-binary system with the eutectic at 30 mole % TiC (15 at.% Ti). The solubility of uranium in TiC is less than 1 at.%, and the solubility of titanium in UC is less than 1 at.%. The (U,Pu)C–TiC system was found to be similar to the UC–TiC system.

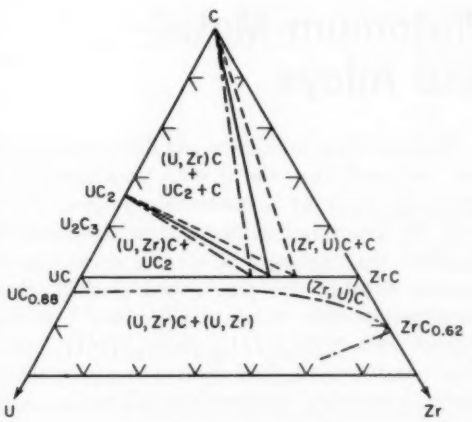

Fig. I-3 Phase fields in UC–ZrC–C system[46] at 1700, 1900, and 2000°C. Arc-melted alloys homogenized 22 hr at 1600°C, then annealed for 22 hr and quenched in helium. Annealing temperature: –·–, 1700°C; ——, 1900°C; – – –, 2000°C.

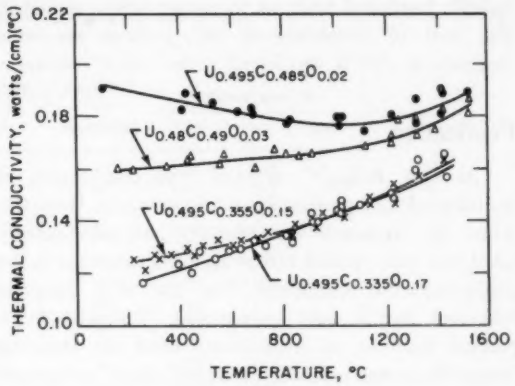

Fig. I-4 Thermal conductivity of uranium oxycarbides calculated from thermal-diffusivity data and heat capacity of uranium monocarbide.[48]

The conductivity of UC is reduced rather rapidly by small amounts of oxygen in solid solution and is reduced more slowly by larger amounts of oxygen in solution according to data obtained by Bates,[48,49] Fig. I-4. If it is recognized that the conductivity of high-purity UC is between 0.22 and 0.23 watt/(cm)(°C) over the temperature range 200 to 1000°C, then Bates' data clearly illustrate the deleterious effect of alloying additions on the conductivity of UC. This deleterious effect has been demonstrated[50] for several alloy additions, including PuC.

The specific heats of UC, UN, and UO_2 have been measured over wide ranges of temperature and compared by Affortit.[51] The heat capacity of UN is similar to that of UC, and over the temperature range 0 to 2000°C is given by the expression

$$C_p = 12 + 3.8 \times 10^{-3} T \text{ cal/(mole)(°C)}$$

The enthalpy of metastable uranium dicarbide ($UC_{1.90}$) has been measured from 400 to 1520°K by Macleod[52] (see Dalton[35] with regard to the stability of UC_2 in this temperature range). The results may be represented by the equation

$$H_T - H_{298} = 17.24\,T + 1.3714 \times 10^{-3}\,T^2 + 3.1605 \times 10^5\,T^{-1} - 6322 \text{ cal/mole}$$

Specific heats and heats of formation were calculated. The heat of formation of $UC_{1.9}$ from the solid elements at 298°K was found to be −21.0 kcal/mole. (W. Chubb)

Fabrication

At Oak Ridge,[53] uniaxial cold compaction of synthesized UN produced sound compacts. However, when the compacts were sintered and subsequently sized, the ends spalled off owing to laminations in the cold-compacted specimens. The use of a camphor lubricant during cold compacting, followed by a gradual increase in temperature until the sintering temperature was reached, produced sound specimens.

Oak Ridge investigators produced bodies with densities of 99% of theoretical by hot-pressing UN powder at 1400°C for 1 hr under a pressure of 3 tsi. The Germans[54] conducted hot-pressing studies on relatively coarse UN powder prepared by a nitride-decomposition cycle. Their "high-purity" UN compacts contained 0.26 wt.% oxygen. Densities on the order of 80% of theoretical were obtained after hot pressing, but higher densities could be achieved by (1) annealing of the hot-pressed compacts, (2) using a finer particle-size powder, and (3) adding either nickel, carbonyl iron, or uranium dialuminide. Relations between hot-pressed densities, time, temperature, and pressure were also investigated.

The fabrication of UC_2–graphite dispersion specimens containing up to 40 wt.% UC_2 was the subject of a study at Battelle–Columbus.[55] Spectrographic carbon, <10-μ UO_2 powder, and furfuryl alcohol were blended as a slurry, vacuum dried, and isostatically compacted. The resulting compact was laminated and showed poor dispersion of UO_2 in carbon. Dry blending, followed by uniaxial vacuum hot pressing, produced a more satisfactory dispersion and a minimum amount of cracking. The UO_2 and carbon were converted to UC_2 and graphite by heating for 3 hr at 2000°C under <50-psi pressure. The specimens were then densified by heating for 1 hr at 2400°C under a pressure of 20,000 psi. By cooling the specimens slowly and releasing the pressure gradually, internal microcracks were kept to a minimum and densities obtained were 97% of theoretical. (W. T. Langendorfer)

Metal–Ceramic Fuels

Oak Ridge is investigating those factors which affect the dimensions and fuel-core structural features of "picture-frame" dispersion fuel elements fabricated by roll bonding.[19e] The use of high-compressive-strength aluminum alloys was found to decrease both dog boning (buildup of fuel at the ends of the fuel core) and the amount of fuel-core porosity developed during rolling. The net effect of the higher strength claddings on in-pile performance is uncertain at this time, since reduced dog boning should improve performance, whereas reduced fuel-core void volume should have the opposite effect. The Oak Ridge research encompasses both the fabrication development and irradiation evaluation of both clad UAl_x–101 aluminum alloy and U_3O_8–101 aluminum-alloy dispersion fuel plates.

The fabrication of UN–W and UN–Mo cermets by sintering and hot isostatic pressing has been investigated at NASA's Lewis Research Center.[56] Table I-2 shows sintering results on powders characterized in Table I-3. The accelerated sintering obtained in nitrogen-free atmospheres is caused by decomposition of the UN to form liquid uranium metal, with attendant liquid-phase sintering of the refractory-metal matrix. The general resistance of the cermets to sintering densification reflects the refractoriness of both the metal matrices and stoichiometric UN. Compatibility experiments showed UN to be considerably more reactive with molybdenum than with tungsten in capsules containing no nitrogen overpressure. These results are in agreement with unpublished Battelle–Columbus observations. (R. A. Smith)

Plutonium Metal and Alloys

Previous X-ray diffraction and dilatometric studies have indicated that the $\alpha \rightleftharpoons \beta$ transformations in plutonium occur by a martensitic process. Furthermore, the anisotropic nature of these transformations suggested the existence of specific crystallographic relations between the parent and product phases. Subsequent work by Nelson and Bowman[57] produced evidence for a $(010)_\alpha \| (\bar{1}11)_\beta$ $[10\bar{2}]_\alpha \| [34\bar{1}]_\beta$ relation in the transformation from alpha to beta plutonium. A rotational and shear translation during transformation was also observed.

Investigators at Los Alamos[58] employed heat-flow experiments, electrical-resistivity measurements, and density determinations on high-purity plutonium to

Table I-2 Properties of Pressed and Sintered W–UN and Mo–UN Cermets[5,6]

Cermet lot (type)	Specimen	Sintering treatment: Temp., °C	Time, hr	Atmosphere (N_2 in Ar), vol.%	Density,* % of theoretical	Chemical analysis: N/U†	ppm	ppm
A(W–UN)	1	2200	10	67	82	1.04	560	23
	2	2200	5	67	82	1.02	800	5
	3	2200	3	67	83	0.98	1195	ND‡
	4	2200	3	0	86	0.99	1485	ND
B(W–UN)	1	1500	8	0	81	1.02	1009	ND
	2	2200	10	67	92	1.00	1290	ND
	3	2200	5	67	90	1.02	1137	11
	4	2200	3	67	86	1.04	1290	54
	5	2200	3	10	88	1.03	1167	76
	6	2200	3	0	97	0.96§	1855	241
	7	2500	5	67	95	0.99	1930	ND
C(W–UN)	1	2200	3	67	95	0.96	2673	ND
	2	2200	3	0	95	0.97	3740	ND
D(Mo–UN)	1	2000	5	67	83	1.02	1135	ND
	2	2200	5	67	89	1.03	1135	52
	3	2200	3	67	87	0.97	1195	52
	4	2200	3	10	89	1.02	1198	112
	5	2200	3	0	98	0.98	1935	ND
E(Mo–UN)	1	2200	3	67	98	0.99	2990	ND
	2	2200	3	0	98	0.97¶	3933	ND

*Determined by water immersion of specimens sealed on their external surfaces with lacquer.

†Stoichiometry ratios were calculated by assuming that all oxygen exists in the form of UO_2; precision of N/U = ±4% of value shown.

‡Not determined.

§Free uranium in grain boundaries.

¶Mo–U phase formed.

Table I-3 Properties of Uranium Nitride, Tungsten, and Molybdenum Powder Before and After Mixing and Cold Pressing[5,6]

Powder lot*	Particle surface area,† m^2/g	Particle size,‡ μ	Chemical analysis, ppm: N/U§	O	C	Si	Ca	Cr	Fe	Ni	Mo
Before Mixing and Pressing											
UN-1	0.18	1.6	1.01	1250	257	20	<5	<10	330	350	90
UN-2	1.07	0.26	0.99	3825	549	15	30	200	300	350	15
W-1¶	0.16	4.5	ND**	250	11	<1	<1	3	2	5	10
W-2¶	1.14	0.88	ND	1255	37	2	<1	5	15	10	50
Mo-1¶	0.34	4.5	ND	53	54	20	5	5	30	ND	ND

After Mixing and Pressing at 70,000 psi (500 MN/m^2)

Cermet lot No.	Uranium nitride lot No.	Metal lot No.	Fuel (UN) loading, vol.%
A	UN-1	W-1	44
B	UN-1	W-2	50
C	UN-2	W-2	56
D	UN-1	Mo-1	48
E	UN-2	Mo-1	49

*UN, W, and Mo denote the chemical symbols of each powder lot.

†BET analysis.

‡Particle sizes of both UN lots were calculated from surface-area measurements assuming spherical particles; particle sizes of tungsten and molybdenum lots were measured by a Fisher subsieve analyzer.

§Stoichiometry ratios were calculated by assuming that all oxygen exists in the form of UO_2.

¶Hydrogen "cleaned" for 18 hr at 800°C.

**Not determined.

determine the cause of the pre $\alpha \rightarrow \beta$ phenomenon observed in some earlier differential thermal analyses. These experiments, performed on specimens having various thermal histories, indicate that the small thermal effect just below the $\alpha \rightarrow \beta$ equilibrium transformation temperature is caused by the exothermic transformation of retained gamma phase to alpha phase, which ceases to occur above the reported temperature (105°C).

The effect of temperature, strain rate, and total strain on the deformation mode of high-purity cast alpha plutonium has been determined at Battelle–Northwest.[59] Deformation was predominantly by grain-boundary sliding at 110°C and at a strain rate of 10^{-4} min^{-1}, whereas slip was the major deformation mode at −10°C and 10^{-1} min^{-1}. Deformation at intermediate temperatures and strain rates was by a mixture of grain-boundary sliding and slip. Recrystallization occurred concurrently with deformation only after a critical strain was reached. The critical strain decreased with increasing temperature and was independent of strain rate in the range 10^{-1} to 10^{-4} min^{-1}. Strains of 14, 6, and 3% were required at 105, 110, and 120°C, respectively, before recrystallization started. Deformation by twinning was insignificant.

The effect of pressures up to 100 kbars on the electrical resistance of plutonium has been studied in England.[60] The difference between the resistivities of alpha and beta plutonium at the transition temperature decreases with increasing pressure, dropping from about 32 μohm-cm at 1 atm to an estimated 20 μohm-cm at 55 kbars. Figure I-5 shows the pressure dependence of the temperature of the onset of the $\alpha \rightarrow \beta$ transition on heating. There appears to be good agreement between this work and that of Stephens[61] who used a different technique. From these data the latent heat associated with the $\alpha \rightarrow \beta$ transition was derived as 967 cal/mole at atmospheric pressure.

The thermal conductivity of three stabilized delta-plutonium alloys is reported[62] in the temperature range 75 to 300°K. The data, shown in Fig. I-6, were obtained from plutonium specimens containing 3.35 and 7.0 at.% gallium and 10.0 at.% cerium. The conductivity of each alloy increases smoothly with temperature. Data for Pu–5.0 at.% Ga from an earlier experiment fall evenly between those for the two present gallium alloys.

A high-temperature X-ray diffraction study was performed by Dow Chemical researchers[63] to investigate the oxidation of plutonium metal between 350 and 420°C. Previous investigators had reported a rate minimum in the oxidation of plutonium metal at about 400°C, suggesting the formation of a protective oxide. This investigation showed that a change in oxide structure occurs in the temperature range where the rate anomaly has been reported. This change is the reaction of αPu_2O_3 with the substrate metal to form PuO, according to $\alpha Pu_2O_3 + Pu \rightarrow 3PuO$. In the region of 400°C, the temperature of the rate minimum, the rate of formation of PuO is sufficiently rapid that a protective film of PuO is always adjacent to the metal, slowing down the overall oxidation rate.

(D. F. Askey)

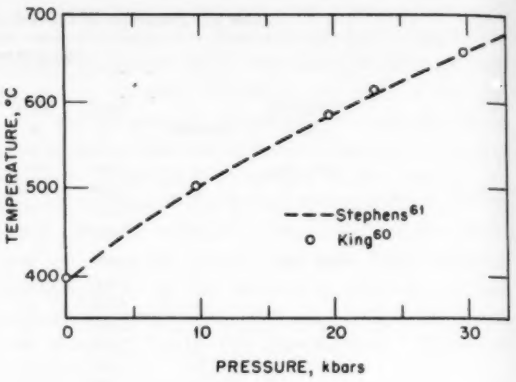

Fig. I-5 Effect of pressure on the $\alpha \rightarrow \beta$ transformation temperature in plutonium.[60]

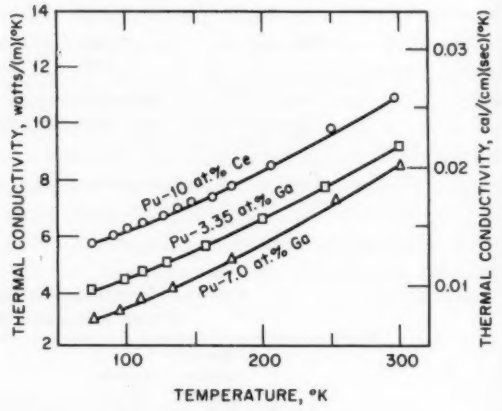

Fig. I-6 Thermal conductivity of three delta-plutonium alloys.[62]

Thorium Metal and Alloys

Information obtained at Los Alamos[64] shows the solubility of oxygen in solid thorium to be less than 0.3 at.%. As can be seen in Fig. I-7, the solid–solid transition of thorium saturated with ThO_2 occurs at 1370 ± 30°C. A Th–ThO_2 eutectic occurs at 1735 ± 20°C with the O/Th ratio of 0.016 ± 0.005. A monotectic occurs at 2740 ± 100°C with thorium-rich and oxygen-rich liquid O/Th ratios of 0.40 and 1.5 ± 0.2, respectively. The thorium-rich ThO_2 solidus has an O/Th ratio of 1.985 ± 0.01 at the eutectic, 1.87 ± 0.04 at the monotectic, and 1.997 ± 0.01 at the melting point (3390°C).

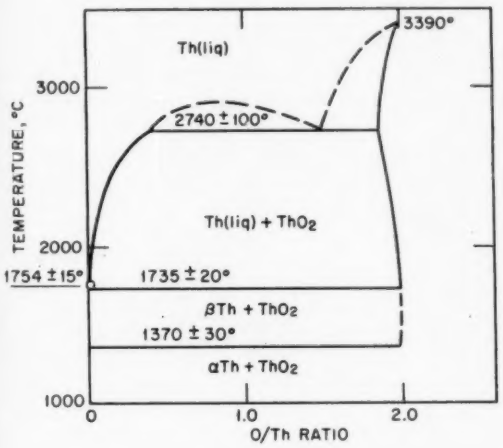

Fig. I-7 The Th–ThO_2 phase diagram.[64]

A comprehensive study of the Th–U–Pu system was carried out at Argonne.[65] Metallography, room- and high-temperature X-ray diffraction, dilatometry, electrical-resistance measurements, and differential-thermal-analysis techniques were employed.

The liquid miscibility gap is restricted to the Th–U side of the system. A eutectic trough connects the Th–U and Th–Pu sides of the diagram. The peritectic reaction $\alpha Th + L \rightarrow C$ ($C = Pu_2Th_{1-x}$) of the Th–Pu binary at 615°C joins the eutectic trough in a ternary peritectic reaction $\alpha Th + \epsilon Pu + L \rightarrow C$ at 630°C. In the solid state, three 4-phase reactions occur involving alphá thorium and the phases on the uranium side of the U–Pu system: a Class III reaction $\alpha Th + \beta U + \gamma U \rightarrow \eta$ at 714°C, a Class III reaction $\alpha Th + \beta U + \eta \rightarrow \zeta$ at 610°C, and a Class II reaction $\alpha Th + \beta U \rightarrow \alpha U + \zeta$ at 595°C. Over a wide range of compositions, the ternary alloys are in equilibrium with alpha thorium and the phases of the binary U–Pu system.

The addition of uranium to the Th–Pu solid solution greatly lowers the solid solubility of plutonium in thorium. Alloys of potential use as fast reactor fuels are restricted to a relatively small range of compositions with no more than 10 at.% plutonium and up to 25 at.% uranium. The Th–U–Pu ternary system resembles other U–Pu systems to which a third element such as molybdenum, titanium, or zirconium has been added. In such systems the zeta phase forms by a peritectoid Class III reaction, and the solubility of zeta for the third element is small. No such uniformity applies to the formation of the eta phase in these ternary systems. (R. L. Martin)

Uranium and Uranium Alloys

Unalloyed Uranium

Microscopic studies of irradiated uranium were utilized by the French[66] to study mechanisms of radiation damage in alpha uranium. Samples irradiated at several burnups were examined. A coherent model was proposed for the fission-particle effects. The number of point defects created by one initial fission is determined for pure and annealed metal. Estimated are (1) the importance of the self-anneal that occurs immediately in each displacement spike and (2) the influence of the anneal due to a new fission on the damage resulting from a previous fission. The focusing distance in the [100] direction is found to be about 1000 A, at 4°K.

Superconducting properties of uranium having alpha, beta, and gamma structures were investigated by Maksimov.[67] It was found that the high-temperature modifications of beta and gamma uranium could be stabilized down to very low temperatures by impurities. The critical temperature of beta uranium stabilized with a 2 wt.% addition of rhodium or platinum is 0.8°K. The critical temperature of gamma uranium stabilized with 15 wt.% addition of molybdenum is 2.1°K. The superconducting properties of these phases differ little from the properties of ordinary superconductors with an electron–phonon pairing mecha-

nism. At atmospheric pressure, uranium does not go over into the superconducting state down to 0.1°K. With increasing pressure to 11 kbars, its critical temperature increases to 2.2°K, and this is not accompanied by any changes in the lattice structure. The isotopic effect in this uranium differs radically from that predicted by the theory of electron–phonon interaction. According to the author, there is evidence of electron–electron interaction in the transition to the superconducting state, due to the existence of the unfilled *f*-shell in the uranium.

Alpha-Phase Uranium Alloys

Precipitate size and morphology effects in ternary and quaternary uranium alloys containing dilute additions of aluminum, iron, and silicon were reported by Czechoslovakian investigators.[68] It was concluded that some particles grow more rapidly on the grain and block boundaries, possibly in individual dislocations, in a U–0.2 Al–0.04 Fe alloy heated 750 hr at 600°C. The basis for this conclusion was the discrepancy between the observed precipitate-particle-size distribution curve and the theoretical curve based on a volume diffusion mechanism. Data were obtained from examination of electron-microscope replicas.

The Soviets studied the effect of small alloying additions to uranium on dimensional stability and surface roughness after thermal cycling.[69a] The additions used were Cr, Nb, Ti, Be, Ni, Zr, Al, Fe, Si, and Ce. Best results were obtained with 0.1 at.% chromium and 0.1 at.% cerium in the binary alloys studied. The best ternary alloys were U–0.1 at.% Si–0.1 at.% Cr, and U–0.1 at.% Nb–0.1 at.% Zr.

Gamma-Phase Uranium Alloys

A study was made[69b] of the tendency of forged alloy samples, gamma-quenched from 800°C and tempered for 20 hr at 500°C, to form bumpy surfaces when subjected to thermal cycling. Binary alloys of uranium containing 10 at.% molybdenum or 15 at.% niobium, were practically unaffected by cyclic heating at temperatures to 900°C.

Dilatometric and metallographic methods, X-ray analysis, and hardness measurements were used[69c] to study the kinetics of gamma-phase transformation in four binary and ternary alloys of uranium with zirconium and niobium. Isothermal transformation diagrams were plotted for three alloys. These studies showed that the mechanism of gamma-phase transformation is different at high and low temperatures. The above methods were found to be insufficiently sensitive to study the decomposition of the gamma phase in a binary alloy of uranium with zirconium.

The effect of composition and heat-treating on the corrosion resistance of alloys in the systems U–Zr–Nb, U–Mo–Zr, and U–Nb–Mo, containing 5 to 30 at.% of alloying elements, to water at 100 and 250°C, has been examined.[69d] Gamma-quenched alloys exhibit much better properties than alloys having a gamma-phase decay structure following tempering.

The Soviets made a study[69e] of the temperature dependence of tensile properties and plasticity in binary uranium alloys containing 20 at.% Zr, Nb, Mo, or Ti at temperatures up to 900°C. They also tested U–70 at.% Zr and several U–Zr–Nb ternaries.

Delta-Phase Uranium Alloys

A review of the literature on U_3Si and U_3Si_2 production and properties has been published[70] by the Australians. The effect of carbon content on the U_3Si peritectoid reaction temperature is shown in Fig. I-8. Other properties pertinent to the use of these compounds as fuels in heavy-water-moderated, water-cooled reactors are also given.

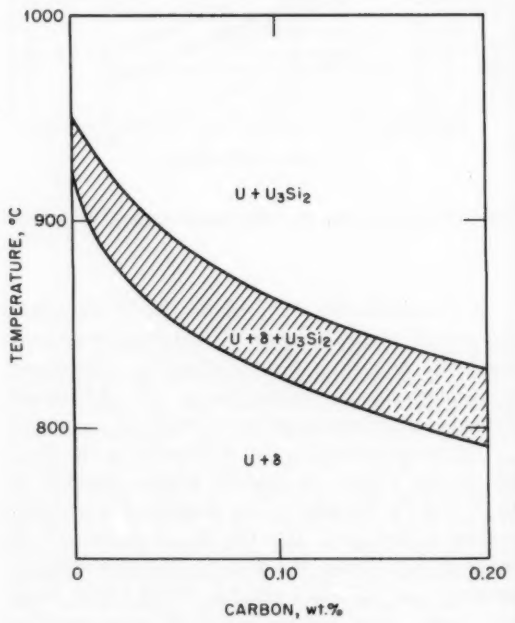

Fig. I-8 Effect of carbon on U_3Si peritectoid temperature[70] (silicon held constant at 20 at.%).

Chalk River Laboratories[71] studied the effect of the primary U_3Si_2 particle size on the transformation to U_3Si in as-cast U–Si alloys. The influence of the dispersion of fine U_3Si_2 particles in the eutectic matrix is also discussed. Samples of a U–4.0 Si alloy were fabricated with particle sizes varying from 8 to 900 μ. It was found that only the samples having primary U_3Si_2 particles smaller than 30 μ could be fully transformed when heat-treated at 800°C for 72 hr. The results suggest that U–Si rods should be cast with as small a U_3Si_2 particle size as possible. One method of minimizing the particle size is to cool the melt as quickly as possible during casting.

Chalk River has prepared for its contractors a set of specifications for uranium silicide fuel elements, covering chemical and isotopic composition, manufacturing and inspecting requirements, density, microstructure, and corrosion resistance. (J. M. Fackelmann)

References

1. G. P. Tiwari, Stability of the Gas Bubbles in Solids, *J. Nucl. Sci. Technol. (Tokyo)*, **5**(12): 648-649 (December 1968).
2. M. August, On the Theory of Swelling, USAEC Report ANL-Trans-736 [from *Kernenergie*, **11**: 186-190 (July 1968)].
3. E. M. Baroody, Calculations on the Collisional Coalescence of Gas Bubbles in Solids, *J. Appl. Phys.*, **38**(12): 4893-4903 (November 1967).
4. E. E. Gruber, Calculated Size Distributions for Gas Bubble Migration and Coalescence in Solids, *J. Appl. Phys.*, **38**(1): 243-250 (January 1967).
5. V. M. Agranovich, E. Y. Mikhlin, L. P. Semenov, V. Y. Pupko, Y. I. Likhachev, and V. P. Zvonarev, Theory of the Swelling of Fissionable Materials, in *Proceedings of the Third International Conference on the Peaceful Uses of Atomic Energy, Geneva, 1964*, Vol. 11, pp. 162-168, United Nations, New York, 1965.
6. T. M. Guseva, E. F. Davydov, V. N. Syuzev, and Yu. V. Chushkin, Possible Nature of Change in Volume of Fuel Compositions in Solid Swelling, *At. Energ. (USSR)*, **24**(5): 449-471 (May 1968).
7. S. T. Konobeevskii, B. M. Levitskii, and L. D. Panteleev, The Mechanism of the Radiation Growth of Uranium at Small Irradiation Doses, *At. Energ. (USSR)*, **24**(4): 312-316 (April 1968).
8. Yu. V. Chushkin, E. F. Davydov, V. N. Syuzev, and V. V. Kolesov, Radiation Resistance of Fuel Elements in the "Arbus" Reactor, *At. Energ. (USSR)*, **24**(4): 385-386 (April 1968).
9. G. L. Kulcinski, R. D. Leggett, C. R. Hann, and B. Mastel, Fission Gas Induced Swelling in Uranium at High Temperatures and Pressures, *J. Nucl. Mater.*, **30**(3): 303-313 (April 1969)
10. B. Bethune, Structural Transformations in U_3Si, *J. Nucl. Mater.*, **31**(2): 197-202 (June 1969).
11. No reference.
12. K. Taketani and M. Ichikawa, Void Migration in Sodium Chloride Crystal Under Temperature Gradient, *J. Nucl. Sci. Technol. (Tokyo)*, **6**(2): 55-62 (February 1969).
13. J. A. L. Robertson, R. E. Carter, K. W. Lay, and D. Lee, Fundamental Properties of Materials in Nuclear Fuel Assemblies, *J. Nucl. Mater.*, **30**(1 and 2): 1-178 (April 1969).
    a. R. E. Carter, J. S. Nadeau, and J. H. Rosolowski, Temperature Gradient Induced Migration of Helium Filled Pores in KCl, pp. 166-169.
    b. R. M. Cornell, M. V. Speight, and B. C. Masters, The Role of Bubbles in Fission Gas Release from Uranium Dioxide, pp. 170-178.
    c. J. Belle, Oxygen and Uranium Diffusion in Uranium Dioxide (A Review), pp. 3-15.
    d. J. F. Marin and P. Contamin, Uranium and Oxygen Self-Diffusion in UO_2, pp. 16-25.
    e. Hj. Matzke, On Uranium Self-Diffusion in UO_2 and UO_{2+x}, pp. 26-35.
14. W. A. Paulson and R. H. Springborn, Estimation of Fission-Product Gas Pressure in Uranium Dioxide Ceramic Fuel Elements, Report NASA-TN-D-4823, National Aeronautics and Space Administration, Lewis Research Center, November 1968.
15. J. W. Harrison, The Irradiation-Induced Swelling of Uranium Carbide, *J. Nucl. Mater.*, **30**(3): 319-323 (April 1969).
16. R. S. Nelson, The Stability of Gas Bubbles in an Irradiation Environment, *J. Nucl. Mater.*, **31**(2): 153-161 (June 1969).
17. J. W. Harrison, An Extrapolated Equation of State for Xenon for Use in Fuel Swelling Calculations, *J. Nucl. Mater.*, **31**(1): 99-106 (May 1969).
18. D. L. Keller and W. Chubb (Eds.), Progress on High-Temperature Fuels Technology During November 1968–January 1969, USAEC Report BMI-1859, pp. 24-29, Battelle–Columbus, February 1969.
19. P. Patriarca (Comp.) and D. J. Rucker (Ed.), Fuels and Materials Development Program, Quarterly Progress Report for Period Ending December 31, 1968, USAEC Report ORNL-4390, (*a*) pp. 58-64, (*b*) pp. 65-68, (*c*) pp. 5-9, (*d*) pp. 45-48, (*e*) pp. 246-258, Oak Ridge National Laboratory, May 1969.
20. Argonne National Laboratory, Reactor Development Program Progress Report, February 1969, USAEC Report ANL-7553, pp. 113-116, Mar. 25, 1969.
21. J. A. Porter and M. C. Thompson, Preparation of $^{238}Pu^{16}O_2$, USAEC Report DP-1153, Savannah River Laboratory, November 1968.
22. P. H. Bonnell, Fines Analysis of Plutonium Dioxide Microspheres After Impact, USAEC Report MLM-1626, Mound Laboratory, Apr. 18, 1969.
23. J. E. Selle, A Summary of the Phase Diagrams and Compatibility of PuO_2 with Various Materials, USAEC Report MLM-1589, Mound Laboratory, Apr. 21, 1969.
24. A. Lhost and H. Bairiot, Irradiation of Mixed UO_2–PuO_2 Fuels in the BR-3 PWR Reactor, Special Report No. 10, USAEC–Euratom Report 2072, June 1968.
25. Nuclear Materials and Equipment Corp., Irradiation Testing of PuO_2–UO_2 Fuels, 14th Quarterly Report, October–December 1967, USAEC Report NUMEC-3432-41, April 1968.

26. E. R. Astley, Fast Flux Test Facility, Periodic Technical Report, October 1968–February 1969, USAEC Report BNWL-941, pp. 5.37-5.48, Battelle–Northwest, May 1969.
27. M. R. Harvey, A. R. Teter, and R. L. Leggett, Fabrication of Oxide Nuclear Fuel Pellets, USAEC Report RFP-1255, Dow Chemical Co., Rocky Flats Division, Mar. 21, 1969.
28. T. Lauritzen, Compatibility of Urania–Plutonia Fuels with Stainless Steel and Sodium, USAEC Report GEAP-5633, General Electric Company, Advanced Products Operation, June 1968.
29. E. A. Aitken and S. W. Evans, A Thermodynamic Data Program Involving Plutonia and Urania at High Temperatures, Quarterly Report No. 4, USAEC Report GEAP-5672, General Electric Company, Vallecitos Nuclear Center, October 1968.
30. D. R. O'Boyle, F. L. Brown, and J. E. Sanecki, Solid Fission-Product Behavior in Uranium–Plutonium Oxide Fuel Irradiated in a Fast Neutron Flux, *J. Nucl. Mater.*, **29**(1): 27-42 (January 1969).
31. W. Batey, J. I. Bramman, H. W. Irons, and G. Yates, High-Temperature Reactions Between Tantalum and Oxides of Uranium and Plutonium, *J. Nucl. Mater.*, **29**(2): 229-234 (February 1969).
32. P. G. Mardon, D. J. Hodkin, and J. T. Dalton, Some Observations on the Pu–Zr–O System, *J. Nucl. Mater.*, 32(1): 126-134 (August 1969).
33. Los Alamos Scientific Laboratory, Advanced Plutonium Fuels Program, Quarterly Status Report, January 1 to March 31, 1969, USAEC Report LA-4193-MS, pp. 9 and 39, June 17, 1969.
34. Argonne National Laboratory, Reactor Development Program Progress Report, March 1969, USAEC Report ANL-7561, pp. 69-71, Apr. 22, 1969.
35. J. T. Dalton, E. A. Harper, H. J. Hedger, and R. W. Stannard, Phase Relationships in the Uranium–Plutonium Dicarbide System, British Report AERE-R-5948, February 1969.
36. C. A. Milet, Contribution to the Study of U–Ti and U–Pu–Ti Carbides, French Report CEA-R-3656, December 1968.
37. R. Lorenzelli, Contribution to the Study of the System (U,Pu)C,N, USAEC Report ORNL-tr-3019 (CEA-R-3536), May 1968.
38. D. L. Keller, Progress on Development of Materials and Technology for Advanced Reactors, January–March 1969, USAEC Report BMI-1862, pp. A1-A5, A9-A11, A42-A50, Battelle–Columbus, April 1969.
39. L. V. Shiryaeva and Yu. M. Tolmachev, Separation of Molybdenum-99 from Irradiated Samples of Uranium Oxides, *Radiokhimiya*, **10**(4): 439-445 (1968).
40. D. Kolar, B. Breic, B. Zatler, and V. Marinkovic, Influence of Atmosphere on the Sintering of High Surface Area Uranium Dioxide, *Sci. Ceram.*, **4**: 189-200 (1968).
41. C. A. Elyard and T. J. Potter, Sintered Uranium Dioxide, British Patent 1,137,551, Dec. 27, 1968.
42. T. J. Burke, Planetary Ball Milling as a Method of Comminuting Presintered Thoria–Urania Granules, USAEC Report WAPD-TM-789, Westinghouse Electric Corp., Bettis Atomic Power Laboratory, April 1969.
43. R. Benz, UO_2–UN_2–U Phase Equilibria, USAEC Report LA-DC-10417, Los Alamos Scientific Laboratory, Mar. 27, 1969.
44. S. Moench and N. Claussen, Properties of Mixtures of UN and UO_2, *Sci. Ceram.*, **4**:459-464 (1968).
45. H. Holleck, E. Smailos, and F. Thümmler, Solid Solutions of UN with the Nitrides of the Rare Earths: CeN and NdN, *J. Nucl. Mater.*, **28**: 105-109 (October 1968).
46. H. Nickel, O. Inanc, and K. Lucke, A Study of the System: U–Zr–C, *J. Nucl. Mater.*, **28**(1): 79-92 (October 1968).
47. H. Holleck, Ternary Carbides in the System U–M–C, *J. Nucl. Mater.*, **28**(3): 339-340 (December 1968).
48. J. L. Bates, Thermal Conductivity and Electrical Resistivity of Uranium Oxycarbide, USAEC Report BNWL-989, Battelle–Northwest, March 1969.
49. J. L. Bates, Thermal Conductivity of Uranium Oxycarbide, National Bureau of Standards Special Publication 302, Report CONF-671110, pp. 477-489, 1968.
50. J. A. Leary, R. L. Thomas, A. E. Ogard, and G. C. Wonn, Thermal Conductivity and Electrical Resistivity of UC, (U,Pu)C, and PuC, *Carbides in Nuclear Energy*, Vol. 1, pp. 365-372, Macmillan & Co., Ltd., London, 1964.
51. C. Affortit, The Specific Heats of UC, UO_{2+x}, and UN, French Report CEA-CONF-1140, November 1968.
52. A. C. Macleod, High-Temperature Thermodynamic Properties of Uranium Dicarbide, *J. Inorg. Nucl. Chem.*, **31**: 715-725 (March 1969).
53. P. Patriarca and W. O. Harms (Comps.), Fuels and Materials Development Program, Quarterly Progress Report for Period Ending September 30, 1968, USAEC Report ORNL-4350, pp. 33-47, Oak Ridge National Laboratory, February 1969.
54. F. Thuemler, G. Ondracek, and K. Dalal, Preparation and Hot-Pressing Behavior of Uranium Mononitride, USAEC Report ORNL-tr-2098 [from *Z. Metallk.*, **56**: 535-542 (1965)].
55. R. F. Redmond, Progress Letter on Development of a Fuel System for a Fast-Flux Pulse Reactor, January Through March 1969, USAEC Report BMI-X-10255, pp. 6-7, Battelle–Columbus, Apr. 23, 1969.
56. P. D. Takkunen, Fabrication of Cermets of Uranium Nitride and Tungsten or Molybdenum from Mixed Powders and from Vapor Coated Particles, Report NASA-TN-D-5136 (N-69-21404), National Aeronautics and Space Administration, Lewis Research Center, April 1969.
57. R. D. Nelson and F. E. Bowman, The Crystallography of the Alpha to Beta Transformation in Plutonium, *Trans. Met. Soc. AIME*, **245**(4): 967-970 (May 1969).
58. D. R. Harbur, W. J. Anderson, and W. J. Maraman, The Pre $\alpha \rightarrow \beta$ Transformation in High-Purity Plutonium, *J. Nucl. Mater.*, **30**(3): 289-296 (April 1969).
59. R. D. Nelson and S. D. Dahlgren, Microstructures of Deformed Alpha Plutonium, USAEC Report BNWL-981, Battelle–Northwest, April 1969.
60. E. King, The Effect of Very High Pressures on the Electrical Resistance of the Actinide Elements from Thorium to Plutonium, British Report AERE-R-5913, November 1968.
61. D. R. Stephens, The Phase Diagram of Plutonium, *J. Phys. Chem. Solids*, **24**: 1197-1202 (1963).
62. J. F. Andrew, Thermal Conductivity of Some Delta-Plutonium Alloys, *J. Nucl. Mater.*, **30**(3): 343-345 (April 1969).
63. K. Terada, R. L. Meisel, and M. R. Dringman, High-

Temperature X-Ray Investigation of Plutonium Oxidation, *J. Nucl. Mater.*, **30**(3): 340-342 (April 1969).

64. R. Benz, Thorium–Thorium Dioxide Phase Equilibrium, *J. Nucl. Mater.*, **29**(1): 43-49 (January 1969).
65. B. Blumenthal, J. E. Sanecki, and D. E. Busch, Thorium–Uranium–Plutonium Alloys as Potential Fast Power-Reactor Fuels. Part I. Thorium–Uranium–Plutonium Phase Diagram, USAEC Report ANL-7258, Argonne National Laboratory, September 1968.
66. J. Leteurtre, Fission Damage in α-Uranium at 4°K, French Report CEA-CONF-1108, 1968.
67. Y. G. Maksimov, New Data on the Superconducting Properties of Metallic Uranium, *Usp. Fiz. Nauk*, **96**(1): 177-179 (1968).
68. J. Truchly and J. Novak, Dispersion of Precipitates in Low Alloy U–Al–Fe and U–Al–Fe–Si Systems, *Kovove Mater.*, **3**: 290-292 (1968).
69. *Physical Chemistry of Alloys and Refractory Compounds of Thorium and Uranium*, Bykov Metallurgical Institute, USSR Academy of Sciences, Nauka, Moscow, 1968.
    a. N. Golovkina and V. Grigorovich, Behavior of Modified Uranium in the Rolled and Normalized State When Subjected to Cyclic Heating in the Alpha Region, pp. 24-28.
    b. V. Grigorovich and N. Golovkina, Deformation of Binary Alloys of Uranium Containing 0–20 at.% Molybdenum, 0–30 at.% Niobium, 0–100 at.% Zirconium When Subjected to Cyclic Heating Up to 600–900°C, pp. 28-37.
    c. V. Kishinevskiy, A. Tret'yakolv, L. Gomozov, and O. Ivanov, Kinetics of Isothermal Transformation of Gamma Solid Solutions of Some Uranium Alloys, pp. 42-52.
    d. V. Kishinevskiy, L. Gomozov, and O. Ivanov, Corrosion Resistance in Water of Some Alloys of Uranium with Zirconium, Niobium, and Molybdenum, pp. 81-86.
    e. V. Bugrov, V. Grigorovich, and O. Ivanov, Temperature Dependence of Strength, Plasticity, and Elastic Properties of Alloys of Uranium with Zirconium, Niobium, and Molybdenum, pp. 62-69.
70. J. Bardsley, A Review of the Physical, Mechanical, and Irradiation Properties of U_3Si and U_3Si_2, Australian Report AAEC/TM-487, December 1968.
71. L. C. Berthiaume and B. S. Wyatt, Effect of Primary U_3Si_2 Particle Size and Distribution on the Peritectoid Reactions in Uranium–Silicon Alloys, Canadian Report AECL-3222, December 1968.

Section II

Reactor Materials

Moderator and Control Materials

Graphite

The vaporization characteristics of graphite in the 2500 to 3500°K temperature range are discussed in Brookhaven Laboratory's annual report.[1a] The major findings were that: (1) C_2 is probably the most prevalent species in "free" evaporation from graphite, (2) disappearing-filament and photoelectric-pyrometer temperature readings on graphite above 3000°K in the presence of inert gases are in error owing to soot formation, and (3) active species can be stabilized by condensing vaporized graphite at liquid-nitrogen temperatures.

The rates of vaporization of graphite in vacuum at 2400 to 3400°K are shown in Fig. II-1. The heat of vaporization calculated from these data is 210 ± 10 kcal/mole on the basis of the second law of thermodynamics, or 202 ± 2 kcal/mole on the basis of the third law of thermodynamics and the assumption that the vapor species is C_2.

It was found that when the Pyrex vessel surrounding a graphite filament heated at any temperature in the range 3000 to 3300°K was immersed in liquid nitrogen, active species were trapped on the condensing surface, which emitted light flashes when the liquid nitrogen was removed. It was impossible to measure the emission spectrum. To explain the flashes, the investigators hypothesized that, upon warming to room temperature, the absorbed and stabilized C_2 would react with small carbon aggregates on the surface and release sufficient energy to heat the carbon locally to a high temperature, which would then initiate exothermic recombination of adjacent C_2 molecules in a thermal chain reaction.

Both absorption and emission spectroscopy on the vapor above graphite inside thin-walled resistively heated graphite tubes in both helium and hydrogen atmospheres revealed the C_2 spectrum. In addition, the CH spectrum was observed faintly in runs in hydrogen, but no other C_xH species or C_3 could be detected.

Comprehensive coverage of carbon–graphite technology was presented in the many technical papers of the Ninth Biennial Carbon Conference. Complete preprints of this conference were not available, but a summary of extended abstracts[2] was printed. Because of the large number of papers presented, no attempt is made here to review individual papers. The following subject areas were covered: (1) carbon-product applications, (2) carbon-product preparation, (3) electronic properties, (4) mechanical properties, (5) radiation damage, (6) reactivity studies, (7) surface phenomena, (8) structural studies, (9) thermal properties, and (10) miscellaneous subjects.

Charles L. Mantell's *Carbon and Graphite Handbook*[3] is a valuable contribution to the carbon literature in providing broad subject coverage. It includes a general discussion of the many forms of carbon that are of industrial importance. It covers the manufac-

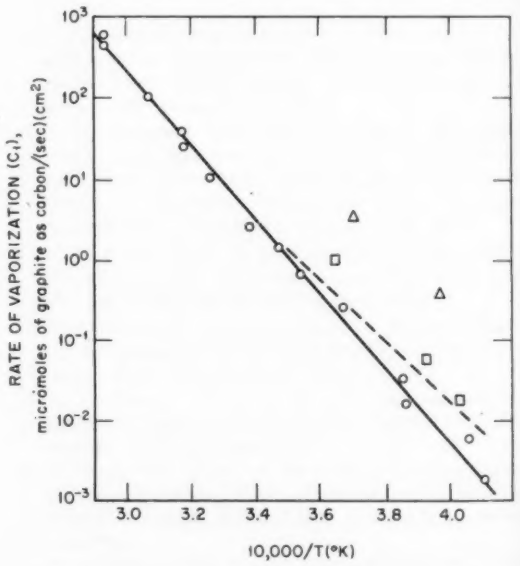

Fig. II-1 Temperature dependence of the rate of vaporization of graphite.[1a] ○, Clarke and Fox; - - -, Marshall and Norton; □, Hoch, Blackburn, Dingledy, and Johnston; △, Honig (Dushman).

turing processes, manufactured forms and types of products, and manufacturing control procedures.

(M. C. Brockway)

Beryllium Metal and Alloys

Mechanical Metallurgy

Mechanical Properties

Table II-1 shows the elastic properties of several commercial beryllium-bearing materials as measured by Lockheed workers.[4] For these materials, Poisson's ratio did not vary much with temperature over the range −320 to 800°F (−200 to 427°C), and elastic stiffness decreased slightly. On the basis of biaxial stressing by both three-point and four-point bending at 75°F (24°C), the materials showed the following ranking:

	Minimum bend radius, in.	Maximum fiber strain, %
Be–Al alloy sheet	<2*	>2.7*
Hot-pressed block	3	1.4
High-strength sheet	7	0.7
PR-20 sheet	6	0.6
S-200 sheet	7	0.5
Ingot beryllium sheet	16	0.3

*No failure or cracks obtained.

Workers at Langley Research Center[5] concluded that Be–38 Al (Lockalloy) tubing can be extruded commercially to dimensional tolerances comparable to those of aluminum tubing. Mechanical properties of the tubing, presented in Table II-2, are comparable to those of other forms of the Be–38 Al alloy. Comparisons of column mass-strength relations of Lockalloy with beryllium and with an aluminum alloy (7075-T6) show beryllium to be most efficient in the elastic range, whereas the Be–38 Al alloy is most efficient at higher stress levels.

Microplastic Behavior

The microplastic characteristics of hot isostatically pressed and isoforged beryllium were studied by Shemenski and Maringer.[6] Typical hot-isostatic-pressing parameters are 1675°F (915°C) and 10 ksi for 2 hr. In comparison, isoforging employs a solid pressure-transmitting medium, such as steel, or alumina, enclosed in a cavity and acted on by the ram of a forging press. The two techniques differed in that isoforging employed greater pressures of 30 to 145 ksi and shorter times of 12 to 120 sec. Both processes employ significantly higher pressures and lower temperatures than are normally used to compact beryllium.

The flow stress of isostatically pressed beryllium was found to be a parabolic function of microstrain. The flow curves were characterized by the following three distinct ranges of microstrain: (1) heterogeneous basal glide at low microstrain, (2) dispersion hardening, most probably by a dislocation pileup mechanism at intermediate levels of microstrain, and (3) prismatic glide and cross slip at microstrains greater than 50×10^{-6}. Microflow behavior was found to be a sensitive function of fabrication history. The microyield strength was observed to increase with decreasing processing temperature, increased beryllium oxide content, and small alloying additions of chromium or silver. The highest microyield strength observed was 103.5 ksi for an alloy containing 0.27 wt.% chromium.

Grain-Size Effects

The hardness dependence on grain size of high-purity polycrystalline beryllium produced from SR-grade electrolytic flake melted in high vacuum in an electron-beam furnace has been determined by Bunshah and Armstrong.[7] The principal impurities in the metal (in at. ppm) were as follows: 30 O, 10 C, 5 Al, 4 Cl, 7 Fe, and 2 Ni. All other impurities were 1 ppm or less.

The hardness was found to follow the relation:

$$H = H_0 + K_h d^{-1/2}$$

where d is the grain diameter and H_0 and K_h are constants. This relation is similar to the one for yield strength vs. grain size:

$$\sigma_y = \sigma_{0y} + K_y d^{-1/2}$$

The hardness and yield-strength values for the higher purity materials were significantly lower than those determined by Macres on relatively impure extruded beryllium rod. Armstrong and Bunshah used Macres' data to compute the constants shown in Table II-3.

Table II-1 Elastic Properties of Various Beryllium-Bearing Materials[4]

Property*	Direction†	PR-20 sheet	Ingot sheet	Be–Al alloy sheet	High-strength sheet	Hot-pressed block	S-200‡ sheet
			Test Temperature, 75°F (24°C)				
E	L	41.7	40.1	28.6	42.4		43.3
E	T	42.7	42.7	30.1		42.6‡	42.6
E	ST	51.4	48.9	33.2	50.2		51.5
G	L,T		19.6	12.3			19.9
G	L,ST		22.8	12.3		20.1‡	21.3
TS	L	70	47	57	88	47§	78
TYS	L	50	39	40	75	36§	54
CYS	L	54	39	37	75		
Elong.	L	7	2	11	3	Nil§	16
TS	T	78	53	49	99	56‡	80
TYS	T	53	41	37	84	36‡	56
CYS	T	53	40	35	82		
Elong.	T	11	3	6	4	Nil	16
			Test Temperature, 400°F (204°C)				
TS	L	53	39	39	76	45§	
TYS	L	44	34	33	67	32§	
Elong.	L	45	12	14	22	2.3§	
TS	T	57	45	34	91	48‡	
TYS	T	46	36	30	76	34‡	
Elong.	T	58	33	8	37	14‡	
			Test Temperature, 800°F (427°C)				
TS	L	31	26.3	20.3	55	39§	
TYS	L	30	26.0	17.5	47.6	27§	
Elong.	L	43	27.7	4.7	44.8	8§	
TS	T	32	26.8	18.6	53.4	31‡	
TYS	T	31	26.2	16.3	48.6	24‡	
Elong.	T	54	40.4	2.8	25.0	36‡	

* E = modulus of elasticity, 10^6 psi
G = modulus of rigidity, 10^6 psi
TS = ultimate tensile strength, ksi
TYS = tensile yield strength, ksi
CYS = compressive yield strength, ksi
Elong. = elongation, %

† L = longitudinal
T = transverse
ST = short transverse
‡Perpendicular to axis of pressing.
§ Parallel to axis of pressing.

Table II-2 Room-Temperature Mechanical Properties of Extruded Be–38 Al Alloy Tubing[5]

Outside diameter, in.	Tensile yield strength (0.2% offset), ksi	Ultimate tensile strength, ksi	Compressive yield strength (0.2% offset), ksi	Young's modulus of elasticity, 10^6 psi	Elongation in 2 in., %
		As extruded			
0.2500		66.2	71.2	28.9	<1
0.4375		65.0	74.7	28.7	<1
0.5625	78.8	81.3	76.9	28.6	<1
0.6875	81.3	85.6	78.0	29.0	<1
		Annealed			
0.2500	50.1	56.8	55.7	28.7	2
0.4375	50.3	53.4	48.6	29.1	2
0.5625	48.8	60.3	43.8	30.4	5
0.6875	48.6	54.5	48.8	29.3	3

Table II-3 Hardness and Yield-Strength Grain-Size Constants[7] for Polycrystalline Beryllium

H_0, kg/mm^2	K_h, kg/mm$^{3/2}$	σ_{0y}, kg/mm^2	K_y, kg/mm$^{3/2}$
150	2.7	17.5	0.5

Physical Metallurgy

A novel technique for identifying anisotropic effects and inhomogeneities of defect structures has been presented by Glass and Weissmann.[8] The technique involves the combined analysis of deficiency conics produced by divergent X-ray techniques and X-ray topographs. The method has been applied to the room-temperature deformation of beryllium.

Annealed single crystals of beryllium were found to contain subgrains, columnar in shape, having dimensions of the order of 1 mm along the *c*-axis and about 50 μ in diameter. The misorientation between neighboring subgrains was of the order of 1 or 2 min of arc. Also, the topographs revealed the existence of a finer substructure leading to an additional orientation spread of 1 min of arc. Basal and prismatic changes in response to compressive deformation were found to be inhomogeneous because of variations in the defect structure initially present.

Powder Metallurgy

Hot Isostatic Pressing

A study was conducted at Battelle–Columbus[9] to develop the hot-isostatic-pressing process for the production of powder-metallurgy beryllium equivalent or superior to S-200-type vacuum-hot-pressed block. A nominal 1 wt.% oxide, −200-mesh powder of commercial purity was employed in the program. To produce hot isostatically pressed specimens, workers loaded beryllium powder into a shaped latex bag, which is then evacuated and sealed. Next the powder is cold hydrostatically pressed to pressures of 30 to 100 ksi; this step produces a green pressing that is then sealed into a steel pressing container fitted with an outgassing stem. Typical outgassing conditions are 1200°F (650°C) for 20 to 24 hr. The outgassed assembly is densified by hot isostatic pressing in a hot-gas autoclave [typically at 1675°F (915°C) and 10 ksi for 2 hr]. Finally the pressing container is removed, and the beryllium piece is finish machined.

The variable parameters of outgassing treatment, pressing temperature, annealing temperature, powder-size fraction, and powder grade were studied in terms of the resulting microstructure, density, and room-temperature tensile properties of hot isostatically pressed beryllium. Some of the more significant observations are:

1. Fully densified beryllium that had been insufficiently outgassed has little ductility and swells during annealing.

2. Optimum tensile properties, as controlled by the outgassing procedure, can probably be obtained by imparting a controlled amount of contamination to the powder for strengthening while the volatile constituents (H_2O, CO_2, and CO) are being removed.

3. Powder-size variations do not affect swelling during postpressing annealing.

4. The minimum pressing conditions to achieve full densification were found to be 1300°F (705°C) at 10 ksi for 2 to 3 hr.

5. The microstructure of beryllium densified at 1400°F (760°C) contains a network, unresolved by optical microscopy, with fine-grained areas along it that decrease in extent with increasing pressing or annealing temperature.

6. As the pressing or annealing temperature is increased or as the powder particle size is increased, the room-temperature elongation increases, whereas the ultimate and yield strengths decrease (Fig. II-2).

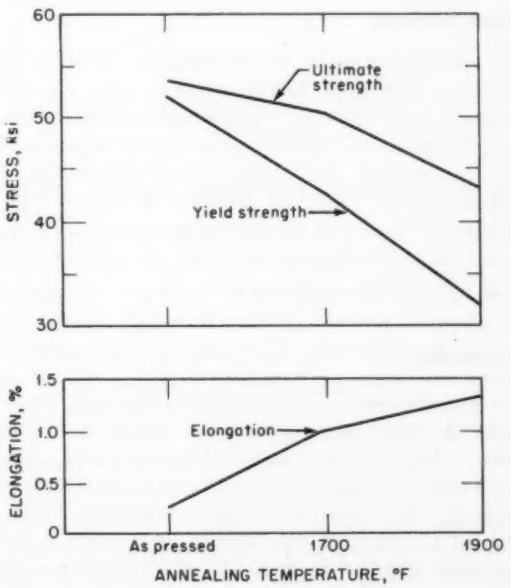

Fig. II-2 Effect of annealing temperature on the tensile properties of isostatically hot-pressed beryllium.[9]

Submicron Powder

National Research Corp.[10] produced submicron beryllium powder by evaporating beryllium metal in an argon atmosphere ranging from about 5 to 300 μ and collecting the vapor on a water-cooled, rotating stainless-steel drum that had been given an adherent beryllium coating to reduce contamination. The oxide content of the resulting powder was found to be dependent on the argon pressure. The beryllium powder produced by this method consisted of black spherical agglomerates with an individual particle size of less than 0.1 μ. This powder was free flowing and pyrophoric.

Two techniques were employed to consolidate the powder. The first was to cold press and then sinter; the second was to cold press and then hot isostatically press. A maximum sintering temperature of 1550°F (845°C) was found to produce fine-grained material, but its density was only about 70% of theoretical. Hot-isostatic-pressing the powder at 1400°F (760°C) and 10 ksi for 2 hr resulted in a density of about 99% of theoretical and a grain size of the order of 1 μ. Failure to produce suitable material for evaluating mechanical properties was due largely to unidentified powder contamination during processing and to non-optimum processing employed in the hot isostatic pressing.

Spark Sintering

Spark sintering is accomplished by an electrical discharge through the beryllium powder while it is held under pressure in a die.[11] Billets with densities as low as 65% and up to 100% of theoretical can be produced by this metho The largest billets presently being fabricated are 7½ in. in diameter by 10 in. high. Transverse tensile and elevated-temperature creep properties of spark-sintered beryllium are presented in Figs. II-3 and II-4, respectively.

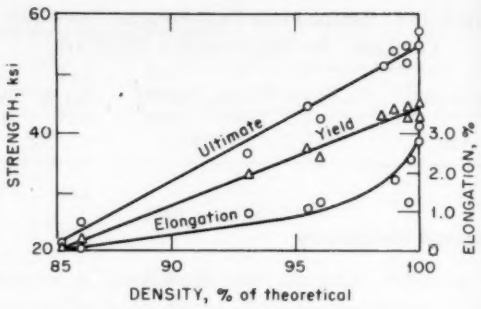

Fig. II-3 Effect of density on room-temperature tensile properties of spark-sintered beryllium (transverse direction).[11]

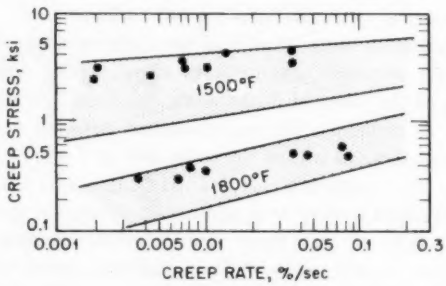

Fig. II-4 Compression-creep properties of spark-sintered beryllium.[11]

Corrosion

The Russians[12,13] have studied the oxidation of sintered beryllium materials with various oxide contents, a Be–5 Ca alloy, and the beryllide $CaBe_{13}$. The corrosion environment employed was a free stream of CO_2 at 700°C with water-vapor contents of 0.0005, 0.2, or .12 vol.% for exposures of up to 1000 hr. All materials tested in the dried CO_2 (0.0005 vol.% water vapor) proved to be corrosion resistant. Raising the moisture content increased the oxidation rate considerably. The best corrosion resistance was exhibited by the beryllide, the Be–Ca alloy, and the higher oxide (10 to 12 wt.% BeO) sintered beryllium. It was found that the more uniform the distribution of beryllium oxide particles in the compacted beryllium, the better was its corrosion resistance. Corrosion resistance was also dependent on the prior treatment of the specimens. For example, preoxidation in dry carbon dioxide increased the corrosion resistance in humid carbon dioxide. Annealing in a humid environment decreased the corrosion resistance. This was attributed to hydrogen pickup, and the original corrosion resistance could be restored by vacuum annealing. Analysis of specimens corrosion tested at 700°C in CO_2 with 0.2 vol.% water vapor showed that the more corrosion-resistant material had a lower hydrogen content. Therefore it was concluded that the low corrosion resistance of beryllium in humid atmospheres is due mainly to hydrogen adsorption.

The Japanese[14] exposed pure beryllium to flowing CO_2 at temperatures of 550 to 700°C and explained the observed reaction rates in terms of oxide morphology. An initial cubic rate stemmed from the formation

of a thin BeO film and the subsequent growth of the oxide which was coherent with the beryllium surface. The second stage was parabolic. This rate change was explained by loss of crystallographic coherency and the growth of coarse crystals in the [10$\bar{1}$0] direction with their (0001) plane parallel to the reacting surface.

Chemical-conversion coatings on beryllium for corrosion protection were studied by Booker and Stonehouse.[15] Coatings of chromate, phosphate–chromate, oxalate, and phosphate were applied by dipping specimens in commercial solutions. Corrosion conditions tested were high-humidity air at 170°F (77°C), salt spray, and high-temperature oxygen at 1290 to 1700°F (700 to 930°C). The chromate coatings were found to provide the greatest protection. The phosphate and oxalate coatings did not impart suitable corrosion resistance to the beryllium.

Physical Properties

Tye and Quinn[16] measured the thermal conductivity and electrical resistivity of S-200 vacuum-hot-pressed beryllium samples taken in the pressing direction and perpendicular to that direction. The results (Figs. II-5 and II-6) showed no appreciable directionality in these properties.

Radiation Effects

NASA–Lewis has reported experiences with beryllium swelling and replacement in the 60-Mw Plum Brook Reactor.[17] Problems were encountered from distortion and failure of major reactor-core components in the high-neutron-fluence regions of the reactor. The beryllium-reflector control rods and core box plates (neutron reflectors) were found to bow toward the fuel elements because of internal helium-gas formation from the fast-neutron ($E > 0.1$ Mev) reaction with beryllium. To prevent a recurrence of this problem, NASA–Lewis changed the design of the core box plates to allow rotation for bowing the plates in both directions and to allow for increases in width, length, and thickness.

To study the behavior of beryllium in the test-reactor environment, Idaho Nuclear[18] photographed the beryllium-reflector face of the Materials Testing Reactor (MTR) and exposed encapsulated beryllium samples to fluences ranging from 2 to 7×10^{21} neutrons/cm^2 ($E > 1$ Mev). The photographs of the reflector revealed a general deterioration, primarily in the form of bowing, spalling, and cracking. Several of the possible mechanisms for this deterioration were

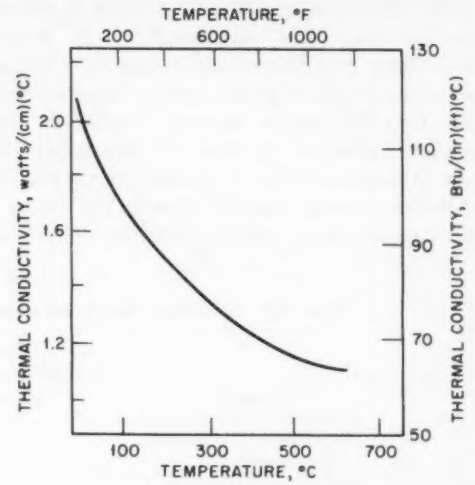

Fig. II-5 Thermal conductivity of S-200 vacuum-hot-pressed beryllium.[16]

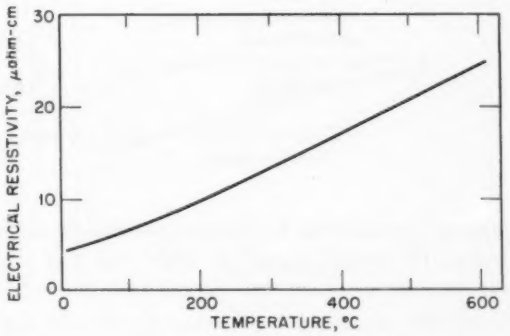

Fig. II-6 Electrical resistivity of S-200 vacuum-hot-pressed beryllium.[16]

evaluated.[19] As a part of this effort, information was assembled on the mechanical and thermal properties of beryllium, gamma heating and neutron-flux intensities across the reflector, coolant flow rates, maximum temperature differences, and stress levels through the beryllium pieces. It was concluded that the most probable cause of the damage is excessive stresses resulting from combined internal and mechanical restraint of both thermal expansion and radiation-induced swelling, coupled with a loss of strength and ductility resulting from extreme radiation damage. Several design changes were recommended which would minimize the stress level in the beryllium-reflector pieces.

The swelling or growth of beryllium at temperatures less than 150°C was found[18] to be approximately linear with fluence and is apparently independent of the beryllium grade or strength, as indicated in Table II-4. The longest exposure, 1.45×10^{22} neutrons/cm^2, produces 7 atoms of helium per 1000 atoms of beryllium. After the irradiations the helium is distributed in small trapping centers. The nature of these trapping centers has not been fully defined, and they are not resolved in electron-transmission micrographs. In samples heated at 600°C for 1 hr after exposure, bubbles were resolved with a size range of 25 to 130 A.

The behavior of beryllium after irradiation in the SM-2 reactor has been studied by the Russians.[20] Corrosion resistance, mechanical properties, dimensional stability, and structural changes were measured as a function of the irradiation dose and fission-gas (helium and tritium) buildup. The effects of various factors on radiation stability were also presented, along with recommendations on beryllium use for conditions analogous to those in the SM-2 reactor.

(F. T. Zurey)

Table II-4 Growth of Beryllium Irradiated at Temperatures Less Than 150°C (Ref. 18)

Material	Fluence, 10^{21} neutrons/cm^2 ($E > 1$ Mev)	$\Delta L/L$, %	$\%/(10^{21}$ neutrons/cm$^2)$ $\Delta L/L$,
Hot-pressed 1.2 wt.% BeO (four samples)	1.5	0.056 ± 0.012	0.038
Hot-pressed 2.0 wt.% BeO (four samples)	2.3	0.068 ± 0.015	0.029
Extruded 1.2 wt.% BeO (five samples)	2.1	0.036 ± 0.007	0.017
Hot-pressed 2.0 wt.% BeO (five samples)	4.4	0.089 ± 0.011	0.024
Extruded 1.2 wt.% BeO (four samples)	4.9	0.118 ± 0.016	0.020
Hot-pressed 1.2 wt.% BeO* (eight pieces)	14.5†		0.020

*MTR lattice pieces on which the bowing strain was computed as percent change in length.
†Maximum value.

Solid Hydrides

Zirconium Hydride

It has been a well-established fact that the primary habit plane for hydride precipitation in zirconium is the $\{10\bar{1}0\}$ plane. However, there has been some uncertainty about the identification of the secondary habit planes of the hydride. Roy and Jacques of the University of Western Ontario, Canada,[21] employed single-crystal zirconium containing 150 ppm by weight hydrogen in their crystallographic studies to identify that the $\{10\bar{1}7\}$ plane is the secondary habit plane of zirconium hydride in zirconium. This plane corresponds with the primary hydride habit planes in Zircaloy-2 and -4.

Hydrided Zirconium–Uranium Alloys

Research on the thermophysical properties of hydrided Zr–U alloys has been conducted for several years at Atomics International to obtain data needed for Systems for Nuclear Auxiliary Power (SNAP) reactors. The results of the work on Zr–10 U hydrided to H/Zr atom ratios of 1.58, 1.65, 1.70, and 1.81 have been summarized in recent publications.[22,23] The first three compositions were studied over the temperature range 0 to 900°C, and the fourth was studied only to 760°C because of its high dissociation pressure. Specific heats were determined from enthalpy measurements, which were obtained using a unique drop calorimeter designed for use with materials in which high-temperature phase transitions or high dissociation pressures occur. This instrument is capable of operating at sample temperatures as high as 1650°C and pressures ranging from 10^{-8} to 10 atm. The values obtained for the specific heats of the four hydrided alloys are shown in Fig. II-7. The specific heats agree, within 10%, with values derived using a theoretical model in which the hydrogen and zirconium atoms are treated as Einstein

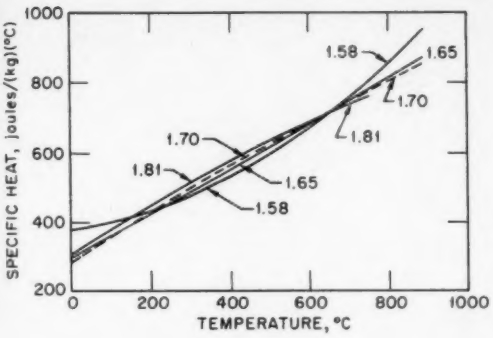

Fig. II-7 Specific heat of hydrided Zr–10 U alloys.[22] Numbers are H/Zr ratios.

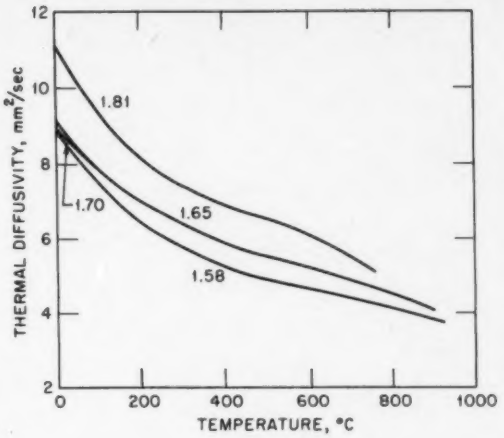

Fig. II-8 Thermal diffusivity of hydrided Zr–10 U alloys.[22] Numbers are H/Zr ratios.

and Debye oscillators, respectively. Thermal diffusivities for the four compositions, obtained by the flash method using a pulsed laser, are shown in Fig. II-8. The thermal conductivities were calculated as the product of specific heat, thermal diffusivity, and density. The results are plotted in Fig. II-9. Polynomial functions of temperature for the thermophysical properties also were calculated with the aid of a computer.

Group V-b Hydrides

The transition metals that constitute Group V-b of the periodic table, vanadium, niobium, and tantalum, form a wide range of solid solutions with hydrogen at elevated temperatures. However, miscibility gaps exist in these systems at lower temperatures. Veleckis and Edwards of the Illinois Institute of Technology[24] have determined thermodynamic properties for the systems V–H (246 to 554°C), Nb–H (352 to 671°C), and Ta–H (350 to 631°C) in the pressure range 1 to 800 torrs by measuring the equilibrium hydrogen pressures as a function of composition. Each of these systems is comprised of a single solid phase in the temperature and pressure range studied. For each system a semi-empirical equation was developed which not only was applicable to the temperature range studied but was also reliable to much lower temperatures. These equations were used to predict the boundaries of the immiscibility regions. Agreement was very good in the case of the one system for which experimental data were available for comparison, namely, the Nb–H system.

The phase diagrams derived for the three systems are shown in Fig. II-10. In the Nb–H diagram, the results of Walter and Chandler, obtained by hot-stage X-ray diffraction and differential thermal analysis, are

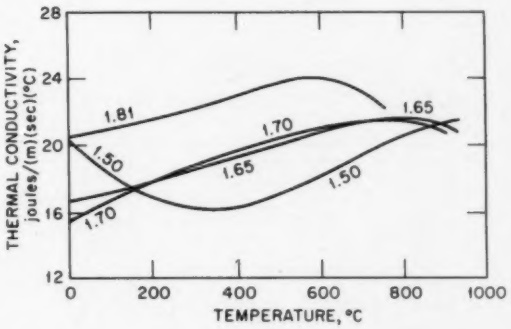

Fig. II-9 Thermal conductivity of hydrided Zr–10 U alloys.[22] Numbers are H/Zr ratios.

shown as dashed lines. The miscibility boundary for the V–H system is compared with that suggested by Maeland from X-ray diffraction studies, and the agreement is poor. For the Ta–H system, the prediction of the two-phase field is confirmed, but the boundary compositions do not agree with those proposed by Waite et al., shown as dashed lines in the figure. However, the values of the partial molal enthalpies, entropies, and free energies obtained from this study are in reasonably good agreement with those of other investigators, where comparable data exist.

Data on V–H compositions up to $VH_{2.0}$ have been reported by Brookhaven.[1b] Vanadium hydride of this composition was prepared by reacting vanadium and hydrogen at 25°C and 950 psia until a composition greater than $VH_{0.9}$ was reached, and then the system

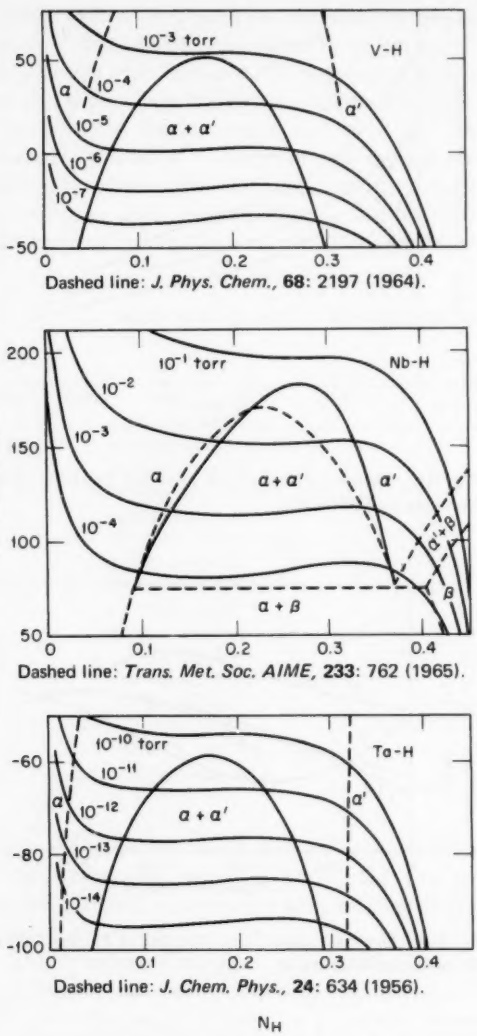

Fig. II-10 Proposed phase diagrams for the systems V–H, Nb–H, and Ta–H.[24]

was cooled to −75°C while the hydrogen pressure was maintained at 950 psia. Several cycles of hydriding and dehydriding were required in order to reach the maximum hydrogen content. The dissociation pressures found for the vanadium hydrides in the composition range VH to VH_2 are shown in Fig. II-11.

Ternary Hydrides

The reactions of hydrogen with a large number of binary alloys have been investigated at Brookhaven.[1b]

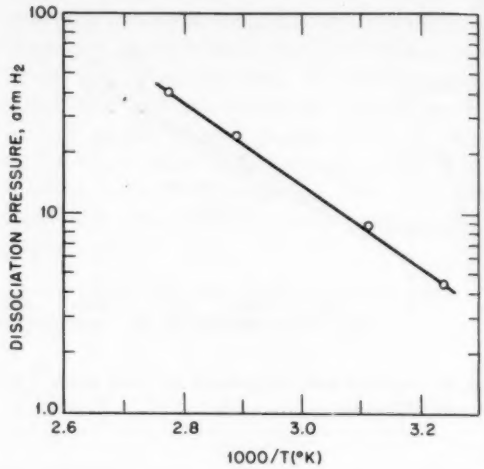

Fig. II-11 Dissociation pressures of vanadium hydrides[1b] in the range VH–VH_2.

The absorption of hydrogen by FeTi was studied up to the composition $FeTiH_{1.7}$ by reaction with hydrogen at room temperature and 950 psia. The dissociation pressures of these hydrides were found to increase rapidly with temperature, as shown in Fig. II-12.

Of the many alloy compositions whose hydrogen uptake was examined, eight absorbed at least 3 wt.% hydrogen:

Alloy composition, wt.%	Phases	Hydrogen absorbed, wt.%
47 Mg–53 Zn	Mg_7Zn_3	3.00
72 Ca–28 Cu	Ca_4Cu	3.00
25 Ti–75 V	Solid solution	3.24
50 Ti–50 V	Solid solution	3.49
41 Cr–59 Mg	$CrMg_3$	3.60
70 Ti–30 V	Solid solution	3.84
42 Ca–55 Mg	Mg_2Ca + Mg	3.88
44 Ca–54 Mg	Mg_2Ca	3.90

The hydride Mg_2NiH_4 was studied in some detail. X-ray diffraction showed that this compound has a tetragonal structure with unit-cell dimensions of $a = 6.464$ A and $c = 7.0333$ A. The density is 2.57 g/cm^3, indicating that there are 4 molecules per unit cell. The thermal-decomposition kinetics follow a first-order law. At 200°C the decomposition rate is low, but at 240°C decomposition is rapid.

(H. H. Krause)

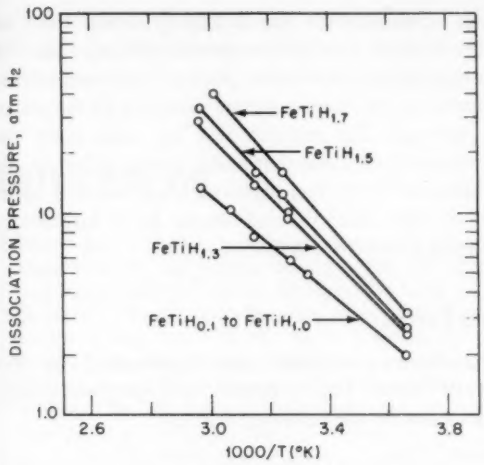

Fig. II-12 Dissociation pressures of $FeTiH_X$ compositions.[1b]

Metallic Poison Materials

An experimental Ag–25 Cd–5 In control rod has been examined nondestructively[25] after 6 years of service in the Army SM-1 Stationary Medium Power Plant 1. The element is a hollow tube 26 1/16 in. long with a 2.308-in.-square central hole and 0.156-in.-thick walls. The sides of the absorber consist of four 0.096-in.-thick strips of absorber alloy clad on both inner and outer surfaces with 30 mils of stainless steel.

It was found that the element had not changed dimensionally, and there was no observable surface damage. Gamma scanning showed no indications of abnormalities in the absorber burnup distribution.

The phase diagram of Gd–Co was determined[26] by means of X-ray diffraction, thermoanalysis, and metallography. The phase diagram is given in Fig. II-13 and shows eight different intermetallic phases. The compounds of $GdCo_5$ and Gd_2Co_{17} were found to possess large homogeneity regions at elevated temperatures.

(M. Kangilaski)

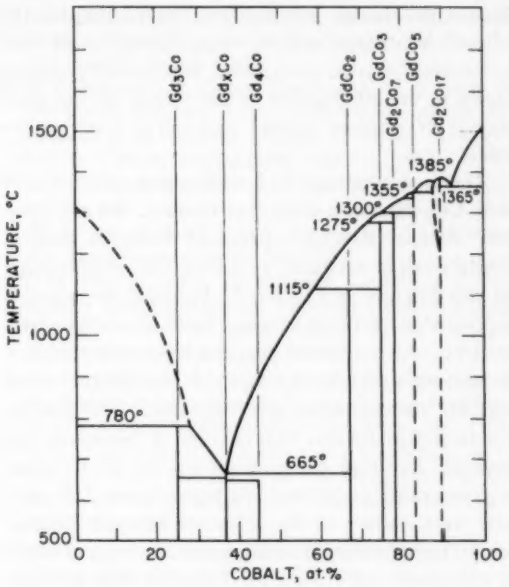

Fig. II-13 Phase diagram of the Gd–Co system.[26]

Dispersions and Nonmetallic Poisons

Boron and Boron Compounds

Scientists at the Carborundum Company[27] have investigated the structure of the SiC phase in the system Si–B_4C–C at 2450 to 2500°C. They found the solubility of boron in alpha SiC at 2450 to 2500°C to be less than 0.2 wt.%. The solubility of silicon in boron carbide is extensive, although it was not accurately determined quantitatively. Boron-saturated alpha SiC and a phase having the general formula $B_{12}(Si,C,B)_3$ are stable in contact with a liquid phase above a eutectic temperature of 2245°C. The eutectic corresponds to a molar ratio of 3 SiC to 7 B_4C plus carbon. No phases harder than B_4C were found.

Compatibility between B_4C and sodium, and the transport of boron and carbon through sodium to stainless steel are being examined by investigators at Battelle Northwest.[28] Test capsules were prepared by filling perforated stainless-steel tubes with −10 +20-mesh B_4C particles. The loaded perforated tubes were then inserted into 304 and 316 stainless-steel tubes, the void space was filled with sodium, and the tubes were subsequently sealed by welding. Tests of 1000 hr at 500°C and 1000 hr at 325°C resulted in a hardening of the 304 stainless-steel tubing to a depth of 2 mils from 150 KHN to 250 and 234 KHN, respectively (0.1-kg load). Similar tests of 100-hr duration showed no hardening zone in the 316 stainless-steel tubing. No evidence of precipitation was found during a metallographic examination of the 316 stainless-steel tubing.

The compatibility results on 99% dense B_4C pellets tested for 100 hr at 500°C showed no weight loss or

dimensional change, although cracking occurred in the pellets. A surface erosion was found to be not preferential at grain boundaries, but instead appeared related to the interception of the surface by the small amount of graphite present as a minor phase in the pellets.

The incorporation of a burnable poison into the 37 wt.% UO_2–stainless steel fuel elements for the presently defunct Argonne Advanced Research Reactor (AARR) was investigated by several laboratories under the coordination of Argonne.[29] Burnable poisons such as uncoated ZrB_2 particles, niobium-coated ZrB_2 particles, and boronated glass beads were dispersed in the stainless-steel matrix material and evaluated metallurgically and chemically at various stages from fabrication to postirradiation examination of miniature fuel elements. Although the program was terminated prior to its scientific conclusion, niobium-coated ZrB_2 particles were chosen as the reference burnable poison. The poison content, irradiation conditions, and swelling data presented in Tables II-5 and II-6 represent fuel plates, irradiated to approximately twice the core design burnup, in which complete depletion of the ^{10}B was calculated to have taken place at about one-fifth to one-sixth of the total exposure sustained by the plates.

Although the research was not exhaustive, the observations indicated that niobium-coated ZrB_2 could be fabricated into fuel plates with a controlled boron loss of less than 5% and would be a satisfactory burnable poison for a high-flux reactor.

Rare Earths

Europium dicarbide was synthesized by the Soviets[30] from Eu_2O_3 powder and spectroscopically pure carbon by the following reaction:

$$Eu_2O_3 + 7C \rightarrow 2EuC_2 + CO\uparrow$$

The blended powders were pressed into a cylinder and heated in a tantalum crucible in argon for 4 hr at 1800°K. The dicarbide has a face-centered cubic (fcc)

Table II-5 Irradiation Test Conditions for Burnable-Poison-Bearing AARR Mark 1 Core Fuel Plates in the G12 Water Loop of the Engineering Test Reactor[29]

Plate	Poison	Ratio (mg of ^{nat}B/g of ^{235}U)	Burnup, % ^{235}U fission		Heat flux, 10^6 Btu/(hr) (sq ft)		Av. temp., °F		Max. temp., °F
			Av.	Peak	Av.	Peak	Plate surface	Plate centerline	
927/48	Nb–ZrB_2	4.2	19.6	21.8	0.93	1.05	262	379	430
928/49	Nb–ZrB_2	4.2	18.0	19.6	0.86	0.94	257	365	400
929/50	Nb–ZrB_2	4.2	20.2	22.5	0.98	1.09	266	390	445
936/77	Nb–ZrB_2	6.6	17.0	22.3	0.82	1.07	254	357	409
938/23	Nb–ZrB_2	6.6*	18.4	23.5	0.88	1.12	240	352	419
939/68	B_2O_3–SiO_2	0.76	17.8	22.8	0.80	1.02	253	354	400

*Overheated during fabrication; ZrB_2 badly reacted with stainless steel; actual amount of boron was probably less than 10% of this value.

Table II-6 Swelling Characteristics of Burnable-Poison-Bearing Plates Irradiated in the Engineering Test Reactor[29]

Plate	Av. burnup, % ^{235}U fission	Initial void fraction in fuel core, %	Total swelling			% measured swelling attributed to	
			Calculated T.D. of UO_2,* %	Measured, %	% of calculated	Li + He	Fission products
927/48	19.6	6.25	7.54	3.27	43.4	0.33	2.93
928/49	18.0	5.63	6.97	2.92	41.9	0.35	2.58
929/50	20.0	5.83	7.85	3.40	43.3	0.35	3.05
936/77	17.0	5.4	6.59	3.25	49.3	0.55	2.71
938/23	18.4	4.31	7.34	5.18	70.4	0.06–0.55	5.12–4.63
939/68	17.8	5.33	6.59	2.90	44.0	0.06	2.84

*Based on 1.6% $\Delta V/V$ per at.% ^{235}U fissioned.

structure with $a = 5.961$ A and a molecular volume somewhat less than the sum of the atomic volumes of its constituents. (D. E. Lozier)

References

1. Brookhaven National Laboratory, Nuclear Engineering Department Annual Report, Dec. 31, 1968, USAEC Report BNL-50149(S-71), (*a*) pp. 32-34, (*b*) pp. 34-39.
2. Summary of Papers, Ninth Biennial Conference on Carbon, Boston College, June 16–20, 1969, compiled by The Defense Ceramic Information Center. Copies available from The American Carbon Committee, 102 Mineral Industries Building, The Pennsylvania State University, University Park, Pa. 16302, Attention: Dr. P. L. Walker, Jr.
3. C. L. Mantell, *Carbon and Graphite Handbook*, Interscience Publishers, New York, 1968.
4. R. W. Fenn, Jr., E. D. Crooks, and W. C. Kinder, Test Methods for Evaluating Mechanical Properties of Anisotropic Materials—Beryllium, Report AFML-TR-68-373(F-33615-67-C-1290), Lockheed Missiles and Space Company, February 1969.
5. D. Rummler, Mechanical Properties and Column Behavior of Thin-Wall Be–38 Al Tubing, Report NASA TN-D-5145, National Aeronautics and Space Administration, Langley Research Center, April 1969.
6. R. S. Shemenski and R. E. Maringer, Microplastic Characteristics of Isostatically Hot-Pressed Beryllium, *J. Less-Common Metals*, **17**(1): 25-45 (January 1969).
7. R. F. Bunshah and R. W. Armstrong, The Dependence of the Hardness on Beryllium Grain Size, *Mater. Res. Bull.*, **4**(4): 239-250 (April 1969).
8. H. L. Glass and S. Weissmann, Interim Progress Report on Synergy of Line Profile Analysis and Selected Area Topography of Beryllium by the X-Ray Divergent Beam Method, Rutgers University, December 1968.
9. F. T. Zurey, H. D. Hanes, and P. J. Gripshover, Final Report on Hot Isostatic Pressing of Beryllium—Vol. I, Battelle–Columbus, Sept. 12, 1968.
10. G. D. Kneip and L. R. Allen, Research on Submicron Beryllium Powder, Report AFML-TR-68-47, National Research Corp., March 1968.
11. Lockheed Missiles and Space Company, Data Sheet on Spark-Sintered Beryllium, Mar. 1, 1969.
12. V. E. Ivanov, V. F. Zelinski, V. K. Khorenko, B. V. Matvienko, and L. A. Kornienko, Sintered Beryllium-Base Compositions—II. Corrosion Properties and Possibilities of Raising Corrosion Resistance in Humid Atmospheres, *Sov. Powder Met. Metal Ceram. (Engl. Transl.)*, No. 8(68): 73-77 (August 1968).
13. V. E. Ivanov, V. F. Zelinski, S. M. Zhdanov, S. I. Faifer, V. K. Khorenko, and B. V. Matvienko, Sintering Beryllium-Base Compositions—I. Preparation and Some Mechanical and Thermophysical Properties, *Sov. Powder Met. Metal Ceram. (Engl. Transl.)*, No. 7(68): 33-36 (July 1968).
14. Ş. Nisigaki and R. Nagasaki, Oxidation of Pure Beryllium in CO_2 at High Temperatures, *Nippon Kinzoku Gakkaishi*, **33**: 134-40 (January 1969).
15. J. Booker and A. J. Stonehouse, Chemical Conversion Coatings Retard Corrosion of Beryllium, *Mater. Protect.*, **8**(2): 43-47 (February 1969).
16. R. P. Tye and J. E. Quinn, The Thermal Conductivity of Hot-Pressed Beryllium Block, in *Proceedings of the 4th Symposium on Thermal–Physical Properties*, American Society of Mechanical Engineers, April 1–4, 1968.
17. W. Fecych, Experiences with Beryllium Swelling and Replacement in the Plum Brook Reactor, Report NASA-TM-X-1794, National Aeronautics and Space Administration, Lewis Research Center, May 1969.
18. J. M. Beeston and W. F. Zelezney, Surveillance of Test Reactor Beryllium, Reactor Engineering Branch Annual Report—Fiscal Year 1968, USAEC Report IN-1228, Idaho Nuclear Corp., February 1969.
19. D. T. Neill and R. H. Morris, Several Deterioration Mechanisms of the Materials Testing Reactor Beryllium, USAEC Report IN-1289, Idaho Nuclear Corp., May 1969.
20. Z. I. Chechetkina, V. P. Golt'sev, F. I. Grechishkin, S. N. Votinov, V. A. Tsyhanov, and V. I. Klimenkov, The Metallic Beryllium Behavior in SM-2 Reactor, Soviet Report SRARI-P-20, 1968.
21. C. Roy and J. G. Jacques, $\{10\bar{1}7\}$ Hydride Habit Planes in Single-Crystal Zirconium, *J. Nucl. Mater.*, **31**(3): 233-237 (June 1969).
22. C. C. Weeks, M. M. Nakata, and C. A. Smith, Thermal Properties of SNAP Fuels, in *Proceedings of the 7th Conference on Thermal Conductivity*, National Bureau of Standards, Special Publication No. 302, pp. 387-398, September 1968.
23. W. A. Young, Specific Heats, Thermal Diffusivities, and Thermal Conductivities of Zirconium Hydrides Containing 4 At.% Uranium, *Trans. Met. Soc. AIME*, **245**(5): 971-980 (May 1969).
24. E. Veleckis and R. K. Edwards, Thermodynamic Properties in the Systems Vanadium–Hydrogen, Niobium–Hydrogen, and Tantalum–Hydrogen, *J. Phys. Chem.*, **73**(3): 683-692 (March 1969).
25. A. E. Richt and V. O. Haynes, Postirradiation Nondestructive Examination of a Silver–Cadmium–Indium Control Rod from the Army SM-1 Power Reactor, USAEC Report ORNL-TM-2506, Oak Ridge National Laboratory, June 1969.
26. K. H. J. Buschow and A. S. Van Der Goot, The Intermetallic Compounds in the Gadolinium–Cobalt System, *J. Less-Common Metals*, **17**(3): 249-255 (March 1969).
27. P. T. B. Shaffer, SiC Phase in the System Si–B_4C–C, *Mater. Res. Bull.*, **4**: 213-220 (March 1969).
28. E. R. Astley, Fast Flux Test Facility Periodic Technical Report, October 1968–February 1969, USAEC Report BNWL-941, pp. 4.41-4.42, Battelle–Northwest, May 1969.
29. C. V. Pearson, Developments in the Elimination of Boron Loss from UO_2–Stainless Steel Dispersion Fuel Plates for the Argonne Advanced Research Reactor Mark I Core, USAEC Report ANL-7477, Argonne National Laboratory, October 1968.
30. N. N. Matiushenko and O. P. Svinarenko, Dicarbides of Europium and Other Rare-Earth Metals, USAEC Report LA-4156-TR [translated by Helen J. Dahlby from *Ukr. Fiz. Zh.*, **13**: 1083 (1968)], May 29, 1969.

Section III

Reactor Materials

Special Fabrication Techniques

Powder-Metallurgy Materials

Los Alamos[1] development work on fabricating refractory-metal tubing by powder extrusion resulted in the production of high-density sintered tungsten tubes. Densities of 97% of theoretical were obtained on tubes ranging from 0.025 to 0.110 in. in wall thickness. A minimum amount of methocel and glycerin in water was found to be a satisfactory binder for the extrusion of 0.7- to 1.32-μ tungsten powders. A low-temperature cure and bake cycle that terminated at 400°C after 32 hr was necessary to remove the binder from the extruded tube. Presintering at 1000°C for 12 hr in a hydrogen atmosphere, followed by 1700°C for 12 hr in a hydrogen atmosphere and a final sintering at 2350°C in vacuum for 1½ hr, yielded tubing having 95 to 96% of theoretical density.

A Canadian patent[2] describes processes such as pulverizing and oxidizing for producing sintered aluminum powder (SAP) material for nuclear applications. Precautions are taken to prevent the introduction of impurities and to promote a uniform distribution of Al_2O_3 in aluminum.

Studies at Oak Ridge[3] involving SAP include the selection of a process for the consolidation of ball-milled $Al-Al_2O_3$ flake for subsequent extrusion into rod. Compacts of the ball-milled powder, fabricated by hot pressing, were vacuum annealed and then extruded. The effects of impurities, the reproducibility, and the mechanical properties of the extruded product are of interest.

A Russian report[4] describes the fabrication of molybdenum sheet from a sintered compact. Hot-rolled, cold-rolled, or warm-rolled sheets of controlled thickness were vacuum annealed at 800 to 1250°C and tested for mechanical properties at 20 to 800°C and for formability at 20 to 500°C. With increasing annealing temperature, the molybdenum-sheet strength decreased and elongation increased. Also, ductility increased as the angle to the direction of rolling increased from 0 to 90°. (W. T. Langendorfer)

Melting, Casting, and Fabrication of Cast Structures

National Lead Co. of Ohio[5] has conducted a study to prevent cold shots in uranium ingots. The effect of orifice configuration on the integrity of a pour stream simulating molten uranium and the effect of the mold bottom shape on the initial metal splash were investigated. The apparatus used consisted of a ⅜-scale acrylic plastic model of the bottom-pouring crucible and mold used in production. Mercury was used as the fluid in these studies because many of its physical properties are similar to those of molten uranium. The changes in the pour stream and in the initial metal splash were recorded with a motion-picture camera. It was found that pour plugs having an orifice with tapered sidewalls and a rounded edge at the top produced the most desirable pour stream. Mold bottoms which were flat or which approached flatness with no abrupt change in contour minimized metal splash.

The Bureau of Mines[6] has published a bulletin that reviews the historical background of cold-mold arc-melting technology, with specific references to the development that led to homogeneous zirconium ingots. Descriptions are given of modern production arc furnaces for vacuum melting of both exotic and conventional metals. Besides zirconium, specific data are given for the production of chromium, thorium, and copper. The development of the skull-casting technique for titanium is detailed, and the application of the technique to such refractory metals as molybdenum and tungsten is described. Factors of operation of the apparatus and furnace design are considered.

The Japanese[7] have prepared a UO_2 single crystal, 10 mm in diameter and 30 mm long, by the floating-zone technique. A sintered UO_2 rod, 17 mm in diameter and 150 mm long having 97% of theoretical density, was heated by high-frequency induction in a graphite pipe in nitrogen at 5 atm pressure. When the

surface temperature of the pipe attained 1100°C, the pipe was removed and the rod was heated at a rate of 500°C/hr directly by induction. When the surface temperature reached 1850°C (power supply 18 kw), about 70% of the cross section of the rod had melted, and the nonmelted outer portion acted as a crucible. Then the rod was rotated at a speed of 100 rpm and at the same time raised at a rate of 5 mm/hr. After it reached a predetermined height, the rod was again lowered at the same rate to its original position. This double pass generated a single crystal in the central portion. Back-reflection Laue photographs taken from different points of the specimen showed that the ⟨111⟩ direction was inclined at about 10° to the axis of the rod. No etch pits were found in the single-crystal area. Spectroscopic analysis revealed that certain kinds of impurities were concentrated in the lower part.

Reed and Pollard[8] have designed a crystal puller using the arc-melting technique for the Czochralski growth of single crystals. The circumference of the melt is heated by three arcs, and the crystal is pulled from the center of the melt with a water-cooled seed rod. The charge is contained in a hollow water-cooled copper hearth fitted with a piston so that the melt can be fed continuously. Use of this apparatus eliminates the difficulty of finding crucible materials suitable for high-temperature growth, since the melt is contained by a solid shell of the same substance in contact with the hearth. The furnace is economical, convenient to use, and requires a relatively small mass of material. Boules of Sn, Ge, Si, Cu_2O, V, VO, Ti_2O_3, Ni, Nb, NbO, and TiC, with melting points between 232 and 3150°C, have been grown.

The Japanese[9] have designed an electron-beam floating-zone-melting apparatus for refractory metals and have used it successfully to melt W, Mo, Ta, Nb, Pt, Pd, and Fe rods. With the use of emission control, it was possible to keep the current constant by automatically adjusting the voltage and filament temperature. This permitted successful floating-zone melting of sintered specimens. The purifying effect of floating-zone melting was confirmed by residual-resistance-ratio measurements. It appeared that the zone-melted rods were purified by both vacuum distillation and zone refining. This apparatus can be used as a single-crystal-growing apparatus for refractory metals. With only one zone-melting pass at about 1 to 4 mm/min, 5-mm-diameter W, Mo, Ta, Nb, Pt, and Pd rods were converted to single crystals without the use of seed crystals. A 4-mm-diameter niobium single crystal was produced by using ⟨100⟩ seed crystals.

The fabrication methods used for the U–Pu–Mo alloy fuel used in the Zero Power Plutonium Reactor are described by Shuck.[10] The elements consist of rectangular plates of the fuel alloy in tight-fitting stainless-steel jackets. Conventional hot-working methods of fabrication required temperatures in excess of 500°C to avoid billet cracking and a high-purity inert atmosphere to prevent oxidation. Vacuum-melting and -casting the U–28.3 Pu–2.5 Mo alloy into reusable, multiple-cavity molds were found to be a practical method for making rectangular-section bars from which the element plates were machined. Directional solidification of the castings from the bottom and continuous feeding of molten metal into the hot-topped molds were necessary to prevent internal shrinkages. The jackets were stretch formed from welded-and-drawn, 304L stainless-steel tubing. The jackets were enclosed in a protective fixture, and the cores were loaded through a funnel that prevented contact of the core with the jacket lip. Close-fitting end plugs were inserted in the jacket sleeves and forced tightly against the cores. The seal welds between the jacket sleeves and end plugs were made at less than 0.5 atm pressure of inert gas. The reduced internal pressure prevented inflation of the fuel element at operating conditions.

The effect of ingot grain structure on the formation of seams during rolling of uranium rods has been studied by National Lead Co. of Ohio.[11] They found that the size of the grains did not change seam depth but that ingots with equiaxed grains had shallower defects than ingots with dendritic or elongated grains.

Workers at Reactive Metals[12] found that an oxide film on a billet of uranium prevents the billet from sticking to steel surfaces during operations such as extrusion and forging. Of several methods of oxidizing the surface, they found chemical oxidation to be the best. This process is carried out by immersing the billet in a 5 wt.% $KMnO_4$ solution for 10 min at 200°F (93°C). This process results in better surface finishes on forged or extruded billets.

Oak Ridge[13a] is studying how Zircaloy-tubing-fabrication procedures interact with crystallographic deformation modes, in order to match the strongest direction with the highest service stress. Twelve experimental fabrications of Zircaloy tubing were completed. The tubing was reduced to final size by tube reducing, cold drawing, swaging, and planetary swaging. Two experimental schedules, which required heavy sinking by swaging, were unsuccessful; all other operations, including sinking by drawing, were completed without difficulty. These experiments have shown the influence

of texture on the biaxial mechanical behavior of Zircaloy tubing. Depending on the texture present, the stress required to produce plastic yielding can vary by 50% or more for materials tested in the same stress state. It should be possible to use information of this type to select Zircaloy tubing with different textures that can optimize resistance to any particular set of operating stress conditions. (D. E. Stellrecht)

Chemical Plating

Workers at Dow Chemical[14] were unable to put metallic coatings on grade-HP BN disks unless they first deposited an approximately 500-A film of beryllium by the accelerated-ion method. The accelerated-ion technique was also used to deposit La, Au, Ag, Cu, or Al over the beryllium. Other metals, i.e., Mo, Ce, and Ti, were more easily deposited on the beryllium film by a triode-sputtering method or from an electron-beam gun. During these deposition processes, care had to be taken to keep the substrate from reaching a higher temperature than that developed during the beryllium deposition.

Plating of Al_2O_3 and UO_2 pellets with Cr_7C_3 and chromium in a fluidized bed by thermal decomposition of dicumene chromium was described by Schneider and Schoenwald.[15] Thermal decomposition of dicumene chromium resulted in Cr_7C_3 coatings containing approximately 10 wt.% carbon (the theoretical carbon content of the Cr_7C_3 is 9 wt.%). When iodine was used as a catalyst in the pyrolysis of dicumene chromium, chromium coatings containing only up to 0.05% wt.% carbon resulted.

Thin diffusion-barrier layers of niobium were deposited by reduction of its halides with hydrogen and zinc.[16] A typical example cited of the need for such barriers in a nuclear application is in thermocouples inserted in a stainless-steel fuel-element plug. The quality of the niobium deposits was demonstrated by numerous tests: micrography, chlorine content, 1000-hr heat-treatment at 620°C, helium leaktightness tests, thermal cycling, hot mechanical tests, overall tests under irradiation, and corrosion tests. Complementary tests showed the method to be suitable for depositing tungsten, tantalum, and alloy coatings as well.

A fluidized-bed coating apparatus and the method for coating nuclear fuel particles are described in a British patent.[17] Pyrolytic carbon coatings can be deposited on oxide or carbide fuel particles of diameters up to 1000 μ on a kilogram scale with a methane–argon flow rate of 45 liters/min.

Development efforts to produce mechanically sound tungsten and W–25 Re tubing by chemical-vapor deposition for liquid-metal containment (e.g., fuel cladding or heat pipes) were summarized by Lawrence Radiation Laboratory.[18] Reaction parameters were evaluated on short-length tubes. Later, apparatus was built to make ½-in.-diameter, 0.040-in.-wall tubing, 1 ft long. Production of longer and larger tubes with thicker walls and different compositions was considered possible with the same basic apparatus design.

At Oak Ridge[13b] the development of a codeposition process for chemical-vapor deposition of W–5 Re alloy sheet has continued. Bend tests of this material to determine the ductile-to-brittle transition temperature and the effects of heat-treatment were started. Several possible remedies were tested to eliminate thickness variations of the alloy deposited on resistance-heated sheet substrates. An increase in deposit thickness from the gas inlet end toward the gas outlet end at a pressure of about 100 torrs was observed. Since the deposit thickness variation at a pressure of 10 torrs was the reverse of that obtained at a pressure of 100 torrs, it is considered possible that uniform thickness would be obtained at some intermediate pressure. To determine the isodeposition temperature for W–25 Re alloys, the deposition temperature was varied between 600 and 1200°C, whereas the other parameters were held constant. At 600°C a rhenium-rich deposit was formed, but at 700°C and above, the rhenium content of the deposit was about the same as that of the gas mixture.

Induction heating was used[13b] in an investigation of the possibility of depositing vanadium by hydrogen reduction of VCl_3 at higher temperatures than 950°C. Reaction of entrained VCl_3 in hydrogen at 1200 and 1300°C on an induction-heated graphite substrate for 2 hr produced bright metallic deposits, identified by X-ray diffraction as vanadium metal.

The formation of high-strength Al_2O_3 shapes by chemical-vapor deposition using $AlCl_3$, CO_2, and hydrogen mixtures was investigated at Lexington Laboratories.[19,20] Using $MgO–SiO_2$ and molybdenum-sheet substrates, the investigators studied deposit growth rate, grain size, porosity, uniformity, and ease of substrate removal.

At Sylvania[21] several fused-silicide-coating compositions were characterized in terms of their structure and chemistry by means of X-ray diffraction and electron-microprobe techniques, and in terms of their applicability and performance by experimental

analyses of wettability and flowability, faying-surface penetration, coating repair, mechanical tests, slow thermal cycling, furnace and torch oxidation, arc-plasma tests, low-temperature cycling, exposure to low pressures at high temperatures, reentry simulation, and statistical reliability analyses. The optimum coating compositions for niobium, tantalum, and molybdenum alloys were identified.

Niobium coatings, 25 to 37 μ thick, on resistance-heated specimens of Nb–20 U were prepared[22] by the hydrogen reduction of $NbCl_5$ at 1100°C. The coatings were dense and well bonded to the substrate.

Gulf General Atomic[23] has been studying process variables in the fabrication of coated fuel particles suitable for use in gas-cooled reactors. Effects of impurities in the process gases (propane, methane, and acetylene) were considered. Other sources of coating contamination were also investigated, using coated particles with ZrO_2 cores. Experiments were planned to evaluate the effect of high levels of hydrogen in the pyrolytic carbon coatings on the thermal stability of the fuel particles. A study was made of the magnitude and effects of variations of pyrolytic carbon-coating densities within a batch of particles.

The use of nitrogen as the carrier gas instead of helium and argon in the pyrolytic carbon-coating process was investigated.[24] Coating rates and coating densities were found to be essentially the same whether helium or nitrogen was used. However, nitrogen pickup was greater when nitrogen was used to deposit coatings from methane above 1600°C. High anisotropy was associated with these high nitrogen levels, within the range studied. X-ray diffraction analyses revealed no phases (in particular, no nitrides) other than those normally associated with production carbide cores.

(J. Zupan)

Explosive Metalworking

The use of pneumatic-mechanical impaction to fabricate radioisotope heat sources has been investigated by Davis and Brite[25] at Battelle–Northwest. Parameters and tooling techniques were developed using a nonradioactive rare-earth oxide. These simulation experiments showed that a metal-encapsulated oxide cylinder having a uniform cross section could be produced by proper design of die tooling. The results of the preliminary experiments were used to fabricate samples of promethium sesquioxide-fueled capsules. Two types of samples were fabricated: compatibility capsules and high-temperature heat sources. A number of compatibility samples, each measuring 1.1 in. in diameter by 1.2 in. long, were compacted and encapsulated with a single impaction; conditions used were 1200°C and 300,000 psi. The heat sources were impacted in a massive molybdenum die at 1600°C. Both types of samples compacted to close to theoretical density.

A novel use of explosives is described in a patent[26] assigned to Du Pont. The shock wave generated in water by a detonating explosive is utilized to stress relieve metal components. The pressures have to be within certain limits (between one and five times the dynamic elastic limit) to effect the desired stress relief. If the pressure is too high, the material is subject to shock hardening; whereas, if the pressure is too low, the material is not plastically strained and no stress relief is produced. An example is given in which a 6- by 12-in. 2014 aluminum plate was shocked by the method described. The initial stress in the plate was 15,000 psi; the stress after this shock-relief treatment was 100 psi.

(D. Laber)

Welding and Brazing

Welding

Studies at Oak Ridge[13c] indicate that hot cracking in tungsten fusion welds is caused by stress-induced interconnection of grain-boundary porosity. This conclusion was reached following electron-fractography studies of gas tungsten-arc welds in 0.050- to 0.060-in.-thick wrought tungsten sheets. Full-penetration, bead-on-plate welds were made on chemically vapor-deposited, powder-metallurgy, and vacuum-arc-melted tungsten sheet. Visible gas porosity (bubbles up to 0.1 mm in diameter) occurred in all but the arc-melted material. It is not known whether the apparent relation of grain-boundary porosity to hot cracking is peculiar to tungsten. If not, it may present a new approach to the understanding of hot cracking in welds.

Along this line, the Russians report a new method for evaluating the susceptibility of niobium-alloy welds to hot cracking.[27] This test utilizes specimens measuring 1 mm thick and 50 or 80 mm wide, with a narrow slit cut in them. A weld bead is deposited on the specimen so that the weld center line goes through the end of the slit. A rate of deformation is then determined by the speed at which the slit opens as a result of welding. This deformation rate increases with

the length of the weld between its starting point and the slit, and with increasing weld speed. The criterion of weld resistance to hot cracking is then defined as the maximum length of the weld at which cracking does not occur. This technique has been successfully applied to a series of niobium alloys.

The long-term safe storage of radioactive fusion isotopes, such as ^{90}Sr or ^{137}Cs, requires a welding operation that is readily adaptable to remote operation in a hot-cell environment. A study at Atlantic Richfield Hanford indicates that inertia welding offers several characteristics which make it attractive for these encapsulating operations.[28] The process is readily adaptable to remote operation and does not require visual observation of welding. Weld quality is controlled by three easily maintained parameters: surface velocity, weld-thrust pressure, and flywheel moment. Also, inertia welding provides excellent mechanical properties with little or no heat-affected zone. Finally, the upsetting during welding provides a capability for flushing surface contaminants and affords a good visual indication of weld quality.

The mechanical properties of gas tungsten-arc welds in Hastelloy N are generally inferior to those of the base metal, according to studies conducted at Oak Ridge.[29] However, a postweld heat-treatment for 8 hr at 1600°F (870°C) improved weldment properties so that they nearly equalled the base-metal properties. The property most severely affected by welding during these studies was strain at fracture, but high-temperature creep-rupture strength was also reduced appreciably. Neutron irradiation of specimens caused a decrease in fracture strain in both welds and base metal. This result appeared to be independent of postweld heat-treatment, unlike the response of unirradiated specimens. Postirradiation fracture strains in the welds approached those in the base metal as the test temperature was increased, and the two were identical at 1600°F. Postirradiation creep-rupture properties at 1200°F (650°C) were about the same for welds and base metal, although the preirradiation properties differed greatly.

The effects of welding temperature, welding pressure, and surface finish on the strength of diffusion welds in Ti–6 Al–4 V have been measured at Atomics International.[30] Specimens ½ in. thick by 1 in. square were welded in a vacuum of better than 5×10^{-4} torr. Satisfactory joints were obtained at temperatures as low as 1440°F (780°C) with 400-psi pressure for 1 hr and at pressures as low as 100 psi at 1500°F (815°C) for 2 hr. The effects of welding pressure and temperature are shown in Figs. III-1 and III-2. In Fig. III-3, weld strength is plotted as a function of deformation for a 1-hr welding time at two ranges of surface finish. For the smoother samples a deformation of 0.010 in. resulted in a perfect bond. At least twice this deformation was necessary for specimens with a coarser finish.

Electron-beam welding has proven a satisfactory process for joining copper to various alloys of interest in nuclear applications. The Russians report electron-beam welding of copper to molybdenum, tantalum, and 18 Cr–10 Ni stainless steel.[31] Table III-1 sum-

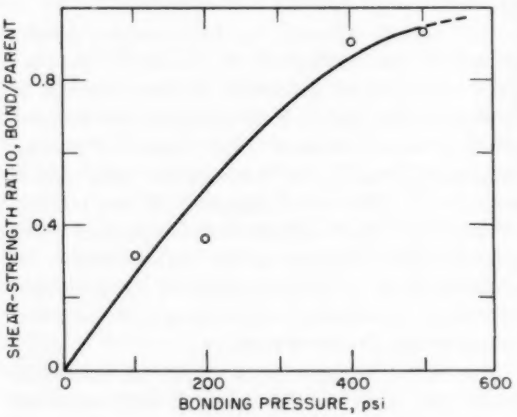

Fig. III-1 Effect of bonding pressure on bond strength in Ti–6 Al–4 V joints[30] bonded in 1 hr at 1440°F (780°C).

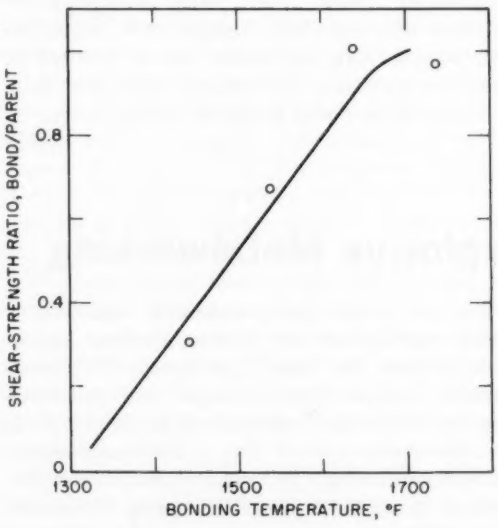

Fig. III-2 Effect of bonding temperature on bond strength in Ti–6 Al–4 V joints[30] bonded in 1 hr at 1440°F (780°C).

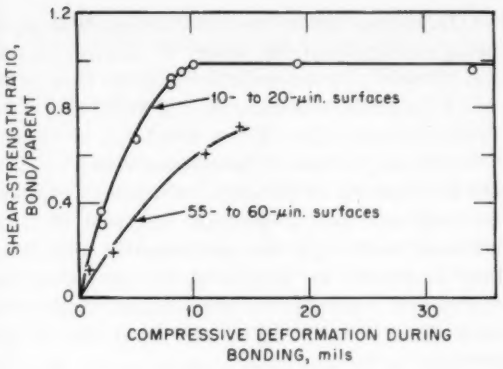

Fig. III-3 Effect of surface finish and deformation during bonding on bond strength in Ti–6 Al–4 V joints[30] bonded in 1 hr at 1440 to 1700°F (780 to 925°C).

marizes their results. In these welds the copper was melted on the surface of both the molybdenum and tantalum, and wettability was good. The copper did not penetrate along the grain boundaries of the stainless steel.

Boeing has also used electron-beam welding to join 321 stainless steel to Kovar (Fe–29 Ni–17 Co) for an engine-cutoff sensor tube.[32] Both a melt-through and a fillet weld were used. Satisfactory welds were obtained as shown by visual and X-ray examination, hardness tests, and microscopic analysis.

Research at Oak Ridge[13d] indicates that various compositions in the Ti–V–Cr system can be used as brazing alloys to join all combinations of graphite, Al_2O_3, and refractory metals. For example, alloys containing 25 to 47.5 wt.% chromium (Ti–V ratio constant) produce excellent joints in Al_2O_3. Alloys with lower chromium content wet the ceramic but do not flow. On graphite, however, those alloys with 5 to 25 wt.% chromium have excellent flowability, and those with more chromium do not flow.

The electron gun for the Astron accelerator requires an accelerating column composed of copper electrodes separated by alumina ring insulators. Active-metal brazing is being used to complete these ceramic-to-metal seals at Lawrence Radiation Laboratory.[34] This process uses titanium hydride coated on the ceramic sealing surface, plus a conventional brazing alloy. In this case, two parts of 200-mesh TiH_2 powder are mixed with three parts nitrocellulose lacquer, and this paint is applied to the alumina. A ring of Ag–Cu–Ni eutectic brazing alloy is placed between the coated alumina insulator and the copper electrode. The accelerating column, consisting of several of these assemblies, is brazed in a vacuum furnace under sufficient pressure to ensure intimate contact. Alloying between the titanium and the braze alloy begins at 810°C, and at 850°C, 6 wt.% of the titanium has been alloyed. This yields a good braze. The furnace must be capable of high pumping speed in the 10^{-5} torr range

Table III-1 Test Results of Copper-to-Dissimilar Metals Electron-Beam Welds[31]

Material combination	Bend-test results	Ultimate strength, ksi	Fracture location
0.06-in. Cu to 0.02-in. Mo	Cracking in Mo at angle of 45°	69.8	In Mo close to joint
0.06-in. Cu to 0.02-in. Ta	No cracks at 90°	22.4	In Cu
0.06-in. Cu to 0.06-in. stainless steel	No cracks at 180°	31.4	

Brazing

Fiat reports the use of a Be–Zr alloy for brazing zirconium strips.[33] Joints with 85 to 90% of parent-metal strength were obtained by brazing for 10 min at 1010°C, followed by 4 to 6 hr at 800°C. The corrosion resistance of these joints was no worse than that of the base metal and their hydrogen content did not increase when they were exposed to water at 340°C.

to reduce the pressure resulting from evolution of hydrogen from the TiH_2.

A technique for forming a solderable/brazable coating on ceramic surfaces by low-temperature deposition has been developed at Sandia.[35] This technique has been used to apply a Nb/Ag metallizing layer to fused silica, which can then be brazed with a high-temperature brazing alloy. Deposition is accomplished in a controlled atmosphere containing a

partial pressure of oxygen. This allows the formation of an interfacial transition oxide region, which increases the adhesion between the resulting coating and the ceramic surface.

A British patent[36] has been issued for a high-temperature brazing alloy for use with tantalum, tungsten, and their alloys.[11] The alloy consists of tungsten plus 35 to 45 wt.% iridium. Rhenium may be substituted for 1 to 10 wt.% of the tungsten.

(J. E. Mortland and R. M. Evans)

Nondestructive Testing

Ultrasonic Techniques

Most piezoelectric materials used to generate and detect ultrasonic energy for nondestructive testing are damaged when they are used in thermally or radioactively hot environments. Contactless electrodynamic transducers are potential alternative methods of generating and detecting the ultrasonic energy for testing metals in such environments, but they require large magnets that preclude their use for in-reactor work. Argonne personnel[37] are attempting to develop a related system using magnetostrictive transducers. They take advantage of the ferromagnetic characteristics of the stainless-steel components of the reactor by making them part of the transducer. Tests were conducted using stainless-steel and nickel rods, 30 cm long and 1.5 cm in diameter. A bank-wound, double-layer pancake coil approximately 1.5 cm in diameter was mounted in the rods and insulated with tape 0.007 cm thick. A PZT-4 detector was located at the opposite end of the rod. Pulses received by the detector indicated that the magnetostrictive transducer was capable of generating suitable pulses for nondestructive testing. However, the magnetostrictive transducer was incapable of detecting pulses transmitted from the PZT-4.

Other work at Argonne shows that the Magnaflux PS-902 ultrasonic instrument is capable of detecting nonwet areas in sodium-filled capsules.

Another approach to inspection at high temperatures is being pursued at Argonne. Lithium niobate has a Curie temperature of 1210°C and should be suitable for high-temperature applications. Argonne personnel are evaluating a transducer consisting of a Pt–Pd–Au coated lithium niobate crystal, about 1 mm thick, brazed to a diaphragm and a backup plate, both made of 304 stainless steel. The brazing material is a Ni–Au alloy.

Techniques similar to ultrasonic spectroscopy are being investigated at Oak Ridge.[13e] Spectrum analysis was obtained of pulses reflected from the back surface of a 1.5-in.-thick aluminum plate in which were drilled flat-bottom holes $\frac{1}{8}$ in., $\frac{5}{64}$ in., and $\frac{3}{64}$ in. in diameter. The reflecting bottom of the hole was about 1 in. from the entry surface of the plate. As would be expected, the amplitude of the spectrum decreased when the ultrasonic wavelength was approximately equal to the hole diameters. By integrating the output of the analyzer, it is possible to obtain a single, quantitative value (read from a digital voltmeter) that is proportional to the area under a spectrum envelope. This makes it possible to compare spectra of different shapes and observe frequency-dependent effects, even though identical amplitude may be indicated with conventional equipment. (D. Ensminger)

NDT Techniques Other Than Ultrasonics

Computer-analysis studies of eddy-current applications are being continued at Oak Ridge.[13f] Solutions have been worked out for the case of a coil encircling a tube, with the signal caused by a defect on the inner surface of the tube directly under the coil. For various tube-wall thicknesses, the response was calculated as a function of the product of frequency, conductivity, and permeability. As the family of curves in the report shows, for a given wall thickness and type of tubing, there is an optimum operating frequency for maximum sensitivity to defects on the inner surface of the wall. In a subsequent calculation for two fixed wall thicknesses, the dimensions of the test coil were varied. Although the sensitivity varied with coil design, all coils had their maximum response at the same frequency if the wall thickness was held constant. Future study is to include differential coils. It is hoped that the details of these continuing studies will be made available in more complete form for industrial use.

Investigators at Mound Laboratory[38] have performed a series of radiographic experiments which permit a comparison of results using three different sources: (1) 150- and 300-kev X rays, (2) equivalent 850-kev gamma radiation from ^{192}Ir, and (3) thermal neutrons. The thermal neutrons were supplied by a 10-Mw reactor operated at 1 Mw, with a thermal flux at the target of 10^7 neutrons/(cm^2)(sec) and a cadmium ratio of ~2.8. The collimator used provided a collimation ratio of 1 : 120 and a half-angle of divergence of 1°. An indium foil 10 mils thick was used as the neutron-radiographic transfer screen in connection with standard industrial Kodak Type T film.

The three specimens radiographed were (1) a Haynes 25 alloy container filled with a 50–50 wt.% mixture of powdered tungsten and molybdenum, (2) a Ta–10 W cylinder with a welded end cap, and (3) a radioactive heat source containing three small capsules of ^{238}Pu metal. Radiographs presented in the report illustrate differences in results with the three radiation sources. Neutron radiography may be more advantageous with materials other than refractory metals and plutonium (e.g., hydrogenous materials). However, the experience of these investigators will help to introduce the technique to those who have not used it.

(A. F. Leatherman)

References

1. W. C. Erickson and C. A. Javorsky, Powder Extrusion of Tungsten Tubing, USAEC Report LA-4099, Los Alamos Scientific Laboratory, December 1968.
2. D. Guslandi and P. Jehenson, Al–Al_2O_3 Structures for Nuclear Applications and Process for Obtaining Same, Canadian Patent 793,244, Aug. 27, 1968.
3. S. Peterson (Comp. and Ed.), Metals and Ceramics Division Annual Progress Report for Period Ending June 30, 1968, USAEC Report ORNL-4370, pp. 133-141, Oak Ridge National Laboratory, October 1968.
4. K. N. Bogoyavlenskii and V. V. Ris, Effect of Temperature on the Mechanical Properties and Formability of Sintered Molybdenum (in Russian), *Tr. Leningrad. Politekh. Inst.*, 271: 9-15 (1966).
5. G. A. Graman and D. E. Kettler, Effects of Pouring Orifice and Mold Bottom Configuration on Ingot Surfaces, USAEC Report NLCO-1026, National Lead Co. of Ohio, March 1969.
6. U. S. Bureau of Mines, Albany Metallurgy Research Center, *Cold Mold Arc Melting and Casting*, U. S. Bureau of Mines Bulletin, No. 646, 1968.
7. S. Yajima and H. Furuya, Preparation of UO_2 Single Crystal by Induction Heating (in Japanese), *Nippon Genshiryoku Gakkaishi*, 10: 632-636 (November 1968).
8. T. B. Reed and E. R. Pollard, Tri-Arc Furnace for Czochralski Growth with a Cold Crucible, *J. Cryst. Growth*, 2: 243-247 (August 1968).
9. K. Masumoto and Y. Tamura, An Apparatus for the Floating Zone Melting of Refractory Metals by Electron Bombardment (in Japanese), *Nippon Kinzoku Gakkaishi*, 32: 1121-1127 (1968).
10. A. B. Shuck, Uranium–Plutonium Alloy Fuel Fabrication, *Nucl. Met., Met. Soc. AIME*, 13: 263-278 (1968).
11. R. Burgett (Ed.), Summary Technical Report for the Period January 1–March 31, 1969, USAEC Report NLCO-1040, pp. 1.1-1.8, National Lead Co. of Ohio, May 1969.
12. Reactive Metals, Inc., Semiannual Progress Summary, July–December 1968, USAEC Report RMI-12.
13. P. Patriarca (Comp.) and D. J. Rucker (Ed.), Fuels and Materials Development Program, Quarterly Progress Report for Period Ending December 31, 1968, USAEC Report ORNL-4390, (*a*) p. 308, (*b*) pp. 162-170, (*c*) pp. 170-175, (*d*) pp. 285-293, (*e*) pp. 182-186, (*f*) pp. 177-179, Oak Ridge National Laboratory, May 1969.
14. R. G. Kurtz and T. Van Vorous, Vacuum Coating of Boron Nitride, USAEC Report RFP-972, Dow Chemical Co., Rocky Flats Division, Apr. 18, 1969.
15. H. Schneider and D. Schoenwald, Vapor Chromium Plating of UO_2 and Al_2O_3 Pellets, German Report EURFNR-572 (KFK-787), July 1968.
16. F. Brossa, R. Debeir, M. Grin, G. Piatti, and H. Venker, Vapor Phase Chemical Deposition of Refractory Metals, *Euratom Information*, 7(4): 265-266 (April 1969).
17. Improvements in Entrained Fluidized-Bed Coating Apparatus and Method Thereof, British Patent 1,144,320, Mar. 5, 1969.
18. L. W. Roberts, Jr., and G. S. Root, Refractory Alloy Development for the Advanced Space Power Reactor Program, USAEC Report UCRL-50603, University of California, Lawrence Radiation Laboratory, Mar. 17, 1969.
19. H. A. Hobbs, Jr., A. Waugh, W. D. Kingery, and L. R. Terrenzio, Chemical Vapor Deposition of Aluminum Oxide Ceramic Shapes, First Quarterly Progress Letter, Lexington Laboratories, June 1, 1968.
20. H. A. Hobbs, Jr., A. Waugh, W. D. Kingery, and B. Albanese, Chemical Vapor Deposition of Aluminum Oxide Ceramic Shapes, Second Quarterly Progress Letter, Lexington Laboratories, Sept. 1, 1968.
21. S. Priceman and L. Sama, Development of Fused Slurry Silicide Coatings for the Elevated-Temperature Oxidation Protection of Columbium and Tantalum Alloys, Report AFML-TR-68-210, Sylvania Electric Products, December 1968.
22. R. F. Redmond, Progress Letter on Development of a Fuel System for a Fast-Flux Pulse Reactor, January–March 1969, USAEC Report BMI-X-10255, pp. 2-3, Battelle–Columbus, Apr. 23, 1969.
23. Gulf General Atomic Incorporated, Public Service Company of Colorado 330-Mw(e) High-Temperature Gas-Cooled Reactor Research and Development Program, Quarterly Progress Report for the Period Ending March 31, 1969, USAEC Report GA-9261, pp. 109-127, Apr. 29, 1969.
24. Gulf General Atomic Incorporated, Public Service Company of Colorado 330-Mw(e) High-Temperature Gas-Cooled Reactor Research and Development Program, Quarterly Progress Report for the Period Ending March 31, 1969, USAEC Report GA-9261(Suppl.), p. 2, Apr. 29, 1969.
25. N. C. Davis and D. W. Brite, Fabrication of Promethium Sesquioxide Heat Sources by High Energy Rate Forming, USAEC Report BNWL-1041, Battelle–Northwest, May 1969.
26. A. H. Holtzman, Process for Relieving Residual Stresses in Metals, U. S. Patent 3,282,743, to E. I. du Pont de Nemours & Co., Nov. 1, 1966.
27. G. N. Klebanov and T. A. Chernysheva, Test for Evaluating the Susceptibility of Niobium-Alloy Welds to Hot Cracking (in Russian), *Svoystva i Primenenive Zharoprochnykh Splavov*, pp. 135-139, Izdatel'stro Nauka, Moscow, 1966.
28. J. C. Wormeli, Evaluation of Inertia Welding for High Level Waste Encapsulation, USAEC Report ARH-1058, Atlantic Richfield Hanford Co., March 1969.

29. H. E. McCoy and D. A. Canonico, Preirradiation and Postirradiation Mechanical Properties of Hastelloy N Welds, *Weld. J. Res. Suppl.*, 48(5): 203s-211s (May 1969).
30. C. A. Smith, Diffusion Bonding of Titanium Alloys, Final Report AMRA-CR-66-10/1, Atomics International, June 30, 1968.
31. G. W. Terebichi, Electron-Beam Welding of Copper to Molybdenum, Tantalum, and KH18NiOT Steel, Welding Production (USSR) (English Translation), 14(10): 14-16 (October 1967) from *Svar. Proizv.*, 14: 8-9 (October 1967).
32. T. Caesar, Investigation of Electron-Beam Welds in a Sensor Tube, Report T-5-6539-102, Vol. I (N68-25523), The Boeing Company, Space Division, Mar. 1, 1968.
33. I. Amato and M. Ravizza, Some Developments in Zircaloy Brazing Technology, *Energ. Nucl. (Milan)*, 16(2): 35-39 (February 1969).
34. R. H. Bulmer, Active Metal Brazing Technique for Metal-to-Nonmetal Seals, USAEC Report UCRL-71542, University of California, Lawrence Radiation Laboratory, Mar. 27, 1969.
35. E. L. Hollar, F. N. Rebarchik, and D. M. Mattox, Composite Film Metallizing for Ceramics, Report SC-TM-68-287, Sandia Laboratories, May 1968.
36. High-Temperature Brazing Alloys for Tungsten and Tantalum, British Patent 1,136,980 to USAEC, Dec. 18, 1968.
37. Argonne National Laboratory, Reactor Development Program Progress Report, March 1969, USAEC Report ANL-7561, pp. 73-74, Apr. 22, 1969.
38. A. G. Barnett, A. R. Bauer, and M. I. Gray, Evaluation of Neutron Radiography for Radioisotopic Heat Sources, USAEC Report MLM-1617, Mound Laboratory, June 5, 1969.

Index

Reactor Materials

Volume 12

The page range for each of the four issues of Vol. 12 is as follows:

No. 1, pages 1 to 72
No. 2, pages 73 to 154
No. 3, pages 155 to 219
No. 4, pages 221 to 256

70/30 cupronickel
  corrosion by water, 178
90/10 cupronickel
  corrosion by H_3BO_3–NaOH solutions, 95
  corrosion by water, 178
90-30 cupronickel
  corrosion by H_3BO_3–NaOH solutions, 95
250 maraging steel
  casting, use of high-temperature dies in, 210

A

Accidents
  loss-of-coolant in water-cooled power reactors, metal–water reactions during, 32–33
Acoustic-emission testing, 69–70, 152, 217–18
Alloy 718
  welding, 215
Aluminum
  bonding to steel by use of explosive-welded inserts, 64
  corrosion by Freon-11, 95
  corrosion of powdered by diphenyl, 103–4
  corrosion by seawater, 27
  corrosion and wear surveillance in the PRTR, 27
  diffusion of Cu in, 134
  diffusion of Nb in, 198
  fluxless brazing of, 215, 217
  phase studies, 2
  reaction with H_2O during loss-of-coolant accidents in light-water power reactors, 32
Aluminum (liquid)
  solubility of C in, 185
Aluminum alloy (6061-T6)
  cavitation damage in H_2O, 95
Aluminum alloy (1100)
  corrosion by H_3BO_3–NaOH solutions, 95
  density, effects of irradiation on, 109–10
  embrittlement, effect of He on, 110
Aluminum alloy (2014)
  development of a rapid stress-corrosion test for, 25
Aluminum alloy (2024)
  development of a rapid stress-corrosion test for, 25
Aluminum alloy (2024-T3)
  rotating cyclic-strain fatigue behavior of, effect of atmosphere on, 117
Aluminum alloy (2219)
  stress corrosion in NaCl solution, 177
Aluminum alloy (2219-T37)
  stress corrosion in NaCl–$AlCl_3$ solutions, 177
Aluminum alloy (3003)
  corrosion by H_3BO_3–NaOH solutions, 95
Aluminum alloy (5052)
  corrosion by H_3BO_3–NaOH solutions, 95
Aluminum alloy (6061)
  corrosion by H_3BO_3–NaOH solutions, 95
Aluminum alloy (7039)
  development of a rapid stress-corrosion test for, 25
Aluminum alloy (7039-T6)
  stress corrosion in NaCl–$AlCl_3$ solutions, 177
Aluminum alloy (7075)
  casting, use of high-temperature dies in, 210
  stress corrosion in NaCl solution, 177
Aluminum alloy (7075-T6)
  stress corrosion in NaCl–$AlCl_3$ solutions, 177
Aluminum alloy (7075-T651)
  development of a rapid stress-corrosion test for, 25
Aluminum alloy (7079-T6)
  stress corrosion in NaCl–$AlCl_3$ solutions, 177
Aluminum alloy (7079-T651)
  development of a rapid stress-corrosion test for, 25
Aluminum alloy (X8001)
  embrittlement, effect of He on, 110
Aluminum alloys
  (see Hastelloy N, Inconel 718, Magnox Al-80, Nimonic 105, SAP, SAP-865, SAP-895, SAP-900, Udimet 700, and XAP-005)
Aluminum alloys (Al–Be)
  elastic properties of sheet, 237–38
  mechanical properties of extruded tubing of, 237–38
Aluminum alloys (Al–B–Cr–Hf–Ta)
  oxidation in air at high temperatures, 178
Aluminum alloys (Al–C–Fe–U)
  creep properties, 157–58
Aluminum alloys (Al–Cu)
  precipitation in supersaturated, effect of irradiation on, 113
  tensile properties, effect of irradiation on, 191
Aluminum alloys (Al–Hf–Ta)
  high-temperature strength properties, 45
Aluminum alloys (Al–Hf–Ta–W)
  high-temperature strength properties, 45
  oxidation tests at 1000°C, 45
Aluminum alloys (Al–Fe–U)
  microstructure of as-cast, 156
Aluminum alloys (Al–Pu)
  diffusion in, 159
  fabrication into fuel rods, 141
Aluminum alloys (Al–Ti–V)
  diffusion welds in, effect of welding temperature and pressure on strength of, 252
Aluminum alloys (Al–U)
  analysis of precipitates in, 156
  irradiation performance, 221
  microstructure of as-cast, 156
Aluminum dispersions (Al–UAl_3)
  compressive strength, 78
  plate fabrication by the picture-frame, hot-rolling technique, 8
  swelling during heat treatments, 78
Aluminum dispersions (Al–U_3O_8)
  compressive strength, 78
  plate fabrication by the picture-frame, hot-rolling technique, 8
  swelling during heat treatments, 78
Aluminum oxide (Al_2O_3)
  brazing, 253
  brazing to Cu, 253
  brazing to Nb–Zr alloy, 215
  chemical plating with Cr_7C_3, 250
  chemical-vapor deposition of, 250
  corrosion by K vapor, effects of Si on, 30
  plating of tubes with Nb, 63
  pressure bonding to Nb, 62
  properties of pressed-forged polycrystalline, 131
  reaction with ThO_2, 164–65
  room-temperature fracture studies of polycrystalline, 131–32
  sintering, application of a microwave-stimulated electrodeless gas discharge to, 55
  Young's modulus, fracture stress and fracture strain of commercially available, 55
Aluminum oxide systems (Al_2O_3–ZrO_2)
  phase studies, 132
Aluminum systems
  (see K-Monel and Nimonic 80A)
Aluminum systems (Al–C–Fe–Si–U)
  precipitation of UAl_3 from 350 to

This index was prepared by Theodore F. Davis of AEC's Division of Technical Information Extension, Oak Ridge, Tenn.

600°C, kinetics of, 73–74
Aluminum systems (Al–C–Fe–Si–U) (Zircaloy-2 clad)
corrosion of beta heat-treated by water at 282°C, 73
Aluminum systems (Al–C–Fe–U)
microstructure of as-cast, 156
Aluminum systems (Al–C–Si–U)
microstructure of as-cast, 156
Aluminum systems (Al–C–U)
microstructure of as-cast, 156
Aluminum systems (Al–Cr–Si–U)
irradiation swelling, 83–84
Aluminum systems (Al–Hf–Nb–N–Ti–W–Zr)
high-temperature strength properties, 45
oxidation tests at 1000°C, 45
Aluminum systems (Al–Fe–Si–U)
alpha-to-beta transition temperature, 73
microstructure of as-cast, 156
structural properties, 73
Aluminum systems (Al–Mo–Si–U)
irradiation swelling, 83–84
Aluminum systems (Al–Si–U)
microstructure of as-cast, 156
Americium hydroxide
electrodeposition of, 64
Arsenical admiralty
corrosion by water, 178
ASTAR 811C
creep properties, 122

B

Barium
diffusion coefficient for H_2 in, 93
diffusion of H_2 in, 199
diffusion in pyrolytic graphite, 16
heat of solution of BaH_2 in, 93
solubility of BaH_2 in, 93
Barium fluoride (BaF_2)
trapping of Xe in, effect of bombardment temperature on, 167
Barium hydride (BaH_2)
heat of solution in Ba, 93
solubility in Ba, 93
Beryllium
annealing of hot-pressed irradiated, gas behavior during, 172
annealing of radiation damage, 89–90
brazing, 91, 216–17
cleavage-crack initiation and propagation in monocrystals of, energy requirement for, 173
corrosion by CO_2, 240–41
corrosion by sodium chloride solution, 91
corrosion by water vapor, 19, 91
corrosion protection with anodized and aluminized coatings, 91
corrosion protection by chemical-conversion coatings, 241
diffusion of C, N, and O in, frequency factors and activation energies for, 51
ductile–brittle behavior, 17–18
effect of improved purity on mechanical properties of wrought polycrystalline sheets, 173–74
elastic constants, 17–18
electron-beam welding, 91
grain size in rolled commercial plate, effect of rapid heating and cooling on, 89
irradiation damage, 89–90, 241–42
microplastic characteristics of hot isostatically and isoforged, 237
physical metallurgy of, book on, 172
plastic deformation of monocrystals at 4.2 to 300°K, 173
powder metallurgy, effect of particle size on the physical properties of press-forged, 18–19
preparation by hot isostatic pressing of powders, 239–40
pressure-sintering of powers, 90–91
stress corrosion in aqueous-salt environments, 91
spark sintering of powders, 240
Beryllium (2-pass zone-leveled SR-Grade)
deformation of single crystals under high pressure, 173
Beryllium (12-pass zone-leveled SR-Grade)
deformation of single crystals under high pressure, 173
Beryllium (A)
mechanical properties of tubing, 90
Beryllium (AMS-7902)
fracture toughness, effect of temperature and strain rate on, 18
Beryllium (B)
mechanical properties of tubing, 90
Beryllium (Berylco Grade Super PEL)
dimensional stability and microplastic properties of, 172–73
Beryllium (bicrystal)
ductile–brittle behavior, 17
Beryllium (BL)
mechanical properties of tubing, 90
Beryllium (Brush Grade I-1400)
dimensional stability and microplastic properties of, 172–73
Beryllium (molten)
development of crucibles for, 60
Beryllium (polycrystalline)
hardness, effect of grain size on, 237, 239
self-diffusion in, study by using ^7B isotope, 18
Beryllium (PS)
mechanical properties of tubing, 90
Beryllium (S-200)
thermal conductivity, 241
Beryllium (SR Grade)
deformation of single crystals under high pressure, 173
Beryllium (zone purified)
flow and fracture characteristics of, 17
Beryllium alloys
elastic constants, 17–18
flow and fracture characteristics of, 17
Beryllium alloys (Al–Be)
elastic properties of sheet, 237–38
mechanical properties of extruded tubing of, 237–38
Beryllium alloys (Be–Cu)
recrystallization studies, 18
Beryllium alloys (Be–Ni)
recrystallization studies, 18
Beryllium boride
diffusion in, frequency factors and activation energies for, 51
Beryllium carbide
diffusion in, frequency factors and activation energies for, 51
Beryllium composites (Al–Be)
fabrication by powder metallurgy, 211–12
Beryllium oxide
diffusion in, frequency factors and activation energies for, 51
Beryllium oxide (BeO)
corrosion by K vapor, effects of Si on, 30
reaction with ThO_2, 164–65
sintering, application of a microwave-stimulated electrodeless gas discharge to, 55
Beryllium oxide dispersions (BeO–UO_2)
irradiation effects on physical properties of, 92
retention of fission products, 92
Bibliographies
on impurity diffusion in oxides, 51
on ionic self-diffusion in simple oxides, 51
on the permeation and diffusion of N, O, and rare gases through stainless steel, 53
Bismuth
deposition on metals by evaporation-abetted bias sputtering, 63
Bismuth (liquid)
solubility of Th in, 185
Books
on physical metallurgy of Be, 172
on physical properties of graphite, 89
Borides
(see also specific borides)
properties of plasma sprayed, 126
Boron
conversion of low-density amorphous type to high-density, high-purity crystalline powder, 22
mechanical properties, improvement by coating with SiC and TiC, 23
packing characteristics of irregularly shaped crystalline particles, 22
Boron alloys
(see Hastelloy N)
Boron alloys (Al–B–Cr–Hf–Ta)
oxidation in air at high temperatures, 178
Boron alloys (B–Mo–W)
phase studies, 127
Boron alloys (B–U)
grain-refining effects and transformation kinetics of, 73–74
Boron carbide
irradiation swelling, 93–94
Boron carbide (B_4C)
compatibility with liquid Na, 245–46
evaluation for use in fast reactors, 23
mechanical properties, improvement by coating with SiC and TiC, 23
reaction with liquid Na, 184
Boron carbide (PyC coated)
irradiation swelling, 93–94
Boron carbide systems (B_4C–UO_2)
irradiation testing, 175–76
Boron nitride (BN)
chemical plating with Al, Cu, Au, La, or Ag, 249
Brass
corrosion by Freon-11, 95
Brass (metastable beta)
effect of irradiation on martensitic transformation in, 44
Brazing, 67–68, 150–51, 215–17, 253–54

C

C-129Y
corrosion by liquid K, 186
development of aluminide and silicide coatings for oxidation protection of, 179
Cadmium
deposition on metals by evaporation-abetted bias sputtering, 63
Cadmium alloys (Cd–In–Ag)
performance as control-rod material, 245

Calcium fluoride (CaF_2)
trapping of Xe in, effect of bombardment temperature on, 167
Carbon
solubility in liquid Al, Pb, and Sn, 185
solubility in liquid Na, 184
Carbon (pyrolytic)
(see Graphite (pyrolytic))
Carbon composites
preparation by arc-melting and centrifugal casting, 203
tensile properties, 203–4
Carbon composites (NbC–C)
thermal expansion, 204
Carbon composites (ZrC–C)
thermal expansion, 204
Carbon steel
corrosion by H_3BO_3–NaOH solutions, 95
Carbon systems
(see ASTAR 811C, Croloy, D-43, HP-9Ni-4Co-0.2C, K-Monel, Monel 400, Nimonic 80A, Su-16, T-222, TZC, TZM, Vanstar-7, and Vanstar-9)
Carbon systems (Al–C–Fe–Si–U)
precipitation of UAl_2 from 350 to 600°C, kinetics of, 73–74
Carbon systems (Al–C–Fe–Si–U)(Zircaloy-2 clad)
corrosion of beta heat-treated by water at 282°C, 73
Carbon systems (Al–C–Fe–U)
creep properties, 157–58
microstructure of as-cast, 156
Carbon systems (Al–C–Si–U)
microstructure of as-cast, 156
Carbon systems (Al–C–U)
microstructure of as-cast, 156
Carbon systems (C–Cr–V)
phase studies, 126
Carbon systems (C–Hf–Mo)
tensile properties at high temperatures, 200–1
Carbon systems (C–Hf–Ta–W–Zr)
oxidation in air, formation of protective coating during, 180
Carbon systems (C–Hf–W)
strength and ductility of, effect of composition, heat-treatment and substructure on, 123
Carbon systems (C–Fe)
radiation-induced increase in yield strength, effect of C content on, 44
Carbon systems (C–Fe–Si–U)
microstructure of as-cast, 156
Carbon systems (C–Fe–U)
microstructure of as-cast, 156
Carbon systems (C–Mo–Nb)
phase diagrams, 126
Carbon systems (C–N–O–U)
phase studies, 81
Carbon systems (C–N–Pu)
studies, 77
Carbon systems (C–N–U)
studies, 77
Carbon systems (C–O–Pu)
phase studies, 77
Carbon systems (C–O–Th)
phase studies, 81
Carbon systems (C–Pu)
phase studies, 161, 224
Carbon systems (C–Si–U)
microstructure of as-cast, 156
Carbon systems (C–Mo–Ta)
phase diagrams, 126
Carbon systems (C–U)
grain-refining effects and transformation kinetics of, 73–74
microstructure of as-cast, 156
Carbon systems (C–U–V)
phase studies, 10
Carbon systems (C–U–Zr)
phase studies, 227
Carbon systems ((Pu,U)–C–N)
studies, 77
Cb-132M
development of aluminide and silicide coatings for oxidation protection of, 179
Cb-752
creep–rupture properties, effect of annealing on, 122
development of aluminide and silicide coatings for oxidation protection of, 179
oxidation behavior of Cr–$MoSi_2$ coated, 180
oxidation in air, effect of LiO_2 additions on, 98
Ceramic fibers
thermal properties of Dynaquartz, Dynaflex, and sapphire wood, 54–55
Ceramic oxides
diffusion mechanisms in, 55
Ceramics
joining to other materials, 215
Cerium alloys (Ce–Co–Pu)(liquid)
irradiation studies, 3
Cerium alloys (Ce–Pu)
Ce diffusion in, 75, 133
Cerium carbide systems (CeC–UC–ZrC)
phase studies, 9
Cerium oxide (CeO_2)
reaction with ThO_2, 164–65
Cesium
diffusion in pyrolytic graphite, 16
Cesium (liquid)
corrosive properties, 103
Cesium (vapor)
erosive effects on turbine buckets, 30
Cesium-137
encapsulation for long-term storage, use of inertia welding for, 252
Cesium iodide (CsI)
diffusion of ^{133}X in, 199
Chromium
creep properties, 46
diffusion in, bibliography on, 132
diffusion in Ti, 134
effect of irradiation on NDT of, 43
effect of irradiation on thermal hardening of, 43
relative partial molar enthalpy in liquid Pu, 3
solubility in liquid Pu, 3
Chromium alloys
(see DH-242, HA-25, Hastelloy C, Hastelloy N, Hastelloy X, Haynes 25, Haynes 188, IN-800, Incoloy 600, Inconel 600, Inconel 625, Inconel 718, L-605 superalloy, Multimet, Nimonic 105, S-1, SANDVIK 12R7 2HV, TD-nickel-Cr, and Udimet 700)
Chromium alloys (Al–B–Cr–Hf–Ta)
oxidation in air at high temperatures, 178
Chromium alloys (Cr–Co)
oxidation behavior, 97
Chromium alloys (Cr–Co–Fe–Mo–Ni–W)
tensile properties of irradiated, effect of Ti additions on, 189–90
Chromium alloys (Cr–Fe–Ni)
effect of irradiation on the superplasticity of, 39
stress-corrosion cracking, "straining"-electrode experiments on, 26
tensile properties, effect of irradiation on, 190–91
Chromium alloys (Cr–Fe–Zr)
beta to alpha transformation temperature of, effect of cooling rate on, 119
development, 48
hardenability, effect of cooling rate on, 193
Chromium alloys (Cr–Mo)
corrosion in high-temperature water, 178
Chromium alloys (Cr–Nb–Zr)
creep properties in air, 48–49
development, 48–49
effect of irradiation on tensile properties of annealed, 34–35
Chromium alloys (Cr–Ti)
diffusion of Cr, Fe, and W in, 198
Chromium alloys (Cr–Ti–V)
burst properties of tubes, effect of irradiation on, 110
compatibility with PuC–UC fuels, 161–62
compatibility with PuO_2–UO_2 systems, 78
corrosion by liquid Na, 28
preparation of high purity, 60
preparation of ingots of, 210–11
Chromium alloys (Cr–U)
grain-refining effects and transformation kinetics of, 73–74
Chromium boride (CrB_2)
irradiation damage, 22–23
Chromium carbide (Cr_3C_2)
chemical deposition of, 250
integral and partial configuration entropies for solid solutions of, 127
structure and hardness, effect of high pressure on, 204
Chromium oxide (Cr_2O_3)
corrosion of powdered by diphenyl, 103–4
Chromium oxide systems (Cr_2O_3–TiO_2)
phase studies, 55
Chromium oxide systems (Cr_2O_3–ZrO_2)
phase studies, 55
Chromium systems
(see Croloy, Nimonic 80A, and Vanstar-7)
Chromium systems (Al–Cr–Si–U)
irradiation swelling, 83–84
Chromium systems (C–Cr–V)
phase studies, 126
Chromium systems (Cr–O)
phase studies, 132
Cladding materials, 25–55, 95–135, 177–205
Cobalt-60
diffusion in Co and Inconel 600, 134–35
Cobalt alloys
(see HA-25, Hastelloy C, Haynes 25, Haynes 188, Haynes Stellite 25, Kovar, L-605 superalloy, Nimonic 105, S-1, Udimet 700, and UMCO 51)
Cobalt alloys (Ce–Co–Pu)(liquid)
irradiation studies, 3
Cobalt alloys (Cr–Co)
oxidation behavior, 97
Cobalt alloys (Cr–Co–Fe–Mo–Ni–W)
tensile properties of irradiated, effect of Ti additions on, 189–90
Cobalt alloys (Co–Gd)
phase diagram, 245
Cobalt systems
(see HP-9Ni-4Co-0.2C)
Computer codes
for analyzing irradiation damage in metals, 11–12
Concrete
creep, strength and elastic properties at elevated temperatures, 54

use for reactor pressure vessels, 205
Concrete (portland cement)
thermal properties, effect of moisture content on, 130–31
Conferences and meetings
on nondestructive testing of graphite, 17
on radiation effects on metals, 33
on the use of Zircaloy and zirconium alloys in the Nuclear Reactors at Marianske Lazne, Czechoslovakia, 34
Control materials, 22–23, 93–94, 175–76, 245–47
Copper
brazing to Al_2O_3, 253
corrosion by Freon-11, 95
corrosion by H_3BO_3–NaOH solutions, 95
corrosion by seawater, 27
diffusion in Al, 134
diffusion in Tl, 134
effect of irradiation on elevated-temperature ductility of, 38
irradiation damage, 114
irradiation damage, effect of impurities on pinning, 44
precipitation in supersaturated, effect of irradiation on, 113
solubility in liquid Na, 29–30
tensile properties, effect of irradiation on, 191
welding to Mo, Ta, and stainless steel, 252–53
Copper alloys
(see 70/30 cupronickel, 9/10 cupronickel, and 90/30 cupronickel)
Copper alloys (Al–Cu)
tensile properties, effect of irradiation on, 191
Copper alloys (Be–Cu)
recrystallization studies, 18
Copper alloys (Cu–Fe–Zr)
corrosion by steam, effects of radiation on, 177
Copper alloys (Cu–Mg)
tensile properties, effect of irradiation on, 191
Copper alloys (Cu–Mo–Zr)
diffusion of Mg in, effect on tensile properties of, 52
Copper alloys (Cu–Nb–Zr)
in-pile relaxation behavior, 34
Copper alloys (Cu–Zr)
diffusion of O in, 52
transformation characteristics of, 49
Copper oxide (Cu_2O)
preparation of single crystals of, 249
Copper systems
(see Aluminum alloy (2024-T3), K-Monel, and Monel 400)
Copper systems (Cu–Si)
effect of irradiation on elevated-temperature ductility of, 38
Cor-Ten
corrosion in high-temperature water, 178
Croloy
corrosion by Na–H_2O reaction products, 181
Crucibles
coatings for, 2–3
Crystals (metal)
irradiation damage, basic studies of, 11–12

D

D-43
corrosion by liquid K, 186
development of aluminide and silicide coatings for oxidation protection of, 179
rupture strength, effect of heat treatment on, 121–22
Deuterium systems (Er–D)
thermodynamic properties, 20–21
DH-242
oxidation behavior of, effects of stress, thermal cycling, and isothermal exposure on, 97
Diffusion studies, 51–53, 132–35, 196–200
Diffusion Information Center
publications, 51
Diphenyl
corrosive properties, 103–4
Dynaflex
thermal properties, 54–55
Dynaquartz
thermal properties, 54–55

E

Eddy-current testing, 69, 152, 217–18
Erbium hydride (ErH_2)
crystal structure, 20
Erbium hydride (ErH_3)
crystal structure, 20
Erbium oxide (Er_2O_3)
diffusion of ^{169}Er in, 53
Erbium systems (Er–D)
thermodynamic properties, 20–21
Erbium systems (Er–H)
phase studies, 20
thermodynamic properties, 20–21
Europium
diffusion in pyrolytic graphite, 16
Europium carbide (EuC_2)
preparation and properties, 246–47
Europium oxide dispersions (Eu_2O_3–stainless steel)
performance as control-rod material in SM-1A Reactor, 176
Explosive metalworking, 64, 147–48, 214, 251
Extrusion
apparatus for, 61

F

F-48
development of $NbSi_2$–Fe–Cr glaze coating for oxidation protection of, 179–80
Fabrication techniques (special), 60–70, 141–52, 210–18, 248–55
Ferrovac Fe
radiation-induced increase in yield strength, effect of C content on, 44
Fission
rate measurements with solid-state track records, 84
Fissium alloys (fissium–Pu–U)
high-burnup properties, 75
Fluoride salts
structural materials for use with, 32
Freon-11
corrosive properties, 95
FS-85
rupture strength, effect of heat treatment on, 121–22
Fuel elements (ceramic)
fabrication of $U_3C_2Si_2$, 141
irradiation damage, basic studies of, 12–13
Fuel elements (metal)
irradiation damage, computer programs for analyzing, 11–12
Fuel elements (U, Zircaloy-2-clad)
irradiation swelling, effect of axial hole in, 73
Fuel elements (Zr clad)
production of, French patent on, 60–61
Fuel and fertile materials, 1–13, 73–85, 155–67, 221–33

G

Gadolinium alloys (Co–Gd)
phase diagram, 245
Gadolinium oxide (Gd_2O_3)
reaction with HfO_2, 176
Gallium alloys (Ga–Pu)
Ga diffusion in, 75
growth of large crystals by using a modified Bridgeman technique, 2
Gallium alloys (liquid)(Ga–Pu)
solubility of Nb in, 158–59
GE2541
corrosion by air at 1000°C, 26–27
Germanium
preparation of single crystals of, 249
Graphite
area density, nondestructive measurement of the fluctuations in, 16
brazing, 253
evaluation of various types for superheat service in reactor cores, 16
growth of large high-quality single crystal of, 89
irradiation damage in isotropic, 171
joining to other materials, 215
manufacturing methods for, 89
mechanical properties, survey of, 89
nondestructive testing, symposium on, 17
orientation of crystallites in polycrystalline, development of densitometer for quick measurement of, 171
physical properties, book on, 89
pressure bonding to Fe, Mo, Ta, W, and Zr, 62
production and properties, 236–37
production from organic materials, effect of heteroatoms on thermal-expansion coefficient of, 171
reaction with liquid Na, effects of irradiation, 183–84
triple points for AGKS, AGOT, AGSR, and LANG, 16–17
use in Rover reactor cores, power-density and thermal-stress limitations for, 17
vaporization characteristics between 2500–3000°K, 236
Graphite (pyrolytic)
chemical deposition on fuel particles, 250–51
coatings on fuel particles, irradiation testing of, 89
creep properties during irradiation, 89
diffusion of Ba, Cs, Eu, and Sr in, 16
fission-fragment damage, 171
optical anisotropy of, effect of surface texture on, 172
oxidation by He–H_2O mixtures, 16
production and properties, 236–37
Graphite composites (NbC–graphite)
mechanical and physical properties, 202–3
Graphite composites (HfC–graphite)
mechanical properties, 204

Graphite composites (TiC-graphite)
mechanical properties, 204
Graphite composites (ZrC-graphite)
mechanical properties, 204
Graphite dispersions (UC–graphite)
fabrication, 228

H

HA-25
corrosion by liquid Na, effect of temperature on, 181
Hafnium
diffusion in, bibliography on, 132
diffusion of C, N, and O in, frequency factors and activation energies for, 51
recrystallization behavior, 22
self-diffusion in, 52
solubility in liquid Li and K, 185
symposium on fabrication and properties of, 117
Hafnium alloys
(see also C-129Y, T-111, and T-222)
symposium on fabrication and properties of, 117
Hafnium alloys (Al–B–Cr–Hf–Ta)
oxidation in air at high temperatures, 178
Hafnium alloys (Al–Hf–Ta)
high-temperature strength properties, 45
Hafnium alloys (Al–Hf–Ta–W)
high-temperature strength properties, 45
oxidation tests at 1000°C, 45
Hafnium alloys (Hf–Nb–Ti–Zr)
high-temperature strength properties, 45
Hafnium alloys (Hf–Nb–W–Zr)
high-temperature strength properties, 45
Hafnium alloys (Hf–Pu)
phase diagram, 159–60
Hafnium boride (HfB_2)
diffusion in, frequency factors and activation energies for, 51
properties of, effect of ceramic additives on, 132
Hafnium boride systems (HfB_2–HfC)
mechanical properties at elevated temperatures, 175
Hafnium carbide (HfC)
compatibility with various refractory metals, 123–24
diffusion in, frequency factors and activation energies for, 51
elastic properties, 205
integral and partial configuration entropies for solid solutions of, 127
mechanical properties at elevated temperatures, 175
microhardness of, effect of stoichiometry on, 127, 129
yield strength of, 127, 130
Hafnium carbide cermets (Mo–Re–HfC)
properties, 124–25
Hafnium carbide composites (HfC–C)
preparation by arc-melting and centrifugal casting, 203
tensile properties, 203–4
Hafnium carbide composites (HfC-graphite)
mechanical properties, 204
Hafnium carbide composites (HfC–Mo)
melting temperature, 204
Hafnium carbide composites (HfC–Nb)
melting temperature, 204
Hafnium carbide composites (HfC–Ta)
melting temperature, 204
Hafnium carbide composites (HfC–Ti)
melting temperature, 204
Hafnium carbide composites (HfC–W)
melting temperature, 204
Hafnium carbide composites (HfC–V)
melting temperature, 204
Hafnium carbide composites (HfC–Zr)
melting temperature, 204
Hafnium carbide systems (HfB_2–HfC)
mechanical properties at elevated temperatures, 175
Hafnium carbide systems (HfC–VC)
phase diagrams, 126
Hafnium carbide systems (HfC–TiC–ZrC)
miscibility gaps in, 126
Hafnium nitride (HfN)
compatibility with various refractory metals, 123–24
Hafnium nitride systems (HfN–UN)
phase studies, 9–10
Hafnium oxide
diffusion in, frequency factors and activation energies for, 51
Hafnium oxide (HfO_2)
compatibility of Y_2O_3 stabilized with various refractory metals, 123–24
reaction with Gd_2O_3, 176
sintering, application of a microwave-stimulated electrodeless gas discharge to, 55
Hafnium oxide systems (HfO_2–Sm_2O_3)
phase studies, 23
Hafnium oxide systems (HfO_2–ZrO_2)
phase studies, 94
Hafnium systems (Al–Hf–Nb–N–Ti–W–Zr)
high-temperature strength properties, 45
oxidation tests at 1000°C, 45
Hafnium systems (C–Hf–Mo)
tensile properties at high temperatures, 200–1
Hafnium systems
(see ASTAR 811C, SU-16, and T-222)
Hafnium systems (C–Hf–Ta–W–Zr)
oxidation in air, formation of protective coating during, 180
Hafnium systems (C–Hf–W)
strength and ductility of, effect of composition, heat-treatment and substructure on, 123
radiation contraction of, 16
Hastelloy C
corrosion by air at 1000°C, 26–27
corrosion by liquid K, 30
corrosion by seawater, 27
Hastelloy N
corrosion by air, inhibition by Si and Ti additions to, 26
corrosion by liquid K, 30
creep strength, effect of Ti additions on, 50
diffusion of Ti in, 197–98
stress–rupture properties of irradiated, effect of Hf, W, and Ti additions on, 191
welding of, 214–15, 252
Hastelloy X
brazing, 68
corrosion by air at 705 to 1095°C, properties of film formed on, 26
corrosion by air at 1000°C, 26–27
corrosion by liquid K, 30
evaluation as fuel-cladding materials for the LMFBR, 29
microstructure stability at high temperatures, 50
oxidation behavior of, effects of stress, thermal cycling, and isothermal exposure on, 97
use as PuC–UC cladding, compatibility studies, 6
Haynes 25
corrosion by air at 1000°C, 26–27
Haynes 188
effects of irradiation on tensile properties of, 40–41
Haynes Stellite 25
effects of irradiation on tensile properties of, 40–41
electrical-discharge and electrochemical machining of, effect on fatigue endurance limit of, 194
HP-9Ni–4Co–0.2C
evaluation as pressure-vessel materials, 195
HS-25
corrosion by liquid K, 30
corrosion by liquid Na, 28
corrosion by Hg vapor, 30–31
Hydrogen
permeation in metals, method for measuring, 199
Hydrogen systems (Er–H)
phase studies, 20
thermodynamic properties, 20–21
Hydrogen systems (H–Nb)
phase studies, 93, 243–44
Hydrogen systems (H–Ta)
phase diagram, 243–44
Hydrogen systems (H–U–Zr)
irradiation testing in the TRIGA Mark F Reactor, 20
pressure-temperature isochores to 1300°C for, 19–20
Hydrogen systems (H–Zr)
phase studies, 92–93

I

IN-800
corrosion by liquid Na, 180
Incoloy 600
stress–corrosion cracking in 100-psi water, inhibition by phosphate additions, 26
Incoloy 800
compatibility with PuN–UN, 70
compatibility with PuO_2–UO_2, 224
compatibility with (U,Pu)N, 162
corrosion by high-temperature steam, properties of film formed on, 26
corrosion by liquid Na, 98–99, 181
corrosion by Na–H_2O reaction products, 181
creep–rupture properties of irradiated, 188–89
effect of C and Ti content on creep properties of irradiated, 39–40
evaluation as fuel-cladding materials for the LMFBR, 29
radiation-induced density changes in, 108–9
rupture properties, effect of irradiation on, 106–7
tensile properties, effect of He impregnation on, 107
use as PuC–UC cladding, compatibility studies, 6
Inconel 600
corrosion by air at 1000°C, 26–27
corrosion by high-temperature steam, properties of film formed on, 26
corrosion in high-temperature water, 178
corrosion by H_3BO_3–NaOH solutions, 95
diffusion of ^{60}Co in, 134–35
electrical-discharge and electrochem-

ical machining of, effect on fatigue endurance limit of, 194
stress–corrosion cracking in 100-psi water, inhibition by phosphate additions, 26
welding, 215
Inconel 625
compatibility with PuN–UN, 7
evaluation as fuel-cladding materials for the LMFBR, 29
rupture properties, effect of irradiation on, 106–7
Inconel 718
brazing, 67–68
corrosion by H_3BO_3–NaOH solutions, 95
evaluation as pressure-vessel materials, 195
mechanical properties, survey of, 195
Inconel X750
effect of irradiation on the impact properties of, 39–40
electrical-discharge and electrochemical machining of, effect on fatigue endurance limit of, 194
Indium alloys (Cd–In–Ag)
performance as control-rod material, 245
Insulating material (thermal)
thermal properties of ceramic fibers, 54
Iridium
chemical deposition on quartz plates, 63
Iron
corrosion of powdered by diphenyl, 103–4
electron-beam floating-zone-melting apparatus for rods of, 249
irradiation damage, mechanisms, 191–92
irradiation damage in various reactors, 114
irradiation hardening of single crystals, effect of C content on, 114–15
phase studies, 2
pressure bonding to graphite, 62
radiation damage, effect of cold working on, 44
radiation-induced increase in yield strength, effect of C content on, 44
solubility in liquid Na, 184
work-hardening coefficient of, effect of irradiation on, 112
Iron (alpha)
in-pile creep tests on, 33–34
Iron alloys
(see HA-25, Hastelloy N, Hastelloy X, Haynes 25, IN-800, Incoloy 600, Kovar, and L-605 superalloy)
Iron alloys (Al–Fe–U)
microstructure of as-cast, 156
Iron alloys (Cr–Co–Fe–Mo–Ni–W)
tensile properties of irradiated, effect of Ti additions on, 189–90
Iron alloys (Cr–Fe–Ni)
effect of irradiation on the superplasticity of, 39
stress–corrosion cracking, "straining"-electrode experiments on, 26
Iron alloys (Cr–Fe–Zr)
beta to alpha transformation temperature of, effect of cooling rate on, 119
development, 48
hardenability, effect of cooling rate on, 193
Iron alloys (Cu–Fe–Zr)
corrosion by steam, effects of radiation on, 177
Iron alloys (Fe–Th)
cracking during fusion welding, effect of Mo addition on, 162
Iron alloys (Fe–Ti)
reaction with H_2, 244–45
Iron alloys (Fe–U)
microstructure of as-cast, 156
Iron systems
(see Aluminum alloy (2024-T3, Croloy, Hastelloy C, Inconel 718, Inconel 625, Inconel 600, Monel 400, Multimet, Vanstar-7, and Vanstar-9)
Iron systems (Al–C–Fe–Si–U)
precipitation of UAl_2 from 350 to 600°C, kinetics of, 73–74
Iron systems (Al–C–Fe–Si–U)(Zircaloy-2 clad)
corrosion of beta heat-treated by water at 282°C, 73
Iron systems (Al–C–Fe–U)
creep properties, 157–58
microstructure of as-cast, 156
Iron systems (Al–Fe–Si–U)
alpha-to-beta transition temperature, 73
microstructure of as-cast, 156
structural properties, 73
Iron systems (C–Fe)
radiation-induced increase in yield strength, effect of C content on, 44
Iron systems (C–Fe–Si–U)
microstructure of as-cast, 156
Iron systems (C–Fe–U)
microstructure of as-cast, 156
Iron systems (Fe–Si–U)
microstructure of as-cast, 156

K

K-Monel
cracking of bolt studs on autoclaves and pumps, causes of, 27
Kovar
electron-beam welding to 321 stainless steel, 65
welding to 321 stainless steel, 253

L

L-605 superalloy
brazing, 68
oxidation behavior from 1000 to 2000°C, 97
Lanthanum boride (LaB_6)
irradiation damage, 22–23
Lead
deposition on metals by evaporation-abetted bias sputtering, 63
electron-beam floating-zone-melting apparatus for rods of, 249
explosive bonding to stainless steel, 64
Lead (liquid)
solubility of C in, 185
structural materials for use with, 32
Lead intermetallic compounds ($PuPb_2$)
identification in Pu–Pb alloys, 75
Lead intermetallic compounds ($PuPb_3$)
identification in Pu–Pb alloys, 75
Lead intermetallic compounds (Pu_3Pb)
identification in Pu–Pb alloys, 75
Lead intermetallic compounds (Pu_5Pb_3)
identification in Pu–Pb alloys, 75
Lead intermetallic compounds (Pu_5Pb_4)
identification in Pu–Pb alloys, 75
Lead iodide
irradiation damage, computer simulation of, 11
Lithium
corrosive properties, 103
Lithium (liquid)
solubility of Hf, Mo, Nb, Re, Ta, and Zr in, 185
Low-silicon bronze
corrosion by water, 178
Lutetium
diffusion of C, N, and O in, 53
Lutetium oxide systems (Lu_2O_3–PuO_2)
phase studies, 77

M

Magnesium
corrosion by organic coolants, inhibition by NH_4OH and CO_2, 32
creep properties of compacted powders of, 47
deposition on metals by evaporation-abetted bias sputtering, 63
Magnesium alloys
(see also Magnox Al-80)
corrosion by organic coolants, inhibition by NH_4OH and CO_2, 32
Magnesium alloys (Cu–Mg)
tensile properties, effect of irradiation on, 191
Magnesium oxide (MgO)
fracture stress of polycrystalline, effect of water vapor on, 132
reaction with ThO_2, 164–65
room-temperature fracture studies of polycrystalline, 131
sintering, application of a microwave-stimulated electrodeless gas discharge to, 55
trapping of Xe in, effect of bombardment temperature on, 167
Young's modulus of polycrystalline, effect of water vapor on, 132
Magnesium systems
(see Aluminum alloy (2024-T3))
Magnox AL-80
creep properties, 47
density, effect of strain during creep testing, 117
fracture mode, effect of grain-boundary sliding on, 117
Manganese
phase studies, 2
solubility in liquid Pu, 3, 158
Manganese systems
(see Aluminum alloy (2024-T3, Nimonic 80A, Monel 400, Hastelloy C, and Hastelloy N)
Mercury (vapor)
corrosive effects on HS-25, 30–31
Metals
casting of high purity, review of methods for, 210
irradiation damage, computer programs for analyzing, 11–12
permeation of H_2 in, method for measuring, 199
radiation effects, symposia on, 33
reaction with H_2O during loss-of-coolant accidents in water-cooled power reactors, 32–33
Methyl iodide (CH_3I)
release from U and UO_2 during reactor accidents, 85
Moderator materials, 16–22, 89–93, 171–75, 236–45
Molybdenum
corrosion by liquid Na, 28
creep properties, 46
diffusion from irradiated UO_2, 226
diffusion in, bibliography on, 132

diffusion in Y, 134
diffusion in W, 133–34
diffusion of C, N, and O in, frequency factors and activation energies for, 51
dislocation-velocity measurements in high-purity single crystals, 46
effect of irradiation on carbide coatings on, 130
electrical resistance of irradiated, effect of pressure on recovery of, 113–14
electron-beam floating-zone-melting apparatus for rods of, 249
fabrication of sheets of, 248
fabrication of tube of, 61
interaction with active gases in vacua and inert gas environments, 97–98
oxidation in air, effect of LiO_2 additions on, 98
oxidation of, effect of foreign gases on kinetics of, 179
oxidation of powders in 20°C air, effect of humidity on, 98
oxygen adsorption on the (100) surface of single crystals of, 179
oxygen absorption and thermal stability of the (111) surface of, 98
pressure bonding to graphite, 62
production of ingots by electron-beam melting, 60
radiation damage, effect of cold working on, 44
radiation damage in, thermal stability of, 43–44
relative partial molar enthalpy in liquid Pu, 3
solubility in liquid Li and K, 185
solubility in liquid Pu, 3
Vickers hardness of, effect of irradiation on, 113
welding to Cu, 252–53
Molybdenum alloys
(see also Hastelloy X, Inconel 625, Inconel 718, Multimet, Nimonic 105, S-1, SANDVIK 12R7 2HV, TZM molybdenum, and Udimet 700)
corrosion by liquid Na in stainless steel pipes, 28
development of fused-silicide coatings for, 250–51
interaction with active gases in vacua and inert gas environments, 97–98
Molybdenum alloys (B–Mo–W)
phase studies, 128
Molybdenum alloys (Cr–Co–Fe–Mo–Ni–W)
tensile properties of irradiated, effect of Ti additions on, 189–90
Molybdenum alloys (Cr–Mo)
corrosion in high-temperature water, 178
Molybdenum alloys (Cu–Mo–Zr)
diffusion of Mg in, effect on tensile properties of, 52
Molybdenum alloys (Mo–Nb)
deformation of single crystals, effect of composition, orientation, and temperature on, 44–45
Molybdenum alloys (Mo–Pu–U)
fabrication in fuel elements for the Zero Power Plutonium Reactor, 249
Molybdenum alloys (Mo–Re)
compatibility with various carbides, 123–24
Molybdenum alloys (Mo–Re–W)
electron-beam welding to T-111, 64–65
Molybdenum alloys (Mo–Ti–Zr)
corrosion by liquid Na, 28
Molybdenum alloys (Mo–W)
corrosion, chemical and galvanic, 98
Molybdenum alloys (Mo–U)
corrosion by diphenyl, 104
corrosion by seawater, 27
grain-refining effects and transformation kinetics of, 73–74
irradiation swelling, 83–84
mechanical and physical properties, 158
recrystallization, effect of B on, 2
specific heat, 74
tensile properties, 2
tensile properties, effect of temperature on, 232
thermal cycling of, effects on surfaces of, 232
transformation of gamma phase on
Molybdenum alloys (Mo–U–Zr)
corrosion by H_2O, effect of composition and heat-treating on, 232
rapid cooling, 74
Molybdenum boride
diffusion in, frequency factors and activation energies for, 51
Molybdenum carbide
diffusion in, frequency factors and activation energies for, 51
integral and partial configuration entropies for solid solutions of, 127
Molybdenum cermets (Mo–Re–HfC)
properties, 124–25
Molybdenum cermets (Mo–Re–ZrC)
properties, 124–25
Molybdenum cermets (Mo–UO_2)
mechanical and thermal properties of, 8
Molybdenum composites (HfC–Mo)
melting temperature, 204
Molybdenum oxide
diffusion in, frequency factors and activation energies for, 51
Molybdenum systems
(see Croloy, SU-16, TZC, and TZM)
Molybdenum systems (Al–Mo–Si–U)
irradiation swelling, 83–84
Molybdenum systems (C–Hf–Mo)
tensile properties at high temperatures, 200–1
Monel 400
corrosion in high-temperature water, 178
corrosion by H_3BO_3–NaOH solutions, 95
Multimet
effects of irradiation on tensile properties of, 40–41

N

Neodymium alloys (Na–Pu)
phase diagram, 159
Neptunium hydroxide
electrodeposition of, 64
Neptunium oxide (NpO_2)
electrodeposition of thin films on metal surfaces, 80
Nickel
diffusion of H_2 in, activation energy for, 199
diffusion of Pu in, 197
effect of irradiation on elevated-temperature ductility of, 38
irradiation damage, 114
preparation of single crystals of, 249
solubility in liquid Na, 184
wetting by liquid Na, 181–82
Nickel (molten)
development of crucibles for, 60
Nickel alloy (15-15N)
properties of, effect of exposure to high temperature steam on, 119
Nickel alloy (16-25-6)
properties of, effect of exposure to high temperature steam on, 119
Nickel alloy (270)
cavitation damage in H_2O, 95
Nickel alloys
(see also 70/30 cupronickel, 90/10 cupronickel, 90/30 cupronickel, HA-25, Hastelloy C, Hastelloy N, Haynes 25, Haynes 188, Haynes Stellite 25, IN-800, Incoloy 600, Inconel 600, Inconel 625, Inconel 718, Kovar, L-605 superalloy, Multimet, Nimonic 105, S-1, SANDVIK 12R7 2HV, TD-nickel, TD-nickel-Cr, and Udimet 700)
corrosion by liquid Na in stainless steel pipes, 28
in-pile creep tests on, 33–34
Nickel alloys (Be–Ni)
recrystallization studies, 18
Nickel alloys (Cr–Co–Fe–Mo–Ni–W)
tensile properties of irradiated, effect of Ti additions on, 189–90
Nickel alloys (Cr–Fe–Ni)
effect of irradiation on the superplasticity of, 39
stress-corrosion cracking, "straining"-electrode experiments on, 26
tensile properties, effect of irradiation on, 190–91
Nickel systems
(see HP-9Ni-4Co-0.2C, K-Monel, Monel 400, and Nimonic 80A)
Nimonic 80A
effect of irradiation on elevated-temperature ductility of, 38
Nimonic 105
rupture properties, effect of heat treatment during testing of, 120
Niobium
adsorption-rate sticking probabilities for O_2 on, 179
chemical deposition, 250
chemical deposition on Al_2O_3 tubing, 63
corrosion by HCl, H_2SO_4, and NaOH solutions, 179
corrosion by liquid Li, 103
corrosion by liquid K containing various amounts of dissolved O_2, 101–2
creep properties, 46
diffusion bonding, 66–67
diffusion bonding to Ta, 66–67
diffusion in, bibliography on, 132
diffusion in Y, 134
diffusion of C, N, and O in, frequency factors and activation energies for, 51
effect of irradiation on carbide coatings on, 130
electron-beam floating-zone-melting apparatus for rods of, 249
electron-beam melting, contamination during, 60
interaction with active gases in vacua and inert gas environments, 97–98
oxidation in air, effect of LiO_2 additions on, 98
oxidation behavior, 97
oxidation behavior between 400 and 1000°C, 178
oxidation in dry air at 485 to 935°C, 178–79
preparation of single crystals of, 249

pressure bonding to Al_2O_3, 62
production of ingots by electron-beam melting, 60
radiation damage, effect of cold working on, 44
relative partial molar enthalpy in liquid Pu, 3
solubility in liquid Ga–Pu alloys, 158–59
solubility in liquid Li and K, 185
solubility in liquid Pu, 3
strain-aging of electron-beam refined, effect of O_2 content on, 45–46
thermodynamic analysis of the solid solution of C, N_2, and O_2 in, 123
Niobium (polycrystalline)
effect of irradiation on yield stress of, 43
Niobium alloys
(see also Cb-132M, Cb-752, C-129Y, DH-242, F-48, FS-85, Inconel 600, Inconel 625, Inconel 718, Multimet, TZM alloys (Nb–TZM), and XB-88)
development of fused-silicide coatings for, 250–51
fusion welds, hot cracking in, 251–52
interaction with active gases in vacua and inert gas environments, 97–98
metallographic features of electron-beam-melted ingots of, 141
Niobium alloys (Cr–Nb–Zr)
creep properties in air, 48–49
development, 48–49
effect of irradiation on tensile properties of annealed, 34–35
Niobium alloys (Cu–Nb–Zr)
in-pile relaxation behavior, 34
Niobium alloys (Hf–Nb–Ti–Zr)
high-temperature strength properties, 45
Niobium alloys (Hf–Nb–W–Zr)
high-temperature strength properties, 45
Niobium alloys (Mo–Nb)
deformation of single crystals, effect of composition, orientation, and temperature on, 44–45
Niobium alloys (Nb–Sn–Zr)
corrosion by steam, effects of radiation on, 177
Niobium alloys (Nb–Ta)
corrosion by K_2CO_3 solutions, 179
oxidation from 550 to 1050°C, 27
Niobium alloys (Nb–Ta–W)
rupture strength, effect of metallic carbide and boride additions on, 45
Niobium alloys (Nb–Ti–V)
creep and stress-rupture properties of, effect of Ti content on, 123
Niobium alloys (Nb–Ti–Zr)
ductility of electron-beam-melted ingots of, 141–42
Niobium alloys (Nb–W)
rupture strength, effect of metallic carbide and boride additions on, 45
self-diffusion of Nb in, 133
Niobium alloys (Nb–TZM)
stress-rupture strength, effect of fabrication variables on, 122
Niobium alloys (Nb–U)
coating with Nb, 251
tensile properties, effect of temperture on, 232
Niobium alloys (Nb–U–Zr)
corrosion by H_2O, effect of composition and heat-treating on, 232
Niobium alloys (Nb–V)
oxidation in air at 500–900°C, 179
Niobium alloys (Nb–V–Zr)
oxidation in air at 500–900°C, 179
Niobium alloys (Nb–Zr)
adsorption-rate sticking probabilities for O_2 on, 179
brazing, 68
brazing to Al_2O_3, 215
compatibility with PuN–UN systems, 78
compatibility with PuO_2–UO_2 systems, 78
corrosion by liquid Cs, 186
corrosion by liquid K, 102–3, 185–86
corrosion by liquid Rb, 186
corrosion by liquid Na, 28, 182
corrosion by steam, effects of radiation on, 177
creep properties, effects of irradiation on, 109
development, 48–49
ductility of electron-beam-melted ingots of, 141–42
evaluation as fuel-cladding materials for the LMFBR, 29
in-pile creep tests on, 33–34
oxidation in air at 500–900°C, 179
oxidation in dry air at 485 to 935°C, 178–79
strain rate dependence of the tensile flow stress of, 45
tensile properties of, effect of H_2 on, 118–19
yield strength, effect of irradiation on, 187
Niobium alloys (NbC)
yield strength of, 127, 130
Niobium boride (NbB_2)
compatibility with Re, 123–24
diffusion in, frequency factors and activation energies for, 51
preparation from Nb_2O_5, 125–26
Niobium carbide
diffusion in, frequency factors and activation energies for, 51
Niobium carbide (NbC)
compatibility with various refractory metals, 123–24
elastic properties, 205
integral and partial configuration entropies for solid solutions of, 127
preparation of ultrafine particles of, 124–25
microhardness, effect of stoichiometry on, 127, 129
structure and hardness, effect of high pressure on, 204
Niobium carbide composites (NbC–C)
thermal expansion, 204
Niobium carbide composites (NbC–graphite)
mechanical and physical properties, 202–3
Niobium carbide systems (NbC–TaC–VC)
miscibility gaps in, 126
Niobium composites (HfC–Nb)
melting temperature, 204
Niobium oxide
diffusion in, frequency factors and activation energies for, 51
Niobium oxide (NbO)
preparation of single crystals of, 249
Niobium oxide (Nb_2O_5)
corrosion of powdered by diphenyl, 103–4
diffusion of O_2 in, 27
Niobium systems (Al–Hf–Nb–N–Ti–W–Zr)
high-temperature strength properties, 45
oxidation tests at 1000°C, 45
Niobium systems (H–Nb)
phase studies, 93, 243–44
Niobium systems (Nb–O)
phase studies, 45
Nitrides
(see also specific nitrides)
properties of plasma sprayed, 126
Niobium systems
(see D-43, SU-16, and Vanstar-9)
Nitrogen systems (Al–Hf–Nb–N–Ti–W–Zr)
high-temperature strength properties, 45
oxidation tests at 1000°C, 45
Nitrogen systems (C–N–Pu)
studies, 77
Nitrogen systems (C–N–U)
studies, 77
Nitrogen systems (N–Th–U)
phase studies, 78
Nitrogen systems ((Pu,U)–C–N)
studies, 77
Nondestructive testing
acoustic-emission techniques, 69–70, 152, 217–18
eddy current, 69, 152, 217–18, 254
graphite, symposium on, 17
radiography, 218, 254–55
ultrasonic techniques, 68–69, 151–52, 217, 254

O

Oxygen
solubility in Th, 230
solubility in V, 30
Oxygen systems (C–N–O–U)
phase studies, 81
Oxygen systems (C–O–Pu)
phase studies, 77
Oxygen systems (C–O–Th)
phase studies, 81
Oxygen systems (Nb–O)
phase studies, 45
Oxygen systems (O–Pu)
liquid-miscibility gap at 2500°C, 160
metallographic and X-ray investigations in, 75
Oxygen systems (O–Pu–U)
metallographic and X-ray investigations in, 75

P

Phosphorus alloys (P–U)
grain-refining effects and transformation kinetics of, 73–74
Plating
chemical, 63–64, 145–47, 212–13, 250–51
electrolytic, 64, 213–14
Platinum
electron-beam floating-zone-melting apparatus for rods of, 249
Plutonium
alpha–beta transformation studies, 228, 230
electrical conductivity, effect of pressure on, 230
oxidation behavior between 350 to 420°C, 230
plastic deformation of alpha, effect of temperature and strain rate on, 74–75, 230
production from oxides, single unit process for, 4
self-diffusion studies, 133
Plutonium (liquid)
relative partial molar enthalpies of Cr, Mo, Nb, Ta, Tm, W, and V in, 3

solubility of Cr, Mn, Mo, Nb, Tm, Ti, and V in, 3
solubility of Mn in, 158
solubility of Ti in, 158
Plutonium alloys
phase diagrams and crystal structure of, 160
Plutonium alloys (Al–Pu)
diffusion in, 159
Plutonium alloys (Ce–Co–Pu)(liquid)
irradiation studies, 3
Plutonium alloys (Ce–Pu)
Ce diffusion in, 75, 133
thermal conductivity, 230
Plutonium alloys (fissium–Pu–U)
high-burnup properties, 75
Plutonium alloys (Ga–Pu)
Ga diffusion in, 75
growth of large crystals by using a modified Bridgeman technique, 2
solubility of Nb in, 158–59
solubility of Nb in liquids, 158–59
thermal conductivity, 230
Plutonium alloys (Hf–Pu)
phase diagram, 159–60
Plutonium alloys (Pb–Pu)
identification of $PuPb_2$, Pu_3Pb, Pu_5Pb_3, $PuPb_3$, and Pu_5Pb_4 in, 75
Plutonium alloys (Mo–Pu–U)
fabrication in fuel elements for the Zero Power Plutonium Reactor, 249
Plutonium alloys (Pu–Pr)
phase diagram, 159
Plutonium alloys (Pu–Sm)
phase diagram, 159
Plutonium alloys (Pu–Th–U)
solid solubility properties, 75
Plutonium alloys (Pu–Ti–U)
high-burnup properties, 75
Plutonium alloys (Pu–U)
irradiation swelling, effect of temperature, pressure, burnup, and composition on rate of, 4
Plutonium alloys (Pu–U–Zr)
high-burnup properties, 75
preparation by induction melting, crucible coatings for, 2–3
Plutonium alloys (Pu–Zr)
phase studies, 3
Plutonium alloys (Na–Pu)
phase diagram, 159
Plutonium carbide (PuC)
creep properties, 161–62
free energy of formation of, 77
irradiation behavior, literature survey on, 6
properties, literature survey on, 6
Plutonium carbide (PuC_2)
crystal structure, 162
Plutonium carbide (Pu_2C_3)
free energy of formation of, 77
irradiation behavior, literature survey on, 6
properties, literature survey on, 6
Plutonium carbide mixtures (PuC–Pu_2C_3)
vapor pressures of Pu from 1375 to 2000°K, 77
Plutonium carbide systems (PuC–UC)
compatibility with 316 stainless steel, 161–62
compatibility with 316L stainless steel, effect of Mo addition on, 162
compatibility with Cr–Ti–V alloy, 161–62
compatibility with various cladding materials, 6, 78
irradiation behavior, literature survey on, 6
irradiation swelling, 162
Pu losses during arc-melting, 6
preparation by the metal-methane fluidized-bed process, composition of, 6
preparation of single phase by arc-melting and hydrogen-treatment process, properties of, 6
properties, literature survey on, 6
thermal conductivity, 224
Plutonium carbide systems (PuC_2–UC_2)
phase diagram, 224–25
Plutonium carbide systems (Pu,U)C
compatibility of Na bonded with 316 stainless steel, 100–1
preparation by arc-melting, composition of, 7
Plutonium carbides
thermodynamic properties, 77
vaporization data, 77
Plutonium chloride ($PuCl_3$)
free energy of formation of, 77
Plutonium fluoride (PuF_4)
production from PuO_2, 75
Plutonium fluorides (PuF_3)
conversion to PuO_2, 4
Plutonium hydroxide
electrodeposition of, 64
Plutonium intermetallic compounds ($PuPb_2$)
identification in Pu–Pb alloys, 75
Plutonium intermetallic compounds ($PuPb_3$)
identification in Pu–Pb alloys, 75
Plutonium intermetallic compounds (Pu_3Pb)
identification in Pu–Pb alloys, 75
Plutonium intermetallic compounds (Pu_5Pb_3)
identification in Pu–Pb alloys, 75
Plutonium intermetallic compounds (Pu_5Pb_4)
identification in Pu–Pb alloys, 75
Plutonium intermetallic compounds ($PuRu_2$)
free energy of formation of, 77
Plutonium intermetallic compounds (Pu_2Zn_{17})
crystal structure, 75
Plutonium nitride (PuN)
compatibility with various cladding materials, 7
free energy of formation of, 77
Gibbs free energy of formation, 7
melting behavior as functions of temperature and N pressures, 77–78
thermodynamic properties, 7
vapor pressure, 7
Plutonium nitride systems (P,U)N
compatibility with Incoloy 800, 162
fission gas release studies, 162
irradiation swelling, 162
melting behavior, 162
nitrogen interaction, effect of irradiation on, 225
thermal conductivity, 7
vaporization, 225
Plutonium nitride systems (PuN–UN)
compatibility of Na bonded with 304 stainless steel, 7
compatibility with various cladding materials, 7, 78
irradiation behavior, 7
melting behavior as functions of temperature and N pressures, 77–78
vapor pressure, 7
Plutonium oxide (PuO)
heat of sublimation, 4–5
Plutonium oxide (PuO_2)
conversion to PuF_4, 75
dissolution methods, 4
effect of aging on the crushing strength of microspheres made by the plasma technique, 76
heat capacity of, 4
heat of sublimation, 4–5
He release from plasma spheres from 600 to 1200°C, 76
irradiation performance in BR-5, 167
irradiation swelling of pellets, 77
lattice parameter of microspheres, effect of self-irradiation damage on, 76
outgassing characteristics of, 160
plastic flow of irradiated, 160
preparation of microspheres by the sol-gel process, 76
preparation of ^{17}O and ^{18}O depleted, 223
preparation of particles by the sol-gel process, 76
preparation of spherical particles of, 4
production from PuF_3, 4
reaction of microspheres with soils, 76
release of gaseous fission products from, 77
removal of fine particulate oxide from microspheres by an elutriation process, 76
thermal diffusivity, 4
vapor-pressure isotherms of substoichiometric, 76
Plutonium oxide (Pu_2O_3)
plastic flow of irradiated, 160
Plutonium oxide systems (Lu_2O_3–PuO_2)
phase studies, 77
Plutonium oxide systems (PuO_2–ThO_2)
application as isotropic heat-source material, 77
preparation of microspheres by the sol-gel process, 76
sintering studies, 6
thermal conductivity of irradiated, 161
Plutonium oxide systems (PuO_2–UO_2)
compatibility with Ta, 224
compatibility with vanadium alloys, 161
compatibility with various cladding
compatibility with various claddings, 77–78, 224
densities of sol-gel prepared pellets of, 223
fabrication by hot pressing, 160
fabrication of pellets, 223
gas-release behavior of irradiated, effect of stoichiometry on, 161
irradiation performance of 304L stainless steel clad, 223
liquidus-solidus curves for, 224
melting heat rating of, effect of stoichiometry on, 5–6
microstructure of irradiated, effect of stoichiometry on, 161
physical and thermal properties, 75–76
preparation of microspheres by the sol-gel process, 76
preparation of pellets for FFTF fuel, 4
preparation of spheres by the sol-gel process, 160
preparation of spherical particles of, 5
shear modulus, 5
solid-fission-product behavior in, 167, 224
thermal conductivity, 5
thermal conductivity, effect of stoichiometry on, 160–61
Young's modulus, 5
Plutonium oxide systems (PuO_2–UO_2–ZrO_2)
burnup studies, 77
melting point, 77
phase studies, 77
Plutonium oxide systems (PuO_2–ZrO_2)
application as isotropic heat-source material, 77

phase studies, 224
Plutonium oxide systems (Pu,U)O_2
reduction by liquid Na containing various amounts of O_2, 100
reduction to Pu, single unit process for, 4
Plutonium phosphate (PuP)
heat capacity, 78
thermal conductivity, 78
Plutonium systems (C–N–Pu)
studies, 77
Plutonium systems (C–O–Pu)
phase studies, 77
Plutonium systems (C–Pu)
phase studies, 161, 224
vapor-pressure studies, 162
Plutonium systems (O–Pu)
liquid-miscibility gap at 2500°C, 160
metallographic and X-ray investigations in, 75
Plutonium systems (O–Pu–U)
metallographic and X-ray investigations in, 75
Plutonium systems (Pu–Th–U)
phase studies, 231
Plutonium systems ((Pu,U)–C–N)
studies, 77
Plutonium sulfide (PuS)
heat capacity, 78
thermal conductivity, 78
Poland
powder-metallurgy developments in, 61
Potassium (liquid)
corrosive properties, 30, 101–3, 185–86
solubility of Hf, Mo, Nb, Re, Ta, and Zr in, 185
solubility of V in, 185
Potassium (vapor)
corrosive properties, 30
Potassium bromide (KBr)
trapping of Xe in, effect of bombardment temperature on, 167
Powder metallurgy, 61–62, 143–45, 211–12, 248
Praseodymium alloys (Pu–Pr)
phase diagram, 159
Pressure bonding, 62–63
Pressure vessels
corrosion of EBWR, 177–78
Promethium oxide
explosive forming, 251
Pyrex glass
diffusion of D_2 in, 199–200
Pyrolytic carbon
(see Graphite (pyrolytic))
Quartz
coating with Ir and Ta, 63

R

Radiography
literature survey of neutron, 218
Rare-earth oxides
diffusion of metals in, 53
diffusion of O_2 in, 53
Reactor control rods
performance of Eu_2O_3–stainless steel dispersion, 176
Reactor fuel elements
(see also specific materials use as fuel elements)
fabrication for Masurca Reactor, 160
radiation swelling, 221
Reactor pressure vessels
production from prestressed concrete, 205
Reactors (Dresden)
fuel-element corrosion, 96
Reactors (EBWR)
pressure-vessel corrosion studies, 177–78
Reactors (FFTF)
preparation of PuO_2–UO_2 fuel particles for, 4
Reactors (Fort St. Vrain)
use of concrete pressure vessel in, 205
Reactors (LMFBR)
fuel-cladding materials for, 29
Reactors (Masurca)
fuel-element fabrication, 160
Reactors (MOSEL)
survey of structural materials for, 32
Reactors (Plutonium Recycle Test)
corrosion and wear studies on Al, stainless steel and Zircaloy, 27
Reactors (PM-2A)
fracture strength of pressure vessel, effect of irradiation on, 112–12
Reactors (PNPF)
corrosive effects of the terphenyl coolant, 31
Reactors (water cooled)
metal–water reactions during loss-of-coolant accidents, 32
Refractor carbides
(see also specific refractory carbides)
diffusion studies, 196–97
high-temperature mechanical properties of, 127
Rhenium
compatibility with various carbides, 123–24
diffusion in W, 133–34
diffusion of C in, 198
lattice parameters of single crystals, effect of irradiation on, 113
oxidation from 1127 to 2227°C at low-oxygen pressures, 27
oxidation of powders in 20°C air, effect of humidity on, 98
solubility in liquid Li and K, 185
Rhenium alloys (Mo–Re)
compatibility with various carbides, 123–24
Rhenium alloys (Mo–Re–W)
electron-beam welding to T-111, 64–65
Rhenium alloys (Re–W)
chemical-vapor deposition of sheets of, 250
chemical-vapor deposition of tubes of, 250
deformation at high temperatures, 202
mechanical properties of arc-melted, 122
preparation of tubes from, 63
tensile properties of sintered, 123
tensile properties of wrought recrystallized, 123
thermal conductivity, 200–1
Rhenium alloys (Ta–Re)
yield strength, work hardening and cleavage in, 45
Rhenium cermets (Mo–Re–HfC)
properties of, 124–25
Rhenium cermets (Mo–Re–ZrC)
properties of, 124–25
Rhenium systems
(see ASTAR 811C)
Ruthenium
diffusion beta Zr, 134
Ruthenium intermetallic compounds ($PuRu_2$)
free energy of formation of, 77

S

S-1
corrosion by liquid Na, 180
effects of irradiation on tensile properties of, 40–41
Samarium alloys (Pu–Sm)
phase diagram, 159
Samarium oxide systems (HfO_2–Sm_2O_3)
phase studies, 23
Samarium oxide systems (Sm_2O_3–ZrO_2)
phase studies, 23
SANDVIK 12R72HV
stress-rupture properties at 700°C, 194–95
Santowax OM
fretting and wear effects on SAP- and Zircaloy-clad UO_2, 31–32
oxidation tests, 31
SAP
embrittlement, effect of He on, 110
explosive welding to Zircaloy-2, 214
preparation of powders of, 248
welding, 67
SAP 865
cyclic-strain fatigue behavior of, 116–17
SAP-895
mechanical properties at high temperatures, effect of Al_2O_3 particle distribution in, 196
mechanical properties, effects of transverse extrusion on, 61
SAP 930
cyclic-strain fatigue behavior of, 116–17
Sapphire wool
thermal properties, 54–55
Silicon
preparation of single crystals of, 249
Silicon carbide (SiC)
mechanical properties of chemical vapor deposited, 205
Silicon carbide (SiC)(pyrolytic)
effects of neutron irradiation on, 205
properties of fluidized-bed deposited, 130
Silicon oxide (SiO_2)
reaction with ThO_2, 164–65
Silicon systems
(see Aluminum alloy (2024-T3) and Monel 400)
Silicon systems (Al–C–Fe–Si–U)
precipitation of UAl_2 from 350 to 600°C, kinetics of, 73–74
Silicon systems (Al–C–Fe–Si–U)(Zircaloy-2 clad)
corrosion of beta heat-treated by water at 282°C, 73
Silicon systems (Al–C–Si–U)
microstructure of as-cast, 156
Silicon systems (Al–Cr–Si–U)
irradiation swelling, 83–84
Silicon systems (Al–Fe–Si–U)
alpha-to-beta transition temperature, 73
microstructure of as-cast, 156
structural properties, 73
Silicon systems (Al–Mo–Si–U)
irradiation swelling, 83–84
Silicon systems (Al–Si–U)
microstructure of as-cast, 156
Silicon systems (C–Fe–Si–U)
microstructure of as-cast, 156
Silicon systems (C–Si–U)
microstructure of as-cast, 156
Silicon systems (Cu–Si)
effect of irradiation on elevated-temperature ductility of, 38
Silicon systems (Fe–Si–U)
microstructure of as-cast, 156

Silicon systems (Si–O)
phase studies of, 132
Silicon systems (Si–U)
analysis of precipitates in, 156
delta peritectoidal reaction in, effect of C on, 2
grain-refining effects and transformation kinetics of, 73–74
microstructure of as-cast, 156
structure, effect of fabrication and heat-treatment variables on, 158
Silver
diffusion of H_2 in, activation energy for, 199
deposition on metals by evaporation-abetted bias sputtering, 63
Silver alloys (Cd–In–Ag)
performance as control-rod material, 245
Sodium (liquid)
compatibility with B_4C, 244–45
corrosive properties, 28–30, 98–101, 180–85
reaction with UO_2, 83
solubility of Ce in, 101
solubility of Cu in, 29
solubility of C in, 184–85
solubility of Fe in, 184
solubility of Ni in, 184
solubility of N_2 in, 29–30
solubility of O_2 in, 101–2
solubility of Ag in, 101
solubility of Zn in, 101
Solids
rare-gas behavior in, 223
stability of gas bubbles in, 221–22
Special fabrication techniques, 60–70, 141–52, 210–18, 248–55
Stainless steels
compatibility with Cr- and V-stabilized UC, 10
corrosion by Na–H_2O reaction products, 181
corrosion by seawater, 27
corrosion and wear surveillance in the PRTR, 27
diffusion of Fe in, 53
effects of irradiation on, review of, 187
explosive bonding to Pb, 64
in-pile creep tests on, 33–34
permeation and diffusion of N, O, and rare gases through, 53
reaction with H_2O during loss-of-coolant accidents in light-water power reactors, 32
wetting by liquid Na, 181–82
Stainless steels (16/13 CrNi)
irradiation embrittlement of, effect of cold-working and thermomechanical treatment on, 106
rupture properties, effect of irradiation on, 106–7
Stainless steel (17-4PH)
effect of irradiation on the impact properties of, 39–40
electrical-discharge and electrochemical machining of, effect on fatigue endurance limit of, 194
Stainless steel (20/25 CrNi)
rupture properties, effect of irradiation on, 106–7
Stainless steel (304)
biaxial-stress-rupture in high-purity liquid Na, 29
compatibility with PuN–UN systems, 7, 78
compatibility with PuO_2–UO_2 systems, 78, 224
corrosion by fuel pastes of Na–UC, Na–UN, and Na–UO_2, 182
corrosion by H_3BO_3–NaOH solutions, 95
corrosion in high-temperature water, 178
corrosion by liquid Na, 28, 98–99, 181
corrosion in liquid Na, 98–99
creep measurement during irradiation, 188–89
ductility of irradiated, 188–89
effect of annealing on yield strength of irradiated, 35
effect of irradiation on yield strength of, 34–35
electrical-discharge and electrochemical machining of, effect on fatigue endurance limit of, 194
electron-beam welding, 65
evaluation as fuel-cladding materials for the LMFBR, 29
mechanical properties, 194
plasma/electron-beam welding, 65
pseudomorphs in irradiated, 192
radiation-induced cavities in, 108
radiation-induced embrittlement, 37–38
radiation-induced embrittlement of fine grained, 37
radiation-induced volume change in, 107–8
radiation swelling, 108–9
rupture properties, effect of irradiation on, 106
solubility of nitrogen in, 119–20
strain–stress properties of irradiated, 106–7
stress corrosion in boiling HNO_3–$Fe_2(SO_4)_3$–H_2SO_4, effect of explosive shocking on, 178
stress–corrosion cracking in 100-psi water, inhibition by phosphate additions, 26
stress–corrosion cracking in boiling $MgCl_2$, effect of explosive shocking on, 178
stress–rupture properties of irradiated, 187–88
stress–rupture properties in liquid Na, 181
tensile properties of cold worked and annealed after fast reactor irradiation of, 106
tensile properties of, effect of irradiation on, 106–7
use as PuC–UC cladding, compatibility studies, 6
wear resistance, improvement of, 194
Stainless steel (304L)
distribution of voids in irradiated foils, effect of thickness on, 191–92
evaluation as fuel-cladding materials for the LMFBR, 29
hydrogen embrittlement, 120, 178
wetting by liquid Na, 182
Stainless steel (310)
corrosion by high-temperature steam, properties of film formed on, 26
hydrogen embrittlement, 120, 178
properties of, effect of exposure to high temperature steam on, 119
stress corrosion in boiling HNO_3–$Fe_2(SO_4)_3$–H_2SO_4, effect of explosive shocking on, 178
stress–corrosion cracking in boiling $MgCl_2$, effect of explosive shocking on, 178
Stainless steel (316)
biaxial-stress-rupture in high-purity liquid Na, 29
brazing to Ta, 68
cavitation damage in H_2O, 95
compatibility with PuC–UC fuels, 78, 161–62
compatibility with PuN–UN, 7
compatibility with PuO_2–UO_2, 224
corrosion by H_3BO_3–NaOH solutions, 95
corrosion by liquid K, 185–86
corrosion by liquid Na, 98–99, 180
corrosion by liquid NaK, 99
effect of annealing on yield strength of irradiated, 35
effect of C content on postirradiation elongation of, at 700°C, 36
effect of C content on radiation-induced embrittlement of, 36
effect of irradiation on creep rates, 36–37
effect of irradiation on yield strength of, 34–35
evaluation as fuel-cladding materials for the LMFBR, 29
mechanical properties, 194
properties of, effect of exposure to high temperature steam on, 119
rupture properties, effect of irradiation on, 106–7
stress–rupture properties of irradiated and unirradiated, 36
stress–rupture properties in liquid Na, 181
tensile properties of, effect of irradiation on, 187–88
Stainless steel (316L)
ductility of irradiated, 188–89
radiation-induced volume change in, 108–9
Stainless steel (318)
corrosion by liquid K, 30
Stainless steel (321)
compatibility with PuO_2–UO_2, 224
corrosion by liquid Na, 28
corrosion by liquid Na, effect of temperature on, 181
electron-beam welding to Kovar, 365
evaluation as fuel-cladding materials for the LMFBR, 29
mechanical properties, 194
properties of, effect of exposure to high temperature steam on, 119
radiation-induced volume change in, 107–8
welding to Kovar, 253
Stainless steel (347)
brazing to fuel plates, 215
compatibility with PuO_2–UO_2, 224
corrosion in liquid Na, 98–99
effect of He bubbles on grain-boundary weakening and embrittlement in irradiated, 35–36
effect of irradiation on elevated-temperature ductility of, 36
evaluation as fuel-cladding materials for the LMFBR, 29
mechanical properties, 194
properties of, effect of exposure to high temperature steam on, 119
radiation-induced volume change in, 107–8
stress–rupture properties at 700°C, 194–95
stress-rupture properties of irradiated, 37
Stainless steels (348)
effect of irradiation on yield strength of, 34–35
evaluation as fuel-cladding materials for the LMFBR, 29

tensile properties of cold worked and annealed after fast reactor irradiation of, 106
Stainless steel (403)
impact strength, effect of irradiation on, 189–90
Stainless steel (405)
tensile properties, effect of He impregnation on, 107
Stainless steel (Al–Cr–Fe–Y)
corrosion by CO_2 at 800 to 1000°C, structure and composition of film formed on, 25–26
Stainless steel (Cr–Mo–Ni)
transition temperature of temper-embrittled and nonembrittled, effect of irradiation on, 111
Stainless steel (Cr–Ni)
welding to Cu, 252–53
Stainless steel (Cr–Ni–Ti)
effect of irradiation on elevated-temperature ductility of, 38
Stainless steels (austenitic)
growth of $M_{23}C_6$ particles at grain boundaries of, 119
in-pile creep tests on, 33–34
mechanical properties, effect of Nb additions on, 194
Stainless steels (Oak Ridge)
compatibility with PuN–UN, 7
Stainless steel dispersions (Eu_2O_3–stainless steel)
performance as control-rod material in SM-1A Reactor, 176
Steam
bonding to Al and Ti by use of explosive-welded inserts, 64
erosive effects on turbine buckets, 30
reaction with UO_2, 83
Steel
corrosion by Freon-11, 95
diffusion welding to Zr, 215
explosive forming, 64
Steel (0.3C–3Mo–Cr)
isothermal tempering characteristics of, effect of Cr content on, 195
Steel (7.5 Ni–Cr–Mo)
evaluation as pressure-vessel materials, 195
Steel (12Ni–5Cr–3Mo)
evaluation as pressure-vessel materials, 195
Steel (15Mo3)
radiation-induced embrittlement, 38–39
Steel (17Cr–2Ni)
corrosion by Freon-11, 95
Steel (1015)
corrosion-fatigue behavior in H_2O and NaCl solutions, 97
Steel (A-212B)
radiation-induced increase in yield strength, effect of C content on, 44
Steel (A-286)
creep rate of irradiated, effect of He content on, 188–90
Steel (A-302B)
effect of Cu and P content on the radiation-induced NDT, 41–42
irradiation embrittlement, 191
Steel (A-350LFI)
annealing of radiation-induced shift in the NDT of, 42
irradiation embrittlement, 191
Steel (A-533B)
irradiation embrittlement, 191
Steel (A-533C)
irradiation embrittlement, 191
Steel (A542)
strength, effect of welding on, 50
Steel (AS17A)
strength, effect of welding on, 50
Steel (AS17E)
strength, effect of welding on, 50
Steel (AS17F)
strength, effect of welding on, 50
Steel (ASTM A-20063T)
creep properties, effect of intermittent thermal cycling on, 195–96
Steel (austenitic)
corrosion by high-temperature steam, properties of film formed on, 26
Steel (carbon)
corrosion in high-temperature water, 178
corrosion by H_2O at 250°C with 0.1 ppm O_2, 96
graphitization and decarburization in liquid Na containing 30ppm O_2, 99–100
tempering of quenched, effect of irradiation on, 112–13
Steel (C–Mo)
effect of high-velocity steam on tube bends of, 96
Steel (Cr–Fe)
radiation-induced embrittlement, 38–39
Steels (Cr–Mo)
corrosion by Hg, 186
performance of tubes exposed to high-pressure steam, 120–21
Steel (Cr–Mo–Ni)
effect of irradiation on welded joints of, 42–43
Steel (Cr–Mo–Nb–V)
creep-rupture properties, effect of tempering temperature and C and B content of, 50
Steels (Cr–Mo–Si)
performance of tubes exposed to high-pressure steam, 120–21
Steels (Cr–Mo–Ti)
performance of tubes exposed to high-pressure steam, 120–21
Steel (ferritic)
corrosion by high temperature steam, properties of film formed on, 26
Steel (HY80)
radiation-induced increase in yield strength, effect of C content on, 44
Steel (HY80 modified)
effect of irradiation on welded joints of, 42–43
Steel (low alloy)
corrosion by CO_2 containing small amounts of CO and H_2O, 25
stress-corrosion cracking in H_2O–Co–CO_2 system, 178
Steels (low-carbon)
boron hardenability of, effect of N, Ti, and Zr on, 121
Steel (martensitic PH13 Cr–8Mo)
evaluation as pressure-vessel materials, 195
Steel (mild)
corrosion by CO_2 containing small amounts of CO and H_2O, 25
stress-corrosion cracking in H_2O–Co–CO_2 system, 178
Steels (Mo–B)
mechanical properties of, effect of V content on, 121
Steels (pressure vessel)
(see also Steel (A-302B), Steel (A-350LFI), Steel (A-533B), Steel (A-533C), and Steel (HY80 modified))
corrosion in EBWR, 177–78
fracture strength of PM-2A, effect of irradiation on, 111–12
long-time stress-rupture tests on, 50
radiation-induced shift in ductile-to-brittle transition temperature, effect of Cu and Ni content on, 111
strength, effect of welding on, 50
Strontium
diffusion in pyrolytic graphite, 16
Structural materials, 25–55, 95–135, 177–205
Strontium-90
encapsulation for long-term storage, use of inertia welding for, 252
SU-16
development of $NbSi_2$–Fe–Cr glaze coating for oxidation protection of, 179–80
rupture strength, effect of heat treatment on, 121–22
Sulfur systems
(see Monel 400)
Systems for Nuclear Auxiliary Power (SNAP-2)
corrosion of HS-25 boiler tubes by Hg vapor, 30–31
Systems for Nuclear Auxiliary Power (SNAP-21)
corrosion of components of, by seawater, 27

T

T-111
corrosion by liquid Li, 103
corrosion by liquid K, 186
creep properties, 122
drawing into cup shapes, 61
electron-beam welding to Mo–Re–W alloy, 64–65
T-222
corrosion by liquid Li, 103, 186
Tantalum
brazing, 253
brazing to 316 stainless steel, 68
chemical deposition onto quartz plates, 63
compatibility with PuO_2–UO_2 systems, 224
corrosion by liquid K containing various amounts of dissolved O_2, 101–2
corrosion of TIG welds in tubing of by NaK alloy, 183
creep properties, 46
creep–rupture properties from 1000 1650°C, 122
diffusion bonding, 66–67
diffusion bonding to Nb, 66–67
diffusion in, bibliography on, 132
diffusion of C, N, and O in, frequency factors and activation energies for, 51
diffusion of He in, 199
diffusion of W in, 198
effect of irradiation on carbide coatings on, 130
electron-beam floating-zone-melting apparatus for rods of, 249
hardness, effect of irradiation on, 110–11
interaction with active gases in vacua and inert gas environments, 97–98
oxidation in air, effect of LiO_2 additions on, 98
oxidation studies, 27–28
pressure bonding to graphite, 62

radiation damage, effect of cold working on, 44
reaction with CO, 179
relative partial molar enthalpy in liquid Pu, 3
solubility in liquid Li and K, 185
strain-aging of electron-beam refined, effect of O_2 content on, 45–46
thermodynamic analysis of the solid solution of C, N_2, and O_2 in, 123
welding to Cu, 252–53
Tantalum alloys
(see also DH-242, FS-85, T-111, and T-222)
development of fused-silicide coatings for, 250–51
interaction with active gases in vacua and inert gas environments, 97–98
Tantalum alloys (Al–B–Cr–Hf–Ta)
oxidation in air at high temperatures, 178
Tantalum alloys (Al–Hf–Ta)
high-temperature strength properties, 45
Tantalum alloys (Al–Hf–Ta–W)
high-temperature strength properties, 45
oxidation tests at 1000°C, 45
Tantalum alloys (Nb–Ta)
corrosion by K_2CO_3 solutions, 179
oxidation from 550 to 1050°C, 27
Tantalum alloys (Nb–Ta–W)
rupture strength, effect of metallic carbide and boride additions on, 45
Tantalum alloys (Ta–Re)
yield strength, work hardening and cleavage in, 45
Tantalum alloys (Ta–W)
brazed joints of, shear strength of, 215–16
creep–rupture properties from 1000 to 1650°C, 122
oxidation in air, effect of LiO_2 additions on, 98
oxidation behavior of W–Si coated, 180
Tantalum boride
diffusion in, frequency factors and activation energies for, 51
Tantalum boride (TaB_2)
compatibility with various refractory metals, 123–24
preparation from Ta_2O_5, 125–26
shrinkage behavior of power compacts in vacuum at 1100 to 2100°C, 23
Tantalum carbide (TaC)
compatibility with various refractory metals, 123–24
diffusion in, frequency factors and activation energies for, 51
elastic properties, 205
integral and partial configuration entropies for solid solutions of, 127
microhardness of, effect of stoichiometry on, 127, 129
preparation of ultrafine particles of, 124
structure and hardness, effect of high pressure on, 204
thermodynamic properties, 127–28
yield strength of, 127, 130
Tantalum carbide systems (NbC–TaC–VC)
miscibility gaps in, 126
Tantalum composites (HfC–Ta)
melting temperature, 204
Tantalum nitride (TaN)
preparation from Ta and nitrogen plasma, 126
preparation of ultrafine particles of, 125
Tantalum oxide
diffusion in, frequency factors and activation energies for, 51
Tantalum oxide (Ta_2O_5)
corrosion of powdered by diphenyl, 103–4
Tantalum systems
(see ASTAR 811C and T-222)
Tantalum systems (C–Hf–Ta–W–Zr)
oxidation in air, formation of protective coating during, 180
Tantalum systems (H–Ta)
phase diagrams, 243–44
TD-nickel
brazing, 68
oxidation behavior of, effects of stress, thermal cycling, and isothermal exposure on, 97
TD nickel-Cr
corrosion by air at 1000°C, 26–27
Technetium
electrodeposition of thin films on metal surfaces, 80
Technetium alloys (Tc–V)
phase studies, 46
Terphenyl
corrosion effects in the PNPF, 31
thermal decomposition experiments on irradiated and unirradiated, 31
Testing
nondestructive techniques, 68–70, 151–52, 217–18, 254–55
Thallium
deposition on metals by evaporation-abetted bias sputtering, 63
relative partial molar enthalpy in liquid Pu, 3
solubility in liquid Pu, 3
Thorium
diffusion of C, N_2, and O_2 in, 51–52, 162
refining by the iodide process, 8
solubility in liquid Bi, 185
solubility of O_2 in, 231
summary of fuel technology, 78
Thorium alloys
summary of fuel technology, 78
Thorium alloys (Fe–Th)
cracking during fusion welding, effect of Mo addition on, 162
Thorium alloys (Pu–Th–U)
solid solubility properties, 75
Thorium alloys (Th–U)
irradiation performance in NaK at 785°C, 166
Thorium alloys (Th–U–Zr)
irradiation swelling, 7–8
Thorium boride
diffusion in, frequency factors and activation energies for, 51
Thorium carbide
diffusion in, frequency factors and activation energies for, 51
Thorium nitride (ThN)
free energy of formation at 1000°C, 78
Thorium oxide
compatibility with various refractory metals, 123–24
diffusion in, frequency factors and activation energies for, 51
diffusion of Th in, 80
Thorium oxide (ThO_2)
diffusion of U in, 53
electrodeposition of thin films on metal surfaces, 80
preparation of SiC coated particles of, 8–9
reaction with Al_2O_3, BeO, CeO_2, MgO, SiO_2, TiO_2, and ZrO_2, 164–65
sintering, application of a microwave-stimulated electrodeless gas discharge to, 55
thermal conductivity of powdered, 163
trapping of Xe in, effect of bombardment temperature on, 167
Thorium oxide systems (PuO_2–ThO_2)
application as isotropic heat-source material, 77
preparation of microspheres by the sol-gel process, 76
sintering studies, 6
thermal conductivity of irradiated, 161
Thorium oxide system (Th–ThO_2)
phase diagram, 163–64, 231
Thorium oxide systems (ThO_2–UO_2)
diffusion of U in, 53
Thorium oxide systems ((Th,Pu)O_2)
thermal stability of particles of, 77
Thorium systems (C–O–Th)
phase studies, 81
Thorium systems (N–Th–U)
phase studies, 78
Thorium systems (Pu–Th–U)
phase studies, 231
Thorium systems (Th–ThO_2)
phase diagram, 163–64, 231
Timken alloy (16-15-6)
use as PuC–UC cladding, compatibility studies, 6
Timken alloy (16-25-6)
use as PuC–UC cladding, compatibility studies, 6
Tin
preparation of single crystals of, 249
Tin (liquid)
solubility of C in, 185
Tin alloys
(see Zircaloy-2 and Zircaloy-4)
Tin alloys (Nb–Sn–Zr)
corrosion by steam, effects of radiation on, 177
Titanium
bonding to steel by use of explosive-welded inserts, 64
corrosion by Freon-11, 95
crevice corrosion by bromide, chloride, iodide, and sulfate solutions, 27
diffusion in, bibliography on, 132
diffusion of C, N, and O in, frequency factors and activation energies for, 51
diffusion of Cr and Cu in, 134
diffusion of Cr, Fe, and W in, 198
production of ingots by electron-beam melting, 60
self-diffusion in, 52
solubility in liquid Pu, 3, 158
Titanium alloy (811)
casting, use of high-temperatures in, 210
Titanium alloys
(see also Inconel 718, Nimonic 105, SANDVIK 12R7 2HV, TZM molybdenum, and Udimet 700)
explosive forming, 64
Titanium alloys (Al–Ti–V)
diffusion welds in, effect of welding temperature and pressure on strength of, 252
Titanium alloys (Cr–Ti)
diffusion of Cr, Fe, and W in, 198
Titanium alloys (Cr–Ti–V)
burst properties of tubes, effect of irradiation on, 110
compatibility with PuC–UC fuels, 161–62
compatibility with PuO_2–UO_2 systems, 78
corrosion by liquid Na, 28
preparation of high purity, 60
preparation of ingots of, 210–11

Titanium alloys (Hf–Nb–Ti–Zr)
high-temperature strength properties, 45
Titanium alloys (Fe–Ti)
reaction with H_2, 244–45
Titanium alloys (Mo–Ti–Zr)
corrosion by liquid Na, 28
Titanium alloys (Nb–Ti–V)
creep and stress-rupture properties of, effect of Ti content on, 123
Titanium alloys (Nb–Ti–Zr)
ductility of electron-beam-melted ingots of, 141–42
Titanium alloys (Pu–Ti–U)
high-burnup properties, 75
Titanium alloys (Ti–W)
diffusion of Cr and W in, 198
phase studies, 46
Titanium alloys (Ti–U)
tensile properties, effect of temperature on, 232
Titanium alloys (Ti–V)
compatibility with PuC–UC systems, 78
compatibility with PuO_2–UO_2 systems, 78
corrosion by liquid Na, 28
creep and stress-rupture properties of, effect of Ti content on, 123
effect of irradiation on creep properties of, 41
preparation of ingots of, 210–11
Titanium boride (TiB_2)
diffusion in, frequency factors and activation energies for, 51
irradiation damage, 22–23
oxidation behavior, 93
use as crucibiles for molten Be, 61
Titanium carbide
carbon activity in nonstoichiometric, effect of composition and temperature on, 127
diffusion in, frequency factors and activation energies for, 51
use as crucibles for molten Ni, 61
Titanium carbide (TiC)
elastic properties, 205
integral and partial configuration entropies for solid solutions of, 127
microhardness of, effect of stoichiometry on, 127, 129
preparation of single crystals of, 249
preparation of ultrafine particles of, 125
structure and hardness, effect of high pressure on, 204
yield strength of, 127, 130
Titanium carbide composites (TiC-graphite)
mechanical properties, 204
Titanium carbide systems (HfC–TiC–ZrC)
miscibility gaps in, 126
Titanium carbide systems (TiC–UC)
phase studies, 227
Titanium composites (HfC–Ti)
melting temperature, 204
Titanium nitride systems (TiN–UN)
phase studies, 9–10
Titanium oxide
diffusion in, frequency factors and activation energies for, 51
Titanium oxide (TiO_2)
corrosion of powdered by diphenyl, 103–4
reaction with ThO_2, 164–65
Titanium oxide (Ti_2O_3)
preparation of single crystals of, 249
Titanium oxide systems (Cr_2O_3–TiO_2)
phase studies, 55
Titanium systems
(see Nimonic 80A, TZC, and TZM)
Titanium systems (Al–Hf–Nb–N–Ti–W–Zr)
high-temperature strength properties, 45
oxidation tests at 1000°C, 45
Tophet C
corrosion by air at 1000°C, 26–27
Transmission electron microscopy
use in studying the microstructure of irradiated materials, 113–14
Tubes
explosive bonding of lined bimetallic, 214
Tungsten
adsorption and decomposition of various gases on, 28
brazing, 253
compatibility with various carbides, 123–24
corrosion by KOH solutions, 179
creep properties, 46
deformation at high temperatures, 202
deposition from WCl_6, 212
diffusion in, bibliography on, 132
diffusion in U, 133
diffusion of Mo in, 133–34
diffusion of ^{95}Nb in, 197
diffusion of Re in, 133
diffusion of Ta in, 198
dislocation etch pitting of single crystals in chloride solutions, 179
ductility of, effect of irradiation on, 111
ductility of recrystallized, effect of Tc additions on, 122–23
effect of irradiation on carbide coatings on, 130
effect of Re on the lattice solid solubility of O_2 in, 201–2
electron-beam floating-zone-melting apparatus for rods of, 249
fabrication into tubes by powder extrusion, 248
fracture strength of, effect of irradiation on, 111
fusion welds, hot cracking in, 251
high-temperatures of chemical-vapor deposited, 201
interaction with active gases in vacua and inert gas environments, 97–98
mechanical properties of arc-melted, 122
oxidation of, 179
oxidation from 1127 to 2227°C at low-oxygen pressures, 27
oxidation in air, effect of LiO_2 additions on, 98
oxidation of, effect of foreign gases on kinetics of, 179
oxidation of powders in 20°C air, effect of humidity on, 98
oxygen interaction with polycrystalline ribbin of, 98
preparation of single crystals of, 63
preparation of tubes by chemical-vapor deposition, 250
pressure bonding to graphite, 62
properties of CVD sheets, 122
radiation damage, effect of cold working on, 44
relative partial molar enthalpy in liquid Pu, 3
thermal properties, 8
Tungsten alloys
(see also C-129Y, Cb-752, FS-85, HA-25, Hastelloy C, Haynes 25, Haynes 188, L-605 superalloy, Multimet, T-111, and T-222)
interaction with active gases in vacua and inert gas environments, 97–98
Tungsten alloys (Al–Hf–Ta–W)
high-temperature strength properties, 45
oxidation tests at 1000°C, 45
Tungsten alloys (B–Mo–W)
phase studies, 127
Tungsten alloys (Cr–Co–Fe–Mo–Ni–W)
tensile properties of irradiated, effect of Ti additions on, 189–90
Tungsten alloys (Hf–Nb–W–Zr)
high-temperature strength properties, 45
Tungsten alloys (Mo–Re–W)
electron-beam welding to T-111, 64–65
Tungsten alloys (Mo–W)
corrosion, chemical and galvanic, 98
Tungsten alloys (Nb–Ta–W)
rupture strength, effect of metallic carbide and boride additions on, 45
Tungsten alloys (Nb–W)
rupture strength, effect of metallic carbide and boride additions on, 45
self-diffusion of Nb in, 133
Tungsten alloys (Re–W)
chemical-vapor deposition of, 212
deformation at high temperatures, 202
mechanical properties of arc-melted, 122
preparation of tubes from, 63
tensile properties of wrought recrystallized, 123
thermal conductivity, 200–1
Tungsten alloys (Ta–W)
brazed joints of, shear strength of, 215–16
creep–rupture properties from 1000 to 1650°C, 122
oxidation in air, effect of LiO_2 additions on, 98
oxidation behavior of W–Si coated, 180
Tungsten alloys (Ti–W)
diffusion of Cr and W in, 198
phase studies, 46
Tungsten carbide (WC)
crystal structure, 204–5
elastic properties, 205
integral and partial configuration entropies for solid solutions of, 127
preparation of spherical granules of, 125
structure and hardness, effect of high pressure on, 204
thermal expansion, 204
thermodynamic properties, 127–28
Tungsten cermets (W–UN)
fabrication by sintering and hot isostatic pressing, 228
Tungsten cermets (W–UO_2)
thermal conductivity, 78
Tungsten cermets (W–UO_2)(W clad)
fabrication by gas-pressure bonding, 62–63
Tungsten composites (HfC–W)
melting temperature, 204
Tungsten dispersions (W–ThO_2)
yield strength, 202
Tungsten dispersions (W–UO_2)
thermal properties, 8
Tungsten systems
(see ASTAR 811C, D-43, SU-16, and T-222)
Tungsten systems (Al–Hf–Nb–N–Ti–W–Zr)
high-temperature strength properties, 45
oxidation tests at 1000°C, 45
Tungsten systems (C–Hf–W)
strength and ductility of, effect of composition, heat-treatment and substructure on, 123
Tungsten systems (C–Hf–Ta–W–Zr)
oxidation in air, formation of protective

coating during, 180
Turbine buckets
erosion and cavitation damage by steam, Cs vapor, and K vapor, 30
TZC
creep properties, 122
tensile properties at high temperatures, 200–1
TZM
brazed joints of, shear strength of, 215–16
corrosion by liquid Na, 182
corrosion by liquid K, 186
creep properties, 122
stress–rupture strength, effect of fabrication variables on, 122
tensile properties at high temperatures, 200–1
TZM alloys (Nb–TZM)
stress–rupture strength, effect of fabrication variables on, 122
TZM molybdenum
corrosion, chemical and galvanic, 98
oxidation behavior of Durak B and Vought IX silicide coated, 180

U

Udimet 700
creep properties, effect of stress cycling on, 120–21
fabrication by powder-metallurgical techniques, 61
Ultrasonic testing, 68–69, 151–52, 217, 254
UMCO-51
corrosion by liquid Na, 28
effects of irradiation on tensile properties of, 40–41
Uranitride (UN)
solubility of USi in, 10
Uranium
cold shots in ingots, prevention of, 248
corrosion by diphenyl, 104
creep properties of beta-quenched, 156–57
deformation mechanisms in alpha phase, 1
diffusion of W in, 133
diffusion studies of Ni plated, 197
effect of ingot grain structure on the formation of seams during rolling of rods of, 249
effects of irradiation on electrical conductivity of single crystals of, 84
electroplating with Zr, 64
electropolishing, 64
extrusion, 249
fission damage at 4°K, 166
fission gas bubbles in, effect of annealing on distribution of, 73
fission gas bubbles in, post-irradiation behavior of, 73
grain growth, thermodynamics of, 1
growth and electrical-resistivity changes in irradiated wires of, 84
ignition temperature in O_2, 155
irradiation damage in alpha phase, 231
irradiation swelling, 166, 221
length changes of irradiated single crystals of, 84
release of CH_3I from, during reactor accidents, 85
room-temperature ductility, effect of annealing on, 73
tensile and impact properties of extruded, 155
Uranium (adjusted)
effect of thermal cycling on density of, 155
Uranium (nickel plated)
ductility at room temperature, effect of annealing under vacuum on, 73
room-temperature ductility, effect of annealing on, 73
Uranium-233
fission cross section, 84
neutron-capture cross section, 84
Uranium alloys (adjusted)
structural changes during high-temperature deformation, 1–2
Uranium alloys (Al–Fe–U)
microstructure of as-cast, 156
Uranium alloys (Al–U)
analysis of precipitates in, 156
irradiation performance, 221
microstructure of as-cast, 156
Uranium alloys (B–U)
grain-refining effects and transformation kinetics of, 73–74
Uranium alloys (Cr–U)
grain-refining effects and transformation kinetics of, 73–74
Uranium alloys (Cr–U)(molten)
evaluation of Y as container material for, 31
Uranium alloys (fissium–Pu–U)
high-burnup properties, 75
Uranium alloys (Fe–U)
microstructure of as-cast, 156
Uranium alloys (Mo–Pu–U)
fabrication in fuel elements for the Zero Power Plutonium Reactor, 249
Uranium alloys (Mo–U)
corrosion by seawater, 27
grain-refining effects and transformation kinetics of, 73–74
irradiation swelling, 83–84
mechanical and physical properties, 158
recrystallization, effect of B on, 2
specific heat, 74
tensile properties, 2
tensile properties of, effect of temperaon, 232
thermal cycling of, effect on surfaces of, 232
transformation of gamma phase on rapid cooling, 74
Uranium alloys (Mo–U–Zr)
corrosion by H_2O, effect of composition and heat-treating on, 232
Uranium alloys (Nb–U)
coating with Nb, 251
tensile properties of, effect of temperature on, 232
Uranium alloys (Nb–U–Zr)
corrosion by H_2O, effect of composition and heat-treating on, 232
Uranium alloys (P–U)
grain-refining effects and transformation kinetics of, 73–74
Uranium alloys (Pu–Th–U)
solid solubility properties, 75
Uranium alloys (Pu–Ti–U)
high-burnup properties, 75
Uranium alloys (Pu–U)
irradiation swelling, effect of temperature, pressure, burnup, and composition on rate of, 4
Uranium alloys (Pu–U–Zr)
high-burnup properties, 75
preparation by induction melting, crucible coatings for, 2–3
Uranium alloys (Th–U)
irradiation performance in NaK at 785°C, 166
Uranium alloys (Th–U–Zr)
irradiation swelling, 7–8
Uranium alloys (Ti–U)
tensile properties of, effect of temperature on, 232
Uranium alloys (U–Zr)
grain-refining effects and transformation kinetics of, 73–74
specific heat, 155–56
tensile properties of, effect of temperature on, 232
thermophysical properties of hydrided, 242–43
Uranium aluminide dispersions (Al–UAl_3)
compressive-strength, 78
plate fabrication by the picture-frame, hot-rolling technique, 8
swelling during heat treatments, 78
Uranium boride (UB)
solubility in UN, 9–10
Uranium carbide (PuC)
irradiation behavior, literature survey on, 6
properties, literature survey on, 6
Uranium carbide (UC)
casting into fuel rings for the HWOCR, 210
Cr and V stabilized, compatibility with stainless steel, 10
compatibility with stainless steel, 10, 164
compatibility with vanadium, 164
compressive creep, 11
corrosion of powdered by diphenyl, 103–4
creep properties, 161–62, 166
diffusion of C in, 81–82
diffusion of ^{131}I in, 196
diffusion studies, 197
diffusion of Xe in, 165
effect of burnup on lattice parameters of, 85
electron-beam melting and casting of, 60
fission induced sorption of Kr in, 85, 165
gas release of irradiated, 165–66, 222
irradiation damage, basic studies of, 12–13
irradiation swelling, 165–66, 222
preparation from UF_4, 82
preparation from UO_2, U_3O_8, or UO_3, 82–83
production from U–UC mixture by warm pressing and reactive sintering, 11
production from UC_2, 11
solubility of Xe in, 165
specific heat, 227
thermal conductivity, effect of O_2 in solid solution with, 227
Uranium carbide (UC)(SAP clad)
performance in Santowax OM and HB-40, 32
Uranium carbide (UC_2)
diffusion of C in, 81–82
enthalpy, 227–28
Gibbs free energy of formation at 740 to 890°C, 82
irradiation behavior, literature survey on, 6
properties, literature survey on, 6
reduction to UC by heat-treating in H_2 atmosphere, 11

Uranium carbide (U_2C_3)
  diffusion of C in, 81–82
  irradiation behavior, literature survey on, 6
  properties, literature survey on, 6
Uranium carbide dispersions (UC_2–graphite)
  fabrication, 228
Uranium carbide systems (CeC–UC–ZrC)
  phase studies, 9
Uranium carbide systems (PuC–UC)
  compatibility with 316 stainless steel, 161–62
  compatibility with 316L stainless steel, effect of Mo addition on, 162
  compatibility with Cr–Ti–V alloy, 161–62
  compatibility with various cladding materials, 6, 78
  irradiation behavior, literature survey on, 6
  irradiation swelling, 162
  Pu losses during arc-melting, 6
  preparation by the metal-methane fluidized-bed process, composition of, 6
  preparation of single phase by arc-melting and hydrogen-treatment process, properties of, 6
  properties, literature survey on, 6
  thermal conductivity, 224
Uranium carbide systems (PuC_2–UC_2)
  phase diagram, 224–25
Uranium carbide systems (Pu,U)C
  compatibility of Na bonded with 316 stainless steel, 100–1
  preparation by arc-melting, composition of, 7
Uranium carbide systems (TiC–UC)
  phase studies, 227
Uranium carbide systems (UC–UN)
  stability of solid solutions of, 10
Uranium carbonitride (U(C,N))
  preparation from UO_2, 82
Uranium hydroxide
  electrodeposition, 64
Uranium intermetallic compounds (UAl_2–UFe_2–UMn_2)
  phase studies, 2
Uranium intermetallic compounds (U–UFe_2–UMn_2)
  phase studies, 2
Uranium nitride (UN)
  compressive creep, 11
  creep properties of stoichiometric, 82
  effect of burnup on lattice parameters of, 85
  gas release of irradiated, 165–66
  fabrication of compacts of, 228
  irradiation swelling, 165–66
  melting behavior as functions of temperture and N pressures, 77–78
  Poisson's ratio, 10–11
  self diffusion of ^{233}U in, 165
  shear modulus, 10–11
  solubility of UB in, 9–10
  specific heat, 227
  thermal diffusivity of, effect of stored energy on, 222–23
  wetting by liquid Na, 182
  Young's modulus, 10–11
Uranium nitride (U_2N_3)
  determination of the partial pressure of N_2 over, 10
Uranium nitride cermets (UN–Mo)
  fabrication by sintering and hot isostatic pressing, 228–29
Uranium nitride cermets (UN–W)
  fabrication by sintering and hot isostatic pressing, 228–29
Uranium nitride systems (HfN–UN)
  phase studies, 9–10
Uranium nitride systems (PuN–UN)
  compatibility of Na bonded with 304 stainless steel, 7
  compatibility with various cladding materials, 7, 78
  irradiation behavior, 7
  melting behavior as functions of temperature and N pressures, 77–78
  vapor pressure, 7
Uranium nitride systems ((Pu,U)N)
  fission gas release studies, 162
  irradiation swelling, 162
  melting behavior, 162
  nitrogen interaction, effect of irradiation on, 225
  vaporization of, 225
Uranium nitride systems (TiN–UN)
  phase studies, 9–10
Uranium nitride systems (UC–UN)
  stability of solid solutions of, 10
Uranium nitride systems (UN–UO_2)
  phase studies, 226–27
Uranium nitride systems (UN–ZrN)
  phase studies, 9–10
Uranium oxide (UO_2)
  chemical plating with Cr_3C_2, 250
  columnar-grain formation, 222
  columnar-grain growth, inhibition by Ir addition, 9, 226
  diffusion of ^{233}U in, 199
  compressive creep, 11
  corrosion of powdered by diphenyl, 103–4
  densification behavior of powders prepared by the reaction of UF_6 with H_2 and O_2 in a flame reactor, 164
  effect of burnup on lattice parameters of, 85
  enthalpy of, 163
  fabrication of shapes by plastic deformation techniques, 80
  fission damage, survey of, 166
  fission gas bubbles in, resolution of, 85, 166, 222
  fission gas bubbles in, trails of migrating, 166
  fission-gas release from, 85, 165–66, 222
  fission gas release, effect of power changes on, 167
  heat of fusion, 163
  ionic motion in, 223, 226
  irradiation damage, basic studies of, 12–13
  irradiation swelling, 165–66
  molybdenum diffusion from irradiated, 226
  oxygen diffusion in, 225–26
  oxygen redistribution in during irradiation, 79–80
  preparation of hollow spherical particles of, 9
  preparation of large single crystals of, 248–49
  production from UO_3 by arc fusion process, 164
  reaction with H_2O during loss-of-coolant accidents in light-water power
  reaction with liquid Na, 83
  reaction with steam, 83
  release of CH_3I from, during reactor accidents, 85
  saturation solubility and diffusion of He in, 163
  self diffusion of ^{233}U in, 165
  sintering of powders of, effect of reducing and oxidizing atmospheres on, 226
  specific heat, 227
  surface diffusion coefficient, 9
  thermal conductivity, 9
  thermal conductivity of sintered stoichiometric, 163
  thermal diffusivity of, effect of stored energy on, 222–23
  trapping of Xe in, effect of bombardment temperature on, 167
  uranium diffusion in, 225–26
Uranium oxide (UO_2)(clad)
  fission-product-gas pressure in microscopic void of irradiated, 222
Uranium oxide (UO_2)(SAP clad)
  fretting and wear tests in Santowax OM, 31–32
Uranium oxide (UO_2)(stainless steel-304
  reaction with water during loss-of-coolant accidents in water-cooled power reactors, 32–33
  clad)
Uranium oxide (UO_2)(Zircaloy clad)
  reaction with water during loss-of-coolant accidents in water-cooled power reactors, 32–33
Uranium oxide (UO_2)(Zircaloy-2 clad)
  corrosion in the Dresden Reactor, 96
  fretting and wear tests in Santowax OM, 31–32
  reaction with steam during loss-of-coolant accidents, 104–5
Uranium oxide cermets (Mo–UO_2)
  mechanical and thermal properties of, 8
Uranium oxide cermets (W–UO_2)
  thermal conductivity, 78
Uranium oxide cermets (W–UO_2)(W clad)
  fabrication by gas-pressure bonding, 62–63
Uranium oxide dispersions (Al–U_3O_8)
  compressive-strength, 78
  plate fabrication by the picture-frame, hot-rolling technique, 8
  swelling during heat treatments, 78
Uranium oxide dispersions (BeO–UO_2)
  irradiation effects on physical properties of, 92
  retention of fission products, 92
Uranium oxide dispersions (W–UO_2)
  thermal properties, 8
Uranium oxide systems (B_4C–UO_2)
  irradiation testing, 175–76
Uranium oxide systems (PuO_2–UO_2)
  burnup studies, 76–77
  compatibility with Ta, 224
  compatibility with vanadium alloys, 161
  compatibility with various claddings, 77–78, 224
  densities of sil-gel prepared pellets of, 223
  fabrication by hot pressing, 160
  fabrication of pellets, 223
  gas-release behavior of irradiated, effect of stoichiometry on, 161
  irradiation performance of 304L stainless steel clad, 223
  liquidus–solidus curves for, 223
  melting heat rating of, effect of stoichiometry on, 5–6
  microstructure of irradiated, effect of stoichiometry on, 161
  physical and thermal properties, 75–76
  preparation of pellets for FFTF fuel, 4
  preparation of spherical particles of, 5, 76, 160
  shear modulus, 5

solid-fission-product behavior in, 167, 224
thermal conductivity, 5
thermal conductivity, effect of stoichiometry on, 160–61
thermal diffusivity, 5
Young's modulus, 5
Uranium oxide systems (PuO_2–UO_2–ZrO_2)
burnup studies, 77
melting point, 77
phase studies, 77
Uranium oxide systems $(Pu,U)O_2$
reduction by liquid Na containing various amounts of O_2, 100
Uranium oxide systems (ThO_2–UO_2)
comminutation of persintered granules by planetary ball milling, 226
diffusion of U in, 53
Uranium oxide systems $((Th,Pu)O_2)$
thermal stability of particles of, 77
Uranium oxide systems (UN–UO_2)
phase studies, 226–27
Uranium rods (Zircaloy-2 clad)
irradiation swelling, effect of axial hole on, 73
Uranium silicide (USi)
solubility in UN, 10
Uranium silicide (U_3Si)
corrosion by H_2O, 158
fission-fragment damage, 166–67
production and properties, 232–33
structure of, effect of irradiation on, 221
Uranium silicide (U_3Si)(Zircaloy-2 clad)
corrosion by high-temperature water, effect of defected cladding on, 83
Uranium silicide (U_3Si_2)
production and properties, 232–33
Uranium sulfide (US)(Nb–Zr clad)
burnup studies, 82
Uranium systems (Al–C–Fe–Si–U)
precipitation of UAl_2 from 350 to 600°C, kinetics of, 73–74
Uranium systems (Al–C–Fe–Si–U) (Zircaloy-2 clad)
corrosion of beta heat-treated by water at 282°C, 73
Uranium systems (Al–C–Fe–U)
creep properties, 157–58
microstructure of as-cast, 156
Uranium systems (Al–C–Si–U)
microstructure of as-cast, 156
Uranium systems (Al–C–U)
microstructure of as-cast, 156
Uranium systems (Al–Cr–Si–U)
irradiation swelling, 83–84
Uranium systems (Al–Fe–Si–U)
alpha-to-beta transition temperature, 73
microstructure of as-cast, 156
structural properties, 73
Uranium systems (Al–Mo–Si–U)
irradiation swelling, 83–84
Uranium systems (Al–Si–U)
microstructure of as-cast, 156
Uranium systems (C–Fe–Si–U)
microstructure of as-cast, 156
Uranium systems (C–Fe–U)
microstructure of as-cast, 156
Uranium systems (C–N–O–U)
phase studies, 81
Uranium systems (C–N–U)
studies, 77
Uranium systems (C–Si–U)
microstructure of as-cast, 156
Uranium systems (C–U)
grain-refining effects and transformation kinetics of, 73–74
microstructure of as-cast, 156
phase studies, 161
Uranium systems (C–U–V)
phase studies, 10
Uranium systems (C–U–Zr)
phase studies, 227
Uranium systems (H–U–Zr)
irradiation testing in the TRIGA Mark F Reactor, 20
pressure-temperature isochores to 1300°C for, 19–20
Uranium systems (Fe–Si–U)
microstructure of as-cast, 156
Uranium systems (N–Th–U)
phase studies, 78
Uranium systems (O–Pu–U)
metallographic and X-ray investigations in, 75
Uranium systems ((Pu,U)–C–N)
studies, 77
Uranium systems (Pu–Th–U)
phase studies, 231
Uranium systems (Si–U)
analysis of precipitates in, 156
delta peritectoidal reaction in, effect of C on, 2
grain-refining effects and transformation kinetics of, 73–74
microstructure of as-cast, 156
structure, effect of fabrication and heat-treatment variables on, 158

V

Vanadium
compatibility with PuC–UC systems, 78
compatibility with PuN–UN, 7
corrosion by liquid Na, 182
creep properties, 46
deposition from VCl_3, 250
deposition from VCl_3, VCl_4, and VF_5, 212
diffusion in, bibliography on, 132
irradiation damage, 114
preparation of single crystals of, 249
pressure bonding to Zr, 62
production of cavities in by irradiation, 110
relative partial molar enthalpy in liquid Pu, 3
solubility in liquid Pu, 3
solubility in liquid K, 185
solubility of O_2 in, 30
Vanadium alloys
compatibility with UO_2–PuO_2, 161
Vanadium alloys (Al–Ti–V)
diffusion welds in, effect of welding temperature and pressure on strength of, 252
Vanadium alloys (Cr–Ti–V)
burst properties of tubes, effect of irradiation on, 110
compatibility with PuC–UC fuels, 161–62
compatibility with PuO_2–UO_2 systems, 78
corrosion by liquid Na, 28
preparation of high purity, 60
preparation of ingots of, 210–11
Vanadium alloys (Nb–Ti–V)
creep and stress-rupture properties of, effect of Ti content on, 123
Vanadium alloys (Nb–V)
oxidation in air at 500–900°C, 179
Vanadium alloys (Nb–V–Zr)
oxidation in air at 500–900°C, 179
Vanadium alloys (Nb–Zr)
compatibility with PuN–UN systems, 78
compatibility with PuO_2–UO_2 systems, 78
Vanadium alloys (Tc–V)
phase studies, 46
Vanadium alloys (Ti–V)
compatibility with PuC–UC systems, 78
compatibility with PuO_2–UO_2 systems, 78
corrosion by liquid Na, 28
creep and stress-rupture properties of, effect of Ti content on, 123
effect of irradiation on creep properties of, 41
preparation of ingots of, 210–11
Vanadium alloys (V–Zr)
compatibility with PuO_2–UO_2 systems, 78
Vanadium carbide (VC)
carbon activity in nonstoichiometric, effect of composition and temperature on, 127
integral and partial configuration entropies for solid solutions of, 127
microhardness of, effect of stoichiometry on, 127, 129
yield strength of, 127, 130
Vanadium carbide systems (HfC–VC)
phase diagram, 126
Vanadium carbide systems (NbC–TaC–VC)
miscibility gaps in, 126
Vanadium carbide systems (VC–ZrC)
phase diagram, 126
Vanadium composites (HfC–V)
melting temperature, 204
Vanadium oxide (VO)
preparation of single crystals of, 249
Vanadium systems
(see Croloy, Vanstar-7, and Vanstar-9)
Vanadium systems (C–Cr–V)
phase studies, 126
Vanadium systems (C–U–V)
phase studies, 10
Vanadium systems (H–V)
phase diagram, 243–44
Vanstar 7
compatibility with PuO_2–UO_2 systems, 78
corrosion by liquid Na, 182–83
preparation of ingots of, 210–11
Vanstar 8
compatibility with PuO_2–UO_2 systems, 78
preparation of ingots of, 210–11
Vanstar 9
compatibility with PuO_2–UO_2 systems, 78
corrosion by liquid Na, 182–83
preparation of ingots of, 210–11

W

Welding, 64–67, 148–50, 214–15, 251–53

X

XAP 005
cyclic-strain fatigue behavior of, 116–17
XB-85
development of aluminide and silicide coatings for oxidation protection of, 179

Y

Yttrium
diffusion of Mo and Nb in, 134
diffusion of Zr in, 134
use as container material for molten U–Cr alloys, 31
Yttrium alloys
(see C-129Y)

Yttrium hydride (YH_2)
use as moderator in a fuel element, 20
Yttrium oxide (Y_2O_3)
diffusion of ^{91}Y in, 53
use as crucible coating, 2–3
Yttrium oxide dispersions (Y_2O_3)
production, 119
Yttrium oxide dispersions (Zr–Y_2O_3)
chemical reactions in, effect of sintering times and temperatures on, 49
creep and rupture properties, effect of Y_2O_3 content on, 49

Z

Zinc
deposition on metals by evaporation-abetted bias sputtering, 63
Zircaloy
corrosion by high-temperature steam, effects of silicate ions on, 25
corrosion by H_2O, distribution of hydride precipitates during, 97
corrosion and wear surveillance in the PRTR, 27
deformation behavior, 117–18
effect of radiation on corrosion, mechanical properties, and hydride formation of, 34
fabrication of tubes of, 249–50
hydride precipitates in, 174–75
reaction with H_2O during loss-of-coolant accidents in light-water power reactors, 32
removal of oxide films from by pickling, 95–96
supersaturation of H_2 in, theoretical predictions for, 48
Zircaloy-2
acoustic emission from tubes during tension and fatigue testing, 119
corrosion by H_3BO_3–NaOH solutions, 95
corrosion by steam, effects of radiation on, 177
creep properties, effects of irradiation on, 109, 187
diffusion of Cr and Fe in, 198
explosive welding to SAP, 214
failure stress of flawed tubes of, effect of neutron radiation and H_2 content on, 187
heavy-water pressure-tube technology, review of, 192
hydrogen transport in, 175
in-pile creep tests on, 33–34
in-reactor corrosion by D_2O, 96
orientation of hydride platelets in tubes of, effect of diameter and wall thickness on, 118
strain aging, effects of irradiation on, 109
tensile properties, 192
Zircaloy-4
corrosion and hydriding of tubing in a pressurized-water system, effect of heat transfer and isothermal conditions on, 25
corrosion by steam, effects of radiation on, 177
plasma/electron-beam welding, 65
in-pile relaxation behavior, 34
in-pile tensile tests on, 34
mechanical properties at high temperatures, 192–93
recovery and recrystallization kinetics of cold-worked plates and tubes of, 47–48
surface cracking during rolling at 795°C, 47
Zirconia
(see Zirconium oxide (ZrO_2))
Zirconium
brazing of strips, 253
casting of ingots of, 248
deformation behavior, 117–18
deformation behavior, effect of O_2 content on, 118
diffusion in X, 134
diffusion of C, N, and O in, frequency factors and activation energies for, 51
diffusion of Mo in, 198
diffusion of ^{95}Nb in alpha, effect of temperature on, 52
diffusion of O in, 51–52
diffusion of Ru in, 134
diffusion welding to steel, 215
electrodeposition on U, 64
electromigration of C, N, and O in, 52
flow stress at low temperatures, effect of O_2 content on, 118
hydride habit planes in single-crystal, 242
oxidation, 96
preparation of high-purity by electron-beam refining, 142
pressure bonding to graphite, 62
pressure bonding to V, 62
production of ingots by electron-beam melting, 60
reaction with H_2O during loss-of-coolant accidents in light-water power reactors, 32
self-diffusion in, 52
solubility in liquid Li and K, 185
strength of tubing of, effect of cold working on, 210
symposia on fabrication and properties of, 117
tensile properties, effect of He and Li on, 34
solubility and precipitation of H_2 in, 118
Zirconium alloys
(see also Cb-752 and FS-85)
effect of radiation on corrosion mechanical properties, and hydride formation of, 34
hydride precipitates in, review of, 192
in-pile creep tests on, 33–34
oxidation in high-temperature steam effects of radiation on, 177
symposium on fabrication and properties of, 117
Zirconium alloys (Cr–Fe–Zr)
beta to alpha transformation temperature of, effect of cooling rate on, 119
development, 48
hardenability, effect of cooling rate on, 193
Zirconium alloys (Cr–Nb–Zr)
creep properties in air, 48–49
development, 48–49
Zirconium alloys (Cu–Fe–Zr)
corrosion by steam, effects of radiation on, 177
Zirconium alloys (Cu–Mo–Zr)
diffusion of Mg in, effect on tensile properties of, 52
Zirconium alloys (Cu–Nb–Zr)
effect of irradiation on tensile properties of annealed, 34–35
in-pile relaxation behavior, 34
Zirconium alloys (Cu–Zr)
diffusion of O in, 52
transformation characteristics of, 49
Zirconium alloys (Hf–Nb–Ti–Zr)
high-temperature strength properties, 45
Zirconium alloys (Hf–Nb–W–Zr)
high-temperature strength properties, 45
Zirconium alloys (Mo–Ti–Zr)
corrosion by liquid Na, 28
Zirconium alloys (Mo–U–Zr)
corrosion by H_2O, effect of composition and heat-treating on, 232
Zirconium alloys (Nb–Sn–Zr)
corrosion by steam, effects of radiation on, 177
Zirconium alloys (Nb–U–Zr)
corrosion by H_2O, effect of composition and heat-treating on, 232
Zirconium alloys (Nb–V–Zr)
oxidation in air at 500–900°C, 179
Zirconium alloys (Nb–Zr)
adsorption-rate sticking probabilities for O_2 on, 179
brazing, 68
brazing to Al_2O_3, 215
compatibility with PuN–UN systems, 78
compatibility with PuO_2–UO_2 systems, 78
corrosion by liquid Ce, 186
corrosion by liquid K, 102–3
corrosion by liquid Rb, 186
corrosion by liquid Na, 28, 182
corrosion by steam, effects of radiation on, 177
development, 48–49
ductility of electron-beam-melted ingots of, 141–42
evaluation as fuel-cladding materials for the LMFBR, 29
in-pile creep tests on, 33–34
oxidation in air at 500–900°C, 179
oxidation in dry air at 485 to 935°C, 178–79
strain rate dependence of the tensile flow stress of, 45
tensile properties of, effect of H_2 on, 118–19
yield strength, effect of irradiation on, 187
Zirconium alloys (Nb–Ti–Zr)
ductility of electron-beam-melted ingots of, 141–42
Zirconium alloys (Pu–U–Zr)
high-burnup properties, 75
preparation by induction melting, crucible coatings for, 2–3
Zirconium alloys (Pu–Zr)
phase studies, 3
Zirconium alloys (Th–U–Zr)
irradiation swelling, 7–8
Zirconium alloys (U–Zr)
grain-refining effects and transformation kinetics of, 73–74
specific heat, 155–56
tensile properties, effect of temperature on, 232
thermophysical properties of hydrided, 242–43
Zirconium alloys (V–Zr)
compatibility with PuO_2–UO_2 systems, 78
Zirconium boride
diffusion in, frequency factors and activation energies for, 51
Zirconium boride (ZrB_2)
irradiation damage, 22–23, 246
oxidation behavior, 93
properties of, effect of ceramic additives on, 132
sintering by chemical activation, 125
Zirconium carbide
diffusion in, frequency factors and activation energies for, 51

integral and partial configuration entropies for solid solution of, 127
Zirconium carbide (ZrC)
compatibility with various refractory metals, 123–24
elastic properties, 205
hot hardness of sintered, 205
production, 125
microhardness, effect of stoichiometry on, 127, 129
yield strength of, 127, 130
Zirconium carbide cermets (Mo–Re–HfC)
properties, 124–25
Zirconium carbide composites (ZrC–C)
thermal expansion, 204
Zirconium carbide composites (ZrC-graphite)
mechanical properties, 204
Zirconium carbide hydrides
crystal structure, 21
Zirconium carbide systems (C–ZrC)
preparation, 142
Zirconium carbide systems (CeC–UC–ZrC)
phase studies, 9
Zirconium carbide systems (HfC–TiC–ZrC)
miscibility gaps in, 126
Zirconium carbide systems (VC–ZrC)
phase diagrams, 126
Zirconium carbide systems (Zr–ZrC–ZrN)
constitution diagram of, 127
Zirconium composites (HfC–Zr)
melting temperature, 204
Zirconium dispersions (Zr–Y_2O_3)
chemical reactions in, effect of sintering times and temperatures on, 49
creep and rupture properties, effect of Y_2O_3 content on, 49
production, 119
Zirconium hydride
neutron-thermalization process in, 93
Zirconium hydride (ZrH)
corrosion of powdered by diphenyl, 103–4
Zirconium hydride (ZrH_2)
measurement of internal friction in polycrystalline wires with a low-temperature torsion pendulum, 174
Zirconium nitride hydrides
crystal structure, 22
Zirconium nitride systems (UN–ZrN)
phase studies, 9–10
Zirconium nitride systems (Zr–ZrC–ZrN)
constitution diagram of, 127
Zirconium oxide
diffusion in, frequency factors and activation energies for, 51
Zirconium oxide (ZrO_2)
corrosion of powdered by diphenyl, 103–4
diffusion of oxygen-ions in, 52
reaction with ThO_2, 164–65
sintering kinetics of ultra-fine calcia stabilized, 55
Zirconium oxide systems (Al_2O_3–ZrO_2)
phase studies, 132
Zirconium oxide systems (Cr_2O_3–ZrO_2)
phase studies, 55
Zirconium oxide systems (HfO_2–ZrO_2)
phase studies, 94
Zirconium oxide systems (PuO_2–UO_2–ZrO_2)
burnup studies, 77
melting point, 77
phase studies, 77
Zirconium oxide systems (PuO_2–ZrO_2)
application as isotropic heat-source material, 77
phase studies, 224
Zirconium oxide systems (Sm_2O_3–ZrO_2)
phase studies, 23
Zirconium systems
(see D-43, TZC, TZM molybdenum, TZM, Vanstar-7, Vanstar-9, Zircaloy-2, and Zircaloy-4)
Zirconium systems (Al–Hf–Nb–N–Ti–W–Zr)
high-temperature strength properties, 45
oxidation tests at 1000°C, 45
Zirconium systems (C–Hf–Ta–W–Zr)
oxidation in air, formation of protective coating during, 180
Zirconium systems (C–U–Zr)
phase studies, 227
Zirconium systems (H–U–Zr)
irradiation testing in the TRIGA Mark F Reactor, 20
pressure-temperature isochores to 1300°C for, 19–20
Zirconium systems (H–Zr)
phase studies, 92–93
Zirconium systems (Zr–ZrC–ZrN)
constitution diagram, 127
Zirconium tritide (ZrT_2)
formation of ^3He in by ^3T decay, 83

LEGAL NOTICE

This journal was prepared under the sponsorship of the U. S. Atomic Energy Commission. Neither the United States, nor the Commission, nor any person acting on behalf of the Commission:

A. Makes any warranty or representation, expressed or implied, with respect to the accuracy, completeness, or usefulness of the information contained in this journal, or that the use of any information, apparatus, method, or process disclosed in this journal may not infringe privately owned rights; or

B. Assumes any liabilities with respect to the use of, or for damages resulting from the use of any information, apparatus, method, or process disclosed in this journal.

As used in the above, "person acting on behalf of the Commission" includes any employee or contractor of the Commission, or employee of such contractor, to the extent that such employee or contractor of the Commission, or employee of such contractor prepares, disseminates, or provides access to, any information pursuant to his employment or contract with the Commission, or his employment with such contractor.

AEC Critical Review Series

SOURCES OF TRITIUM AND ITS BEHAVIOR UPON RELEASE TO THE ENVIRONMENT

by D. G. Jacobs, Oak Ridge National Laboratory

The author surveys the published information on tritium production and the major factors affecting tritium's behavior in the environment. He projects tritium production in an expanding nuclear power economy and estimates the impact of increased production on local and worldwide populations.

Contents

Properties of Tritium and Tritium Compounds
Sources of Tritium Production and Its Release
Procedures for Tritium Enrichment
Monitoring Practices and Instruments for the Detection and Assay of Tritium
Movement in the Environment
Projected Tritium Production in a Nuclear Power Economy and Its Impact Upon Local and Worldwide Populations
Summary and Conclusions
Index

Available as TID-24635 from:

Clearinghouse for Federal Scientific and Technical Information
Springfield, Virginia 22151 $3.00

This book is the first of a series of state-of-the-art reviews the AEC will be publishing under the series title AEC Critical Review Series. Next to be released will be *Reactor-noise Analysis in the Time Domain* by Nicola Pacilio and *Atmospheric Transport Processes*, Part 1, by Elmar R. Reiter.

REACTOR-NOISE ANALYSIS IN THE TIME DOMAIN

Nicola Pacilio
Argonne National Laboratory
Comitato Nazionale per l'Energia Nucleare

Recent research and new instrumentation emphasize once again the importance of time-analysis methods in the study of neutron noise. The second book in the AEC Critical Review Series is therefore a timely summary and evaluation of past and present research in this field and an indication of future developments in noise analysis.

The author organizes the state of the art of time analysis into four main categories under which he describes 15 different methods. For each method he gives the mathematical formulation, the means of data collection, and the experimental procedure. More important, however, he interprets the results and looks ahead to the uses, limitations, and potentialities of each method. With this added dimension the book becomes a valuable guide for reactor personnel. (102 pp., 18 figs., paperbound, chronological list of references.)

FOUR MAIN CATEGORIES

I: Time-correlation analysis among the neutron-detection pulses

II: Analysis of the moments of neutron distribution

III: Analysis of the probability of neutron detection

IV: Correlation analysis among the signs of the fluctuations

The contents also include:

General considerations on reactor-noise analysis
Synopsis of neutron statistics methods
Conclusions
Index

Available for $3.00 as TID-24512 from

Clearinghouse for Federal Scientific and Technical Information
Springfield, Virginia 22151

AEC Symposium Series

ABUNDANT NUCLEAR ENERGY

This symposium, sponsored by the U. S. Atomic Energy Commission and Oak Ridge Associated Universities, explores the applications of abundant low-cost nuclear energy, particularly within the context of the agro-industrial complex. Following a prediction of future cost and per capita consumption of electricity, the papers examine the effects of projected energy costs on energy-intensive processes, such as phosphorus, aluminum, chlorine, and electrolytic hydrogen, and on the large-scale uses of process heat from large nuclear plants. Discussions cover aspects peculiar to nuclear power plants: plant location and independence from fuel sources; the cost–size relation; and the cost–energy demand relation. 355 pages, 133 figures, 6 by 9 in.

Contents

Abundant Energy
Rationale for Low-Cost Nuclear Heat and Electricity
Energy-Intensive and Heat-Intensive Processes for a Nuclear Energy Center

Production of Basic Chemicals
Phosphorus
Effect of Low-Cost Nuclear Energy on the Chlorine–Caustic Industry
Acetylene and Low-Cost Power
The Fixation of Nitrogen in Arc Processes
The Economics of Hydrogen and Oxygen Production by Water Electrolysis and Competitive Processes
Production of Ammonia Using Low-Cost Nuclear Energy

Electrowinning of Metals and Metal Refining
Aluminum
Magnesium
Iron and Steel with Hydrogen
Electrowinning of Metals

Productive Uses of Process Heat
A Bleached Straw Pulp Mill for an Agro-Industrial Complex
Space Heating in Urban Environments
Application of Low-Cost Energy to Processing of Sewage Water for Reuse
Marine Chemical Recovery
Potable Water from Seawater by High-Temperature Electrodialysis
Nuclear Desalting

Panel Discussion
The Effects on University Engineering Programs of Abundant Nuclear Energy

Available for $3.00 as CONF-680810 from

Clearinghouse for Federal Scientific and Technical Information, Springfield, Virginia 22151

Announcing the publication of

LATE SOMATIC EFFECTS OF IONIZING RADIATION by C. D. Van Cleave

This book is a compilation of what is known about the late effects of radiation at the various levels of biological organization. It is directed primarily to the nonspecialist.

Contents

The Nature of the Problem

Part 1 Manifestations of Late Effects in Whole Organisms, Especially Mammals

Life Shortening by Ionizing Radiation
Radiation Leukemogenesis
Radiation Tumorigenesis in Animals and Man
Nonneoplastic Late Effects of Radiation
Prenatal Irradiation and Late Life Vigor

Part 2 Manifestations of Late Effects in Tissues, Cells, and Macromolecular Assemblies

Late Effects in Organs and Tissues
Late Effects in Individual Cells
Late Effects in Subcellular and Extracellular Entities

Part 3 Degradative Change and Aging

Similarities and Differences Between the Manifestations of Late Radiation Effects and of Natural Aging
Biological Organization and Degradative Change
General Summary

Available as TID-24310 from:

Clearinghouse for Federal Scientific and Technical Information
National Bureau of Standards, U. S. Department of Commerce
Springfield, Virginia 22151 $3.00

Nuclear Science Abstracts

The U. S. Atomic Energy Commission, Division of Technical Information, publishes *Nuclear Science Abstracts (NSA)*, a semimonthly journal containing abstracts of the literature of nuclear science and engineering.

NSA covers (1) research reports of the U. S. Atomic Energy Commission and its contractors; (2) research reports of government agencies, universities, and industrial research organizations on a worldwide basis; and (3) translations, patents, books, and articles appearing in technical and scientific journals.

Complete indexes covering subject, author, source, and report number are included in each issue. These indexes are cumulated and sold separately.

Availability of NSA

SALE *NSA* is available on subscription from the Superintendent of Documents, U. S. Government Printing Office, Washington, D. C. 20402, at $42.00 per year for the semimonthly abstract issues and $38.00 per year for the cumulated-index issues. Subscriptions are postpaid within the United States, Canada, Mexico, and all Central and South American countries, except Argentina, Brazil, Guyana, French Guiana, Surinam, and British Honduras. Subscribers in these Central and South American countries, and in all other countries throughout the world, should remit $52.50 per year for subscriptions to semimonthly abstract issues and $47.50 per year for the cumulated-index issues. The single-copy price for the abstract issues is $1.75 postpaid, with this exception: Add one-fourth of $1.75 for mailing to the countries to which the $52.50 subscription rate applies.

EXCHANGE *NSA* is also available on an exchange basis to universities, research institutions, industrial firms, and publishers of scientific information. Inquiries should be directed to the Division of Technical Information Extension, U. S. Atomic Energy Commission, P. O. Box 62, Oak Ridge, Tennessee 37830.

UNITED STATES
ATOMIC ENERGY COMMISSION
P.O. BOX 62
OAK RIDGE, TENNESSEE 37830

OFFICIAL BUSINESS

POSTAGE AND FEES PAID
U.S. ATOMIC ENERGY COMMISSION

1

MR. R.E. CHAPIN
DIRECTOR OF LIBRARIES
MICHIGAN STATE UNIVERSITY
EAST LANSING, MICHIGAN 48823

DOCUMENTS

DEC 29 1969

MICHIGAN STATE UNIVERSITY
LIBRARIES

TECHNICAL PROGRESS REVIEWS may be purchased from Superintendent of Documents, U. S. Government Printing Office, Washington, D. C. 20402. *Nuclear Safety* at $3.50 per year (six issues) for each subscription or $0.60 per issue; *Reactor Technology* at $3.00 per year (four issues) for each subscription or $0.75 per issue; each of the other journals at $2.50 per year (four issues) or $0.70 per issue. The use of the order form below will facilitate the handling of your order.

POSTAGE AND REMITTANCE: Postpaid within the United States, Canada, Mexico, and all Central and South American countries except Argentina, Brazil, Guyana, French Guiana, Surinam, and British Honduras. For these Central and South American countries and all other countries: add, for each annual subscription, $1.00 for *Nuclear Safety* and $0.75 for each of the other journals; for single issues, add one-fourth of the single-issue price. Payment should be by check, money order, or document coupons, and MUST accompany order. Remittances from foreign countries should be made by international money order or draft on an American bank payable to the Superintendent of Documents or by UNESCO book coupons.

order form

SUPERINTENDENT OF DOCUMENTS
U. S. GOVERNMENT PRINTING OFFICE
WASHINGTON, D. C. 20402

Please send — 1, 2, or 3 years

- ☐ Isotopes and Radiation Technology _____
- ☐ Nuclear Safety _____
- ☐ Reactor Technology _____
- ☐ Reactor Materials _____

Enclosed: document coupons ☐ check ☐ money order ☐

Charge: Superintendent of Documents No._____

SUPERINTENDENT OF DOCUMENTS
U. S. GOVERNMENT PRINTING OFFICE
WASHINGTON, D. C. 20402

(Print clearly)

_____
Name

_____
Street

_____
City, State, ZIP Code

V
O
I
1
4